Environmental Effects on Interacting Galaxy Pairs in the SDSS

by

Farid Qamar

A thesis submitted to the
Department of Physics, Engineering Physics, and Astronomy
in conformity with the requirements for
the degree of Master of Science

Queen's University
Kingston, Ontario, Canada
September 2014

Abstract

The cause of varying galaxy interaction outcomes in different environments is investigated using a sample of over 505,000 Sloan Digital Sky Survey Data Release 7 galaxies at $0.01 < z < 0.20$. The aim is to distinguish the large-scale environmental effects on galaxies from the small-scale interaction effects in order to identify whether interaction mechanisms vary in different environments, or whether different galaxy populations produce the various outcomes in different environments. To study the properties of paired galaxies, the enhancements in star formation rates (SFRs) and asymmetries are investigated as functions of projected pair separations in different environments. The paired galaxies and control samples were selected using a new technique to distinguish between the influence of nearby neighbours and larger scale environment, and we define four different environmental classes using their dark matter halo masses (the field, poor groups, rich groups, and clusters).

We find the strongest SFR enhancements at projected separations $(r_p) < 40\ h_{70}^{-1}$ kpc in field paired galaxies and the weakest (but statistically significant) in cluster paired galaxies, while the largest asymmetry enhancements are found in cluster paired galaxies, and the least in field paired galaxies. Using the asymmetry offset rather than enhancements reveals no dependence on environmental membership. Mean SFR suppression is found at separations $100 < r_p < 400\ h_{70}^{-1}$ kpc for paired galaxies with

mass ratio < 1 in all environments, but is absent for paired galaxies with mass ratio > 1. For paired galaxies with mass ratio < 1, this suppression is accompanied by a lack of mean asymmetry offset or enhancement at similar separations. Possible explanations of this result include suppression due to an earlier encounter whereby star bursts consume the star forming gas, and given sufficient time the galaxy settles into a symmetric shape. At close separations ($r_p < 40\ h_{70}^{-1}$ kpc), reduced mean SFR enhancements in all environments are found together with increased asymmetry enhancement in comparison with paired galaxies with mass ratio > 1. We hypothesize that the suppression in lower-mass paired galaxies is due to the depletion of their gas reservoirs prior to the interaction, and conclude that interactions in different environments produce various results due to assembly bias rather than differing interaction mechanisms in various environments.

Acknowledgments

There are many that I wish to thank for their contribution and role in making this thesis possible. This research has made use of data from the Sloan Digital Sky Survey (SDSS). Funding for the SDSS and SDSS-II has been provided by the Alfred P. Sloan Foundation, the Participating Institutions, the National Science Foundation, the U.S. Department of Energy, the National Aeronautics and Space Administration, the Japanese Monbukagakusho, the Max Planck Society, and the Higher Education Funding Council for England. The SDSS Web Site is http://www.sdss.org/. The SDSS is managed by the Astrophysical Research Consortium for the Participating Institutions. The Participating Institutions are the American Museum of Natural History, Astrophysical Institute Potsdam, University of Basel, University of Cambridge, Case Western Reserve University, University of Chicago, Drexel University, Fermilab, the Institute for Advanced Study, the Japan Participation Group, Johns Hopkins University, the Joint Institute for Nuclear Astrophysics, the Kavli Institute for Particle Astrophysics and Cosmology, the Korean Scientist Group, the Chinese Academy of Sciences (LAMOST), Los Alamos National Laboratory, the Max-Planck-Institute for Astronomy (MPIA), the Max-Planck-Institute for Astrophysics (MPA), New Mexico State University, Ohio State University, University of Pittsburgh, University of Portsmouth, Princeton University, the United States Naval Observatory,

and the University of Washington.

I wish to thank our research group in the University of Victoria for their invaluable help and guidance throughout the past two years. In particular, I am indebted to Asa Bluck for introducing me to various techniques and approaches to dealing with databases and galaxy mergers. His input and guidance were crucial in many areas of this thesis and in my development in the field. I also want to thank Jorge Moreno for introducing me to cosmological simulations, and for being the role model I aspire to be. I would also like to express my gratitude to Stéphane Courteau for his immeasurable help and support, academically and otherwise. Finally, I want to express how fortunate and thankful I have been to work with David Patton, my supervisor. Without his continuous support, guidance, and most of all his patience with me, this thesis would not have been possible.

A special thanks goes to my family, without them I wouldn't be where I am right now. Mom and Dad, thank you for raising me to be the man I am today, I will always be indebted to you. Doris, Mera, and Lina, your encouragement and support means the world to me. Finally, Samantha, you are the rock that I lean on, and the source of joy and comfort in my life. I dedicate this thesis, with all my love, to you.

Contents

List of Tables

List of Figures

Chapter 1

Introduction

1.1 Galaxy Evolution

In modern day astrophysics, galaxies are used as a tracer population of the underlying matter, and are considered in a sense to be the atoms of the cosmic fabric. To obtain a full picture of the evolution of the universe, understanding galaxy formation and evolution is crucial. It explains the current appearance of the universe, and aids in the prediction of its development in the future. Significant progress has been achieved in this field, and it is one of the most active fields of research in astrophysics today. Yet we have only begun to scratch the surface in terms of fully understanding the specific processes involved and their relative importance when it comes to galaxy evolution.

Once the vast distances to galaxies were known, for much of the 20th century, galaxies were thought to be Island Universes that were forming and evolving in isolation with no contact between one another. However, as galaxy catalogues began to grow, examples of galaxy pairs started to surface, alongside many peculiar galaxies with long, luminous plumes and tails emanating from their bodies (Lundmark and Ark, 1927; Holmberg, 1937). It was later discovered that those galaxies were

interacting, resulting in profound impacts on their properties (e.g., Holmberg 1958; Vorontsov-Vel'Iaminov 1958; Arp 1966; Markarian 1967). This includes intense bursts of star formation, the onset of quasar-like activity in galactic nuclei, and even the transformation of spiral galaxies into elliptical galaxies. Observational studies have shown that there is a significant fraction of interacting and merging systems, and theories of cosmological structure formation indicate that the majority of galaxies have had some form of strong interaction with other galaxies during their lifetime (Lotz et al., 2011). Therefore, studying galaxy mergers and interactions and the variables within provides crucial information for understanding the universe in general, and galaxy evolution in particular.

Galaxy mergers and interactions have been studied in a fair amount of detail in the past few decades. Many variables have been found to affect the outcome of mergers and interactions including the relative masses of the involved galaxies, their rotation, their relative velocities, etc. One of those variables that this thesis will focus on in particular is the density of their environment. Galaxies don't just come in a variety of properties like sizes, shapes, masses, etc. They can also be found to occupy regions with different densities in the universe, where some can be isolated in the field, and some can be found in highly dense clusters. By now, it is well known that environments have an effect on the properties of individual galaxies residing within them, and also on the outcome of the interaction of those galaxies, which is discussed in more detail in the next sections (e.g., Oemler 1974; Dressler 1980; van der Wel et al. 2010). However, little effort has been dedicated to finding whether the physical processes of interactions vary in different environments, or whether the interaction processes are identical but the galaxy populations interacting are different.

In other words, if one accounts and carefully controls for the differences between the galaxy populations in different environments, would the interaction outcomes vary with the environment? Moreover, if environments have an effect on the residing galaxies' properties, and interactions and mergers also affect the interacting galaxies' properties, which of the two influences is more dominant: the environmental effects or interactions? And how far must the interacting galaxies be from each other for the small-scale interaction effects to become negligible in comparison with the large-scale environmental effects?

In this thesis, I focus on exploring the properties of interacting galaxy pairs in different environments. I find the difference in the properties of paired galaxies and their controls in order to understand the extent of the effect of interactions on pairs in each environment. This detailed study is carried out using a sample of galaxy pairs obtained from the Sloan Digital Sky Survey (hereafter SDSS). In this sample the galaxies lie in the redshift range of $0.01 < z < 0.20$, corresponding to a lookback time of 0.14 Gyr to 2.4 Gyr in a concordance cosmology of $\Omega_\Lambda = 0.7$, $\Omega_M = 0.3$, and $H_0 = 70\ h_{70}$ km s^{-1} Mpc^{-1}.

Before embarking on this detailed study, I provide a description of different environments and the physical processes that affect the galaxies that reside within (§1.2). This is followed by a brief description of the physical processes involved in mergers and interactions and the effects they have on the interacting galaxies (§1.3). I then provide a summary of earlier studies done on pairs in different environments and what makes this thesis unique (§1.4). The introduction closes with an overview of this thesis.

1.2 Galaxy Environments

The density of environments in the universe can be defined in various ways, including the use of the number of nearest neighbours of a galaxy, or through the use of fixed apertures (e.g., dark matter halo mass). All methods lead to the inference that galaxies are generally found in three environments: groups, clusters, and the field. Groups and clusters are the largest known bound objects that come from the process of cosmic structure formation. In the large-scale structure of the Universe, they form the densest part and may contain a few to thousands of galaxies. Geller and Huchra (1989) showed that the density of galaxies in the local universe spans from $\sim 0.2\rho_0$ in voids to $\sim 5\rho_0$ in superclusters and filaments, $\sim 100\rho_0$ in the cores of rich clusters, and up to $\sim 1000\rho_0$ in compact groups, with ρ_0 being the average field density. Moreover, galaxies come in many different forms and sizes but they can be broadly divided into two main species: spirals and ellipticals. Spirals generally have flattened, disk-like shapes, blue colours, much gas and dust, and a widespread star formation activity that results in the presence of many young stars within. However, there are spirals that appear red mainly due to dust absorption of UV emissions. Ellipticals on the other hand, generally have a spheroidal shape, red colours, little to no gas and dust, and little star formation activity, therefore containing mostly old stars.

As early as the 1930s, it has been known that the environment in which a galaxy is found has a significant effect on its evolution and properties. Hubble and Humason (1931) pointed out that spiral galaxies dominate the field, while ellipticals and lenticulars (S0s) are more prevalent in dense cluster environments. The dependence of the morphology of galaxies on the environment shows that in denser environments a larger fraction of early-type galaxies is found. This relation was quantified by Oemler

(1974) and Dressler (1980). In his paper, Dressler (1980) studied the galaxy population in 55 rich clusters, and found a well-defined relation between local galaxy density and galaxy type. This relation became known as the Morphology-Density relation, and it shows that the fraction of spiral galaxies decreases from $\sim 60\%$ in the low-density environments to $\sim 10\%$ in the high-density environment, while the elliptical and S0 fractions exhibit the opposite trend. This relation offers clear evidence that the environment has an effect on galaxy type. In fact, it is considered to be the clearest observational signature of significant environmental dependencies of the processes that govern the formation and the evolution of galaxies.

With the rise of large galaxy surveys that are capable of generating accurate photometry for an unprecedentedly large sample of galaxies in the past decade, statistical studies of the behaviour of various galaxy properties became possible. In such studies, the $g-r$ versus $u-g$ colour-colour[1] diagrams show a clear bimodality in galaxy distribution together with a clear minimum between the two peaks (Strateva et al., 2001). Galaxies in those diagrams are found to be either in the "red sequence", which is dominated by old, quiescent stellar populations and dust- reddened spirals, or in the "blue cloud", which is predominantly occupied by late-type galaxies with ongoing star formation, or in the intermediate "green valley" (Bell et al., 2004; Brammer et al., 2009; Schawinski et al., 2014). Since its discovery, the origin of this colour bimodality in galaxy populations has been extensively researched. The majority of the works in this field agree that this bimodality is the result of star-forming galaxies transitioning to a quiescent state, which over time builds the red sequence (e.g.,

[1]Magnitudes are measured in different colours by taking images through filters. The SDSS telescope's filters are green (g), red (r), ultraviolet (u), and infrared (i and z). Colour is quantified by subtracting the magnitudes ($u-g$, $g-r$, etc.). Magnitudes decrease with increased light output, therefore objects with high $g-r$ are redder than objects with lower $g-r$.

Madgwick et al. 2002; Bell et al. 2003; Faber et al. 2007; Cucciati et al. 2012). In particular, it has been shown that a galaxy's environment can play a significant role in the quenching of star formation, where dense environments tend to have galaxy populations that are more massive and dominated by early-type galaxies. There have been many observational studies that were concerned with studying the effectiveness of quenching of star formation by the different environments. These studies were done using many photometric (e.g., Giodini et al. 2012; Cucciati et al. 2012; Li et al. 2012; Scoville et al. 2013) and spectroscopic surveys (e.g., Pelló et al. 2009; Jeltema et al. 2009; Balogh et al. 2011). These studies have found that for fixed stellar masses, the fractions of galaxies found along the red sequence are higher for denser environments than for lower density environments. Since this predominance of early type galaxies in clusters is likely the result of physical processes that suppress star formation and eventually alter galaxy morphology, several mechanisms that drive this quenching have been proposed, and can be grouped into the following categories:

- Interstellar medium (ISM) - Intracluster medium (ICM) interactions
- Galaxy-Cluster interactions
- Galaxy-Galaxy interactions

The following is a brief description of some of the processes that belong to those categories:

Ram Pressure Stripping

Ram Pressure Stripping is an example of an ISM-ICM interaction, first proposed by Gunn and Gott (1972). This process can remove the interstellar medium (ISM) from

a galaxy as it moves through the intracluster medium (ICM) of the cluster. When the ram pressure is greater than the binding force, the cold gas in the galaxy gets stripped, and the remaining gas could be compressed within the galaxy to cause a burst of star formation that would consume the majority of the leftover gas (Abadi et al., 1999; Quilis et al., 2000; Bekki and Couch, 2003; McCarthy et al., 2008). Ram pressure is expected to be an efficient method to remove the hot atmosphere of satellite galaxies in groups and clusters, and mostly effective in the cores of rich clusters (Tanaka et al., 2004).

Viscous Stripping

Viscous Stripping was first introduced by Nulsen (1982) and is another example of an ISM-ICM interaction, in which galaxies suffer gas loss by continuous (sometimes called turbulent or viscous) stripping. In this mechanism the outer layers of the ISM in a galaxy travelling into the ICM experiences a viscosity momentum transfer that could be sufficient to drag out part of its gas (Quilis et al., 2000; Schulz and Struck, 2001; Roediger and Hensler, 2005; Roediger and Brüggen, 2008).

Thermal Evaporation

Thermal Evaporation was introduced by Cowie and Songaila (1977) as another mechanism for ISM-ICM interactions. If the ICM temperature is high in comparison with the galaxy velocity dispersion, at the interface between hot ICM and cold ISM the temperature of the ISM rises rapidly, thus evaporating the gas which cannot be retained by the galaxy's gravitational field (Nipoti and Binney, 2007).

Starvation

Starvation (or Strangulation) was introduced by Larson et al. (1980). This mechanism consists of the removal of the diffuse hot gas reservoir of satellite galaxies as they enter a larger halo in groups and clusters. Since this tenuous halo is less bound than the cold gas in the disk, its stripping is considerably easier. Stripping gas from galactic disks induces a truncation of star formation activity on a short timescale ($\sim 10^7$ yr); however, starvation is expected to affect a galaxy's star formation history on a long timescale (> 1 Gyr) provoking a slowly declining activity, which consumes the disk gas after the supply of cooling gas has been removed (Larson et al., 1980; Balogh et al., 2000; van den Bosch et al., 2008). This mechanism is also an ISM-ICM interaction.

Tidal Interactions

Tidal Interactions are an example of Galaxy-Cluster interactions. In this mechanism, the galaxy interacts with the general potential of the cluster, where the orbiting galaxy can experience tidal forces and perturbations that can strip both gas and stars from the galaxy, as well as compress the gas within to cause increased star formation rates (Byrd and Valtonen, 1990; Bekki et al., 2001; Gnedin, 2003; Coziol and Plauchu-Frayn, 2007). These perturbations can also be violent enough to result in the entire disruption of the galaxy, causing a stellar stream to form.

Galaxy Harassment

Galaxy Harassment is a type of Galaxy-Galaxy interaction. When the tidal forces are not strong enough, or the relative velocities of the galaxies are too large for a merger to occur, the tidal forces can effectively heat the galaxy by transferring

energy from the orbit to internal motions of stars in the galaxy. This heating can result in the expansion of the galaxy, effectively causing the destruction of the cold, ordered structures like the disk. This process works through tidal shocking, where stars in the galaxy experience a rapidly changing tidal field as they are orbiting, which causes them to gain energy in the form of random motions, thus heating the system dynamically and causing it to expand (Moore et al., 1996; Fujita, 1998; Moore et al., 1999; Gnedin, 2003; Park and Hwang, 2009). Harassments are minor events in comparison with the major mergers; however, they occur far more often in dense environments due to the high relative velocities of the galaxies within them.

1.3 Galaxy Mergers and Interactions

Galaxy mergers and interactions are also types of galaxy-galaxy interactions that are thought to contribute to the colour bimodality of galaxies. As galaxies approach one another, the immense gravitational forces tend to wreak havoc on the properties of the interacting galaxies. When inspecting interacting and merging galaxies visually, one can easily see some unique features that are not common in isolated galaxies. They tend to have long bridges, tails, enhanced spiral structure, and are often severely distorted. Initially astronomers thought that the tails and long streams of gas and stars were the product of magnetic fields or nuclear jets. This was justified mainly due to the linearity and thinness of those features, which were at the time associated with stellar jets rather than gravitational interactions. However, Toomre and Toomre (1972) used computer models of interacting galaxies to convincingly show that these features known as “tidal tails” were most likely the product of gravitational tides acting on rotating disk galaxies. Since then, there has been substantial research into

the physics involved in these encounters (e.g., Bournaud et al. 2005; Di Matteo et al. 2007; Cox et al. 2008; Di Matteo et al. 2008; Jian et al. 2012).

1.3.1 How Merging Works

Galaxy composition can be split into three systems: gas, stars, and dark matter. As galaxies approach one another and begin to interact, these systems are affected differently. Systems can be either collisional or collisionless, depending on the interaction cross section between the systems' particles. When the interaction cross section between a medium's particles is sufficiently low as to not significantly affect the overall system, then the medium is collisionless. Otherwise, it is collisional. Stars in galaxies are a collisionless system due to the immense distances between stars with respect to their sizes. During galaxy collisions, the stellar systems pass through one another without sustaining any significant damage (Barnes et al., 1991). Dark matter is also collisionless, while the gas component of galaxies is a collisional system. This is mainly due to the extended and diffuse nature of gas clouds as well as their ability to lose energy due to radiation. The difference between collisional and collisionless systems is then seen when galaxies collide, where the gas in the systems experiences shockwaves and compression. The gas in the densest part of those gas clouds cools rapidly and collapses, which results in the formation of new stars.

Since gravity is the dominant force driving the galaxy-galaxy interactions, the slower the interaction is, the more disruptive it tends to be. This is due to gravity having more time to affect the systems, which is to be expected. As the separation between interacting galaxies decreases, tidal forces acting on the pair become more significant, resulting in tidal tails and bridges. Although the total energy of the

system is conserved during the encounter, energy can be transferred from galaxy motion to stellar motion. The orbital energy of the interacting galaxies gradually converts to internal motions within said galaxies as the interaction progresses. This phenomenon is referred to as dynamical friction (Chandrasekhar, 1943; Binney and Tremaine, 1987), and depending on the properties of the galaxies (including relative velocities, orientation, and masses) this process may eventually lead to the galaxies merging and leaving behind a single merger remnant, whose morphology depends on the initial masses of the merging galaxies. Two galaxies of relatively comparable masses merging (known as a *Major Merger*) results usually in an elliptical galaxy (Barnes, 1988). Galaxies with a high mass ratio merging (a *Minor Merger*) usually results in the larger galaxy being left intact while the smaller one gets cannibalized. In some cases the galaxies do not merge, but the encounter would still have a noticeable effect on the galaxies involved, and in this case, these events are known as interactions rather than mergers.

1.3.2 Properties of Galaxy Pairs

In the past couple of decades, there has been a significant amount of work concerning the properties of galaxy pairs. Such properties include star formation rates (SFR), colours, asymmetries, etc. In this section I summarize the results of some of those works that are concerned with properties that are relevant to this thesis.

It is now well understood that some galaxies experience an enhanced star formation rate (SFR) when interacting. This enhancement is found to be strongly present for galaxy pairs that are separated by a projected physical distance (hereafter r_p) of $< 30 - 40\ h_{70}^{-1}$ kpc (Ellison et al., 2008). Moreover, this enhancement is found to be

strongest for galaxies with equal or comparable masses and is evident in more widely separated galaxy pairs. In other words, SFR enhancement is known to be present in galaxies undergoing major mergers, and is amplified the closer the pairs are.

Few studies have attempted to find the extent in projected separation to which this enhanced SFR is evident in interacting systems. Patton et al. (2013) studied a large sample of star forming galaxies with separations that extend up to 1000 h_{70}^{-1} kpc and compared it with results from merger simulations. They reported clear SFR enhancements that are present even for pairs separated by $\sim 150\ h_{70}^{-1}$ kpc. They concluded that this enhancement at wide separations is the result of starburst activity that is triggered at first pericenter passage which then persists as galaxies move to larger separations after the initial close interaction. Furthermore, the strongest SFR enhancement was found for galaxies with projected separations of $r_p \lesssim 20\ h_{70}^{-1}$ kpc, which is due to highly disturbed systems that are undergoing final coalescence. After coalescence, Ellison et al. (2013) showed that post-merger remnant galaxies still maintain an average central SFR enhancement of a factor of ~ 3.5 over their control sample. They also reported that $\lesssim 20\%$ of post-mergers have a SFR enhancement at least a factor of 10 larger than their control.

Galaxy interactions and mergers are thought to contribute to the colour bimodality of galaxy populations. This is due to research showing that the colours of galaxies are affected by interactions and mergers. Patton et al. (2011) reported that there is a higher fraction of extremely blue galaxies in galaxy pairs than in isolated galaxies, coupled with an offset that shows that close galaxy pairs ($r_p < 30\ h_{70}^{-1}$ kpc) are bluer in colour than wide galaxy pairs ($r_p > 60\ h_{70}^{-1}$ kpc). This is consistent with having close, pericentre passages triggering induced star formation causing the galaxies to

become bluer in colour. As the galaxies separate they begin to gradually redden due to an aging starburst. Therefore, galaxy interactions and mergers contribute to the galaxy bimodality by providing a mechanism where galaxies are turned from star-forming blue, to "red-and-dead".

As stated in previous sections, interactions can significantly affect the morphology of the interacting galaxies. These changes in morphology can be seen in tidal tails, stellar bridges, and even the complete transformation into irregular galaxies. These irregularities in the shapes of galaxies can be quantified and compared. Studies have shown that galaxy pairs tend to be far more likely to be asymmetric than isolated controls. A study of galaxies at intermediate redshift puts $40\% \pm 11\%$ of merging systems as asymmetric, compared to $9\% \pm 3\%$ of isolated galaxies (Patton et al., 2005). This study has also demonstrated that strongly asymmetric galaxy pairs tend to be significantly bluer (rest frame $(B-R)$ colours close to 0.8) than all other galaxy pairs ($(B-R)_0$ of 1.24).

In sum, studies have found that close galaxy pairs tend to have enhanced SFRs, bluer colours, and higher asymmetries than isolated galaxies. These enhancements and offsets are amplified the closer the galaxies are to each other during the interaction, but can have a lasting effect after coalescence.

1.4 Mergers and Interactions in Different Environments

With the effects of the environment on residing galaxies known, as well as the effects of interactions and mergers on paired galaxies, a question arises of whether the interaction processes vary with environmental membership or whether the processes are identical but the outcomes are different. A number of previous works have attempted

to evaluate the role of environment on the properties of interacting galaxy pairs. The purpose of this section is to summarize a few key papers that are focused on this particular topic, and in comparison, present the uniqueness of this thesis.

Alonso et al. (2006) and Perez et al. (2009) studied the effects of galaxy interactions in different environments. They did so by analyzing SFR data (Alonso et al., 2006) and colours (Perez et al., 2009) of galaxy pairs in different environments using the 2-degree Field Galaxy Redshift Survey (2dFGRS) (Alonso et al., 2006) and the Sloan Digital Sky Survey (SDSS) (Alonso et al., 2006; Perez et al., 2009). They observed an increase in the effectiveness of triggering star formation in low and moderate density environments with respect to their control sample of galaxies without a companion. They also report the gap in the red fraction between close pairs and their controls is significantly higher in massive halos than in lower mass ones. To achieve these results, the authors defined their sample of galaxy pairs as galaxies with projected separation $r_p < 100\ h_{70}^{-1}$ kpc and relative velocity $\Delta v < 350$ km s^{-1}. They chose these limits based on the value of r_p and Δv where the enhancement of star formation rates diminishes. This method might introduce a bias due to the fact that different environments have different r_p and Δv distributions. The different distributions imply that the definition of what constitutes a bound pair based on SFR enhancement can vary for different environments. As I describe in §2.1.2, I adopt a different definition for what constitutes a galaxy pair based on an estimate for the minimum binding energy of the pair system, whereby many systems that cannot be gravitationally bound are eliminated from the sample. The proposed method of pair selection in this thesis also allows for the study of paired galaxies separated by distances far larger than 100 h_{70}^{-1} kpc, as well as the removal of some projected pairs from the sample.

Moreover, Alonso et al. (2006) and Perez et al. (2009) define their environment using an estimator calculated through the projected distance to the 5th nearest neighbour (Σ_5). Ellison et al. (2010) used the projected galaxy density from distances to the 4th and 5th neighbours within 1000 km s^{-1}, and adopted similar limits to the different environments as Perez et al. (2009). In a study that applied twenty published environment definitions to a common mock galaxy catalogue that was constrained to resemble the local universe, Muldrew et al. (2012) concluded that there is no universal environment measure and the most suitable method depends on the scale being probed. Nearest-neighbour methods for defining the environments are best suited for defining higher density environments such as rich groups and clusters, but they are not appropriate for defining lower density environments due to the dominating effect of inter-halo separations which smooth out any local density variations. On the other hand, using the total number of galaxies within a dark matter halo may seem like an acceptable method to define the different scales of environment densities. However, due to the limited resolution of telescopes, and the wide range of possible sizes and brightness of galaxies, surveys tend to miss small and faint dwarf and satellite galaxies. Moreover, faint galaxies in closer systems appear brighter than in more distant systems. This is known as the Malmquist Bias (Malmquist, 1920), where for a fixed apparent magnitude limit for a survey, at lower redshifts more faint galaxies are observed that at higher redshifts, producing a bias. In §2.2 I demonstrate that basing the environmental definition on the number of galaxies in the vicinity of the galaxy pairs may not be the best option, while the use of the dark matter halo mass in which the galaxy pairs reside provides a far better indication of the environmental density. In this thesis, I use the dark matter halo masses to define the different environments,

but also match the control galaxies on the halo mass, isolation (distance to closest 2nd neighbour), and the number of galaxies within 2 Mpc of the paired galaxy.

Alonso et al. (2006) find their control sample by matching the redshift and luminosity of galaxies without a companion to the galaxy pairs. The lack of matching on environment implies that their results do not differentiate between the effect of the environment on the individual galaxies and the effect of the environment on the interaction itself. In order to test the effects of the environment on the interactions within, the pairs and the controls must be members of a similar environment for this comparison to be meaningful. As I will describe in more detail in §2.3, for the control sample used in this thesis I matched the redshift, mass, isolation, halo mass, and density of the environment of the controls to their respective pairs in order to remove as much bias as possible from the control sample, and arrive at more meaningful results.

1.5 Organization of Thesis

In order to investigate the origin of the variation in the properties of interacting galaxy pairs in different environments in this thesis I proceed by introducing the sample used and the method of finding pairs, correcting for sources of incompleteness and biases, defining the environments, and finding the appropriate control sample in the next chapter. I then discuss the star formation rate (SFR) and specific star formation rate (sSFR; SFR per unit stellar mass) properties of paired galaxies relative to their controls in different environments in Chapter 3. Chapter 4 describes the asymmetry parameter used in this thesis, and shows and discusses the asymmetry enhancement of paired galaxies in different environments. Chapter 5 summarizes the results from the previous two chapters, and concludes and outlines future work.

Chapter 2

Sample Description

2.1 Pairs of Galaxies in the SDSS DR7

In order to study the different properties of interactions and mergers of galaxies in different environments, a statistically large sample containing both spectroscopic and photometric data is needed. The Sloan Digital Sky Survey Data Release 7 (SDSS DR7, Abazajian et al. 2009) is well-suited for this task as it provides public imaging and spectroscopic data for approximately one million galaxies that cover 11,663 $\deg^2$ on the sky (approximately 30% of the full sky). The large number of galaxies in this survey, combined with the large coverage area they occupy in the nearby universe and the wide range of environments they reside in, makes the SDSS DR7 a suitable survey for the purposes of a statistical study with meaningful results. In this section I briefly summarize the SDSS observations in §2.1.1, and describe the method with which the galaxy pairs were selected in §2.1.2. The environment classification of the galaxy pairs is then discussed and determined in §2.2, followed by a description of the method used to find the control sample for the galaxies in pairs in §2.3.

2.1.1 Input Catalog

Observations for the SDSS were carried out using a dedicated wide-field 2.5 m telescope located at Apache Point Observatory in southern New Mexico. The seventh data release (DR7) of the SDSS covers an imaging area of 11,663 deg^2 and a spectroscopic footprint area of 9380 deg^2. It gives *ugriz* band photometry and 3800 - 9200 Å in spectroscopic coverage. It contains the spectra of over 1.6 million unique objects, which include $\sim$ 930,000 galaxies and $\sim$ 120,000 quasars (Abazajian et al., 2009). The SDSS DR7 provides the largest collection of galaxies at spectroscopically confirmed low redshifts to date, which fits the requirements for this thesis perfectly as it allows for meaningful statistical analysis for the different properties in various environments. For the sake of enhancing the results obtained from this study, I only include galaxies that have secure spectroscopic redshift (zConf > 0.7) that lie in the range $0.01 \leq z \leq 0.2$, as well as being classified photometrically and spectroscopically as a galaxy, with extinction-corrected Petrosian apparent magnitudes of $14.0 \leq m_r \leq 17.77$.

In this thesis, the masses of the stellar component of galaxies (stellar mass, hereafter) used are obtained from the Mendel et al. (2014) catalogue, which is based on the photometry of Simard et al. (2011) which improved on the commonly used stellar masses of Kauffmann et al. (2003). They showed that the photometry of the SDSS DR7 produced in the pipeline can be improved by creating more robust structural parameters and integrated galaxy magnitudes and colors. Using a set of quality assurance metrics, Simard et al. (2011) demonstrate a significant improvement over the standard SDSS pipeline, especially for galaxies in crowded environments, and in particular for close pairs (Patton et al., 2011). Simard et al. (2011) used the

SEXTRACTOR code (Bertin and Arnouts, 1996) on the output images of the SDSS pipeline in order to identify various objects and generate segmentation images that assigned pixels for each detected object as well as identified and masked neighbouring objects. Object-by-object, the local sky levels were redetermined, and using the GIM2D software package (Simard et al., 2002) the galaxies' two-dimensional surface-brightness distributions were mapped with different axisymmetric models of galaxies. This provided structural decompositions of the objects into bulges and disks and produced other structural parameters including position angles, Sérsic indices (i.e., the degree of curvature in the mathematical function that describes how the intensity of a galaxy varies with the distance to the galactic center, Sérsic 1963), etc. The motivation behind this decomposition is the fact that the two components (bulge and disk) are basic features found in the majority of galaxies and appear to be the dominant structural features. With the decompositions, Simard et al. (2011) simultaneously performed parametric fits in the g and r bands by forcing the bulge and disk structural properties in each galaxy to be the same in both bandpasses. The resulting catalogue of Simard et al. (2011) contains the measured $g-r$ colours, as well as an estimate of the bulge and disk size, position angle, inclination and ellipticity of each galaxy, and local sky background and segmentation masks on a galaxy-by-galaxy basis.

Mendel et al. (2014) took the reprocessed SDSS g-band and r-band photometry provided by Simard et al. (2011) and extended it to include the u, i, and z bands. Using the galaxy-by-galaxy based structural information of the SDSS galaxies from Simard et al. (2011), Mendel et al. (2014) used those best-fit single-component Sérsic and bulge+disk photometric models to compute total stellar masses and stellar masses

for bulges and disks separately. By creating a grid of synthetic models that span a wide range of possible ages, star-formation histories, metallicities, and dust extinctions, and comparing the galaxies' enhanced photometry to it, Mendel et al. (2014) derived the masses of those galaxies. Ellison et al. (2013) compared the masses of SDSS galaxy pairs obtained from Mendel et al. (2014) to the commonly used masses of Kauffmann et al. (2003) as a function of projected separation between the pairs. They showed that there is a slight offset to higher masses in the Mendel et al. (2014) catalog, accompanied by a scatter between the two values that becomes larger at the smallest separations. Moreover, they report an overall increase in the trend towards lower masses in the Kauffmann et al. (2003) values at $r_p < 20$ kpc. This result is primarily due to Mendel et al. (2014) using the improved photometry of Simard et al. (2011) in crowded environments for the mass determination. Therefore, for the purpose of increasing the accuracy of the properties of galaxy pairs in this thesis, I use the photometric Sérsic total mass measurements of Mendel et al. (2014), and require that each galaxy's observed fibre $g-r$ colour be within 0.1 mag of its model-predicted Simard et al. (2011) fibre colours in order to increase the reliability of the stellar mass estimates.

2.1.2 Pair Selection

The method used in this thesis in order to collect a sample of galaxy pairs is similar to the one used in Patton et al. (2013), which will be discussed in further detail in Patton et al. (*in prep*). To begin, first we define what a neighbour galaxy is. Simply put, it is a galaxy with a rest-frame relative velocity $\Delta v < 1000$ km s^{-1} in comparison to the galaxy in question, with a stellar mass within a factor of ten ($0.1 <$ mass ratio

< 10) of said galaxy. These criteria are meant to avoid neighbouring galaxies that are either too small to have a significant effect, or are physically well separated but appear as a companion due to projection.

Using the above definition of a neighbour, various properties of galaxies in the input sample are then calculated. Those properties include the projected separation to the closest neighbour (r_p), the projected separation to the second closest neighbour (hereafter r_2), and the total number of neighbours within 2 h_{70}^{-1} Mpc (hereafter N_2). For N_2, 2 h_{70}^{-1} Mpc was selected as the threshold for neighbours due to it being large enough to distinguish between different environments like clusters, groups, and the field, while being small enough to be sensitive to small groups and cluster substructure. It is worth noting that with this limit for N_2, $\sim 67\%$ of galaxies in the catalogue have at least 2 neighbouring galaxies. This allows us later on to match on both isolation and number density when finding the control sample as described in §2.3.

Due to our fixed perspective of the cosmos combined with our current technological limitations, every sample of galaxy pairs is bound to suffer from incompleteness and projection errors. In the remainder of this subsection, I will address those issues and outline the steps taken to eliminate or at minimum reduce their effect on the sample.

Fibre Weights

The SDSS produces images using a dedicated telescope at Apache Point Observatory in New Mexico with a large-format mosaic CCD camera (Gunn et al., 1998). Objects in the imaging survey are then targeted for a spectroscopic follow-up survey using two multiobject fibre spectrographs on the same telescope (Smee et al., 2013). The

target objects are matched to the fibres within each field of view of the fibre plug plates. Due to the finite size of the fibre plugs, there is a minimum separation of 55 arcsec between the centres of adjacent fibres. In order to acquire spectra for both members of a galaxy pair simultaneously, the minimum fibre separation of 55 arcsec sets the limit on the angular separation of the pair (Strauss et al., 2002). This angular separation restriction causes the sample of galaxies in close angular pairs to have lower spectroscopic completeness. This fibre incompleteness is one of the major sources of incompleteness with significant implications when it comes to studying galaxy pairs in the SDSS.

Patton and Atfield (2008) looked at the ratio of spectroscopic to photometric pairs in their SDSS sample plotted as a function of angular separation (θ). They report a substantial deficit of spectroscopic pairs only at small angular separations ($\theta < 55''$). Moreover, in Patton et al. (*in prep*) the authors show the projected separation (r_p) as a function of redshift for all the galaxy pairs in the sample with $r_p < 300\ h_{70}^{-1}$ kpc, and report a sharp drop in the number of detected galaxies with angular separations < 55 arcsec. The majority of the regions of the sky are covered by a single plate, and in those regions only pairs with angular separations > 55 arcsec are detected. However, there are regions covered by two or more overlapping adjacent plates as well as areas covered with multiple plates, which explains the detection of some pairs with angular separations < 55 arcsec. Given a maximum redshift for the sample of $z = 0.2$ the corresponding furthest objects are at an angular size distance of ~ 680 Mpc. Using simple trigonometry, it is clear that galaxy pairs with projected separations $r_p \gtrsim 180\ h_{70}^{-1}$ kpc all have angular separations > 55 arcsec; therefore no spectroscopic incompleteness from fibre collisions exists for those pairs. For smaller

r_p the sample becomes biased towards lower redshifts because of fibre incompleteness, where it is strongest at $r_p \sim 80\ h_{70}^{-1}$ kpc; however, the bias disappears for the smallest separations ($r_p \lesssim 6\ h_{70}^{-1}$ kpc) since all very close pairs have angular separations < 55 arcsec.

Fibre incompleteness has been a well-known issue in the literature, treated usually by culling the galaxy pair sample at larger angular separations in order to reduce the bias (e.g., Ellison et al. 2008, 2010; Scott and Kaviraj 2014). However, Patton and Atfield (2008) showed that due to the use of two or more plates in some regions, the spectroscopic sample contains enough close angular pairs to enable them to model the incompleteness and correct for it using a statistical weight rather than removing detected wide pairs with useful information from the sample. The authors begin by measuring the ratio of spectroscopic to photometric pairs (N_{zz}/N_{pp}) as a function of angular separation (θ). Patton and Atfield (2008) found a sharp drop in N_{zz}/N_{pp} below 55 arcsec, and correct it by modelling the incompleteness through the fitting of a function $g(\theta)$ to the data, followed by the multiplication of each spectroscopic pair by a weight $\omega_\theta = f_s^2/g(\theta)$ (where f_s is the overall spectroscopic completeness of the survey). Therefore, by simply applying the weight $\omega_\theta = 3.08$ to all pairs with angular separation < 55 arcsec, the angular dependence of the small scale spectroscopic incompleteness was removed, and this very significant bias was eliminated from the measurements.

Figure 2.1 shows the effect of applying the corrective fibre incompleteness weight on our sample's galaxy pairs. It is clearly evident that the bias produced by fibre collisions for galaxy pairs with $10 \lesssim r_p \lesssim 150\ h_{70}^{-1}$ kpc is largely removed by applying the corrective weight $\omega_\theta = 3.08$ to all pairs with angular separation < 55 arcsec. In

both panels of Figure 2.1, it is clear that there is a bias in the unweighted sample, especially at $r_p \sim 80\ h_{70}^{-1}$ kpc where this bias appears the strongest. The unweighted sample shows clearly that at separations between $5 \gtrsim r_p \gtrsim 180\ h_{70}^{-1}$ kpc, there is a bias towards lower redshifts and lower masses, while the weighted sample shows fairly smooth and flat trends in redshift and stellar mass.

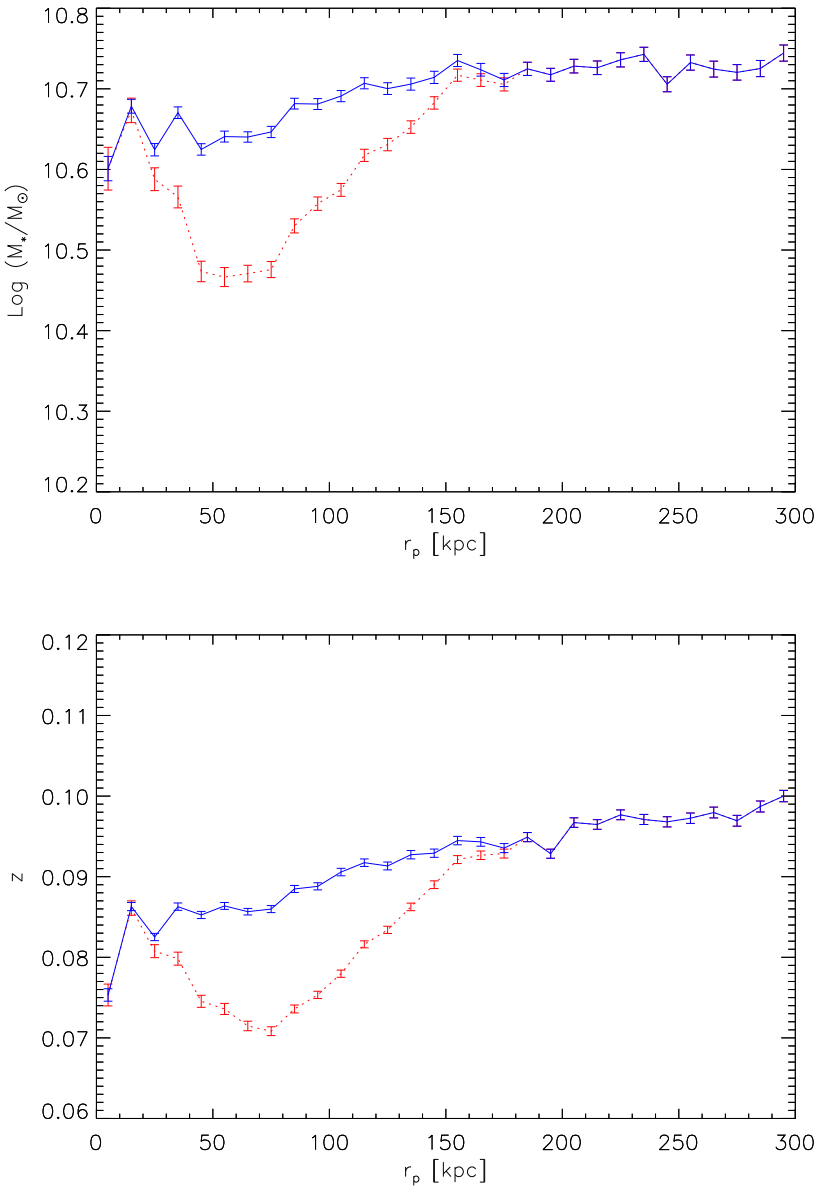

Figure 2.1: (a) The upper panel shows a plot of the mean stellar mass of the SDSS galaxy pairs as a function of r_p. (b) The lower panel shows a plot of the mean redshift of the SDSS galaxy pairs as a function of r_p. In both plots, red dots connected by the dashed red line show the data before the corrective fibre weights, and blue dots connected by the solid blue line show the data after the weight correction. The error bars show the error in the mean.

Resolution

We have an inability to detect pairs at very small separations. There are many factors that contribute to this inability:

1. Angular Resolution

   If the angular separation of a pair of galaxies is comparable to the angular resolution of the images then the pair appears as a single galaxy on the image that is used for galaxy identification. The ground-based imaging of the SDSS has a typical seeing of $\sim$ 1.5 arcsec (York et al., 2000), which indicates that there certainly are missing pairs below those separations.

2. Angular Diameter

   If the angular separation of the pair is comparable to the angular diameter of one or both members of the galaxy pair, then overlapping isophotes might hinder the identification of two galaxies. This particular incompleteness is more significant for galaxies with larger physical diameters, as well as paired galaxies at higher redshifts due to the decrease in angular separation relative to closer pairs with similar projected physical separations.

3. Late Stage Mergers

   If a galaxy pair is in the late stage of a merger then the two galaxies' morphology might be significantly disrupted to the extent that recognizing them as two separate galaxies becomes difficult. Even in the case where the disruption is not as severe, when the galaxies are close enough to one another, the difficulty of discerning the two galactic nuclei increases since both will be covered by a

single common light envelope. Therefore, it is quite challenging to differentiate a single merger remnant from distorted and/or extremely close pair at this stage.

Patton et al. (*in prep*) show that there is an absence of paired galaxies with angular separations < 2 arcsec in our sample, with some close spurious pairs removed by eye, which is broadly consistent with expectations from the SDSS seeing (York et al., 2000). They also note that at angular separations between 2-3 arcsec, there are noticeably fewer detected paired galaxies than what is expected based on the density of detected pairs at larger separations, while at an angular separation ≥ 3 arcsec there are no obvious resolution issues. From the redshift limits on the survey, all galaxy pairs with $r_p > 10\ h_{70}^{-1}$ kpc correspond to angular separations > 3 arcsec, which indicates that it is safe to assume that the sample is complete for any combination of redshift and stellar mass at $r_p > 10\ h_{70}^{-1}$ kpc. However, as r_p goes below $10\ h_{70}^{-1}$ kpc, an increasing fraction of paired galaxies are missed, and this fraction increases for higher redshift and higher stellar mass galaxy pairs. This selective incompleteness causes the mean redshift and mean stellar mass of the population to decrease as projected separation approaches zero, with only very few pairs being detected at $r_p < 3\ h_{70}^{-1}$ kpc which all consist of low mass galaxies at redshifts below 0.05. This is seen in Figure 2.1 where a clear and significant drop in both mean redshift and stellar mass is seen for paired galaxies with projected separations $0 < r_p < 10\ h_{70}^{-1}$ kpc in comparison with paired galaxies with $10 < r_p < 20\ h_{70}^{-1}$ kpc.

The analysis in this thesis requires splitting galaxies into their respective environment category, and then into paired galaxies and their respective controls. Therefore, the subsamples contain significantly smaller sample sizes than the full sample, which

require the binning in r_p to include a wider range in order for the results to be meaningful. The larger bins would then reduce the visible effect of the incompleteness from resolution. Therefore, no corrections are required for this specific incompleteness, but it should be kept in mind when analyzing the properties of paired galaxies at close separations to avoid overanalyzing the results.

Proximity to Survey Boundary

The SDSS DR7 covers an area of $\sim 8000\ deg^2$ which is fairly large in comparison to other surveys (Abazajian et al., 2009). Nonetheless, galaxies will be detected close to the boundaries of the survey that can have many neighbours or even companions that are outside those boundaries. Therefore, due to the boundary effects, a small incompleteness arises that needs to be accounted for. This incompleteness affects studies that require the identification of close galactic companions; however the effect is more significant for studies that require the estimation of local densities at large scales (2 Mpc in this case).

This incompleteness is addressed by first identifying the survey boundaries using a list of right ascensions and declinations for all galaxies in the spectroscopic sample. Then using an automated algorithm, the galaxies that are likely to lie close to the survey boundaries are identified, where $\sim 1\%$ of galaxies in the survey are identified as being close to the boundaries. Following this, for every galaxy in the sample, the projected distance to the nearest boundary galaxy (hereafter r_{bound}) is computed, and it was found that 95.3% of galaxies in the sample lie more than $2\ h_{70}^{-1}$ Mpc from the survey boundaries. Therefore, by simply eliminating any galaxy with $r_{bound} < 2\ h_{70}^{-1}$ Mpc, the incompleteness is effectively removed (Patton et al. *in prep*).

Binding Energy Cut

As with any redshift survey, there is a problem of contamination of the samples of galaxy pairs by projected foreground or background galaxies that are not pairs, but appear as such. This problem arises from the fact that only the projected positions and line-of-sight velocities of galaxies are measured. The measured line-of-sight velocities of galaxies can be split into two components: the velocity due to the Hubble expansion of the universe (hereafter v_z), and peculiar velocities (hereafter v_{pec}). In the absence of independent distance measurements, no information is available on the contribution of each of those velocities to the measured line-of-sight velocity, which is used in determining the distance of those galaxies from our own, and hence from each other. A rest-frame relative velocity (Δv) of zero between two galaxies indicates that they are at the same redshift with r_p being the true physical separation only in the case where the peculiar velocities have no contribution to the measured line-of-sight velocities. However, in the possible case where one galaxy has $v_{pec} = 0$ km s^{-1} while the other has $v_{pec} = 1000$ km s^{-1}, with the system having $\Delta v = 0$ km s^{-1}, the true separation between these galaxies could be as high as 14 Mpc in our sample. This produces a source of contamination that cannot be corrected for with our current data. Moreover, there is a lack of knowledge about the motion perpendicular to the line-of-sight caused by the limitation of current technology to measure the rate of angular motion of galaxies. Due to this lack of knowledge, the process of finding galaxy pairs that are physically bound to one another becomes less straightforward. There have been many examples in the literature of attempts to reduce this contamination, mainly by imposing an upper limit on Δv (e.g., Patton et al. 2000; Alonso et al. 2004; Ellison et al. 2008). The majority of works impose an upper limit on Δv of no more

than 500 km s^{-1}. These limits are usually decided upon using a trade-off between removing the contamination from deceptively projected pairs and keeping the sample size large enough for the statistics to be significant. Even though this technique is widely used in the literature, a more quantitative and physically meaningful solution to removing those contaminants will most likely produce a cleaner sample with better results.

As galaxies approach one another for an interaction, the force of gravity dictates the majority of events prior to the first encounter. Galaxies that are gravitationally bound to one another interact and may eventually merge. Galaxies that are not bound could still merge due to dynamical friction in the interaction causing the galaxies to slow down and eventually coalesce. The calculation of the dynamical friction between a possible galaxy pair is beyond the scope of this thesis. Therefore, for the purpose of this thesis, it is assumed that in order for a galaxy interaction and eventually a merger to take place, the galaxies involved must be gravitationally bound to one another. This process excludes some of the paired galaxies that could potentially be interacting and merging systems; however the trade-off is that the sample left to use as a pairs sample has many projected pairs with no chance of interaction removed.

Due to the lack of information on the motion of the galaxies perpendicular to the line-of-sight and any depth components to the physical separation of the galaxies, it is not possible to calculate the true energies of the systems. However, knowing the motions along a single direction together with the projected separation of the pairs enables us to calculate a minimum energy of the system, where any possible unidentified components of motion perpendicular to it or any unknown depth components to the physical separation would only increase that energy. If the minimum binding

energy of the system is calculated using classical mechanics, where one only considers the minimum relative kinetic (KE_{min}) and minimum potential (U_{min}) energies of the system, then a minimum binding energy $E_{min} > 0$ calculated using only the one known vector of motion and projected separations can only increase if there is motion perpendicular to the known vector or if there are any peculiar velocities contributing to the line-of-sight velocities. Since redshift is incapable of differentiating peculiar velocities of galaxies along the line-of-sight, and velocities caused by the expansion of the universe, the calculated projected distance between two galaxies assuming the redshift is solely an indicator of cosmic distance is the minimum possible separation between the two galaxies. As with the distance component, any velocities perpendicular to the line-of-sight would only increase the velocity difference between the galaxies, thus increasing the energy of the system. Therefore, one can remove any projected pair with $E_{min} > 0$ with some confidence that it is not a gravitationally bound pair. Some caveats to this method remain where there are pairs left with $E_{min} < 0$ which are not interacting pairs due to undetected motions or unknown depth separations, as well as removed pairs with $E_{min} > 0$ that could become bound from dynamical friction or interact through fly-bys.

In this thesis, I defined the minimum binding energy to be

$$E_{min} = U_{min} + KE_{min} \tag{2.1}$$

such that

$$U_{min} = \frac{-GM_{D1}M_{D2}}{r} \tag{2.2}$$

and

$$KE_{min} = \frac{1}{2}\mu v^2 \tag{2.3}$$

where G is the gravitational constant, M_{D1} and M_{D2} are the dynamical masses of the first and second galaxies in the pair, μ is the reduced mass of the galaxies given by $\mu = (M_{D1}M_{D_2})/(M_{D1} + M_{D_2})$, r is the distance between the two galaxies, and v is the absolute difference in the velocities of the galaxies relative to their center of mass. In equation 2.2, r is taken to be r_p, which is calculated using $r_p = D_A * \theta$, where D_A is the angular diameter distance calculated using the mean redshift of the galaxies, and θ is the angular separation calculated using the right ascension (RA) and declination (Dec) of the galaxies. Since r_p is the projected separation, any peculiar velocities that are not taken into account would only serve to increase the true value of r. Therefore, $r = r_p$ is the lowest possible separation between two galaxies, and the addition of depth only increases the value of r. Since the potential energy (U) is a negative value that is proportional to $1/r$, then the calculated binding energy (E_{min}) is minimum for $r = r_p$ and only increases with the addition of a depth component to the separation between the galaxies. In equation 2.3, v is the difference in the velocities of the galaxies relative to their center of mass. Therefore, for v, the value of the known variable Δv obtained from the redshifts of the galaxies is used. Since Δv is calculated from the line-of-sight velocities of the galaxies, the true relative velocity of the pair can be split into two components, the line-of-sight (Δv), and the transverse velocities. Using $v = \Delta v$ and having the kinetic energy (KE) proportional to v^2 and positive indicates that any unknown velocities would only increase the value of KE_{min} and hence increases E_{min}. Therefore, the calculated energy of the system using $r = r_p$ and $v = \Delta v$ is the minimum energy of the system and any additional

components of motion or depth can only increase the value of E_{min}.

The dynamical masses of the galaxies were calculated using the method described in Moster et al. (2010), where they adopt the parametrization similar to that of Yang et al. (2003), described as the following:

$$\frac{M_S(M_D)}{M_D} = 2\left(\frac{M_S}{M_D}\right)_0 \left[\left(\frac{M_D}{M_1}\right)^{-\beta} + \left(\frac{M_D}{M_1}\right)^{-\gamma}\right]^{-1} \tag{2.4}$$

M_S is the stellar mass of the galaxy, $(M_S/M_D)_0$ is the normalization of the stellar-to-halo mass ratio (SHM), M_1 is a characteristic mass for which the SHM ratio is equal to $(M_S/M_D)_0$, and β and γ are the slopes that indicate the behaviour of M_S/M_D at the low and high mass ends respectively. The values for the four free parameters in equation 2.4 were taken from the best fits with scatter performed by Moster et al. (2010), described in Table 2.1.

Figure 2.2 shows the distribution of Δv and r_p for galaxy pairs with $E_{min} < 0$ and $E_{min} > 0$. Out of an initial sample of 505,708 galaxies, 321,230 (64%) are considered paired galaxies under our definition. This is also shown in Figure 2.3 where I plot the fraction of bound galaxies and their dependence on r_p and Δv. It can be clearly seen that the fraction of accepted pairs decreases constantly as Δv increases, where $\sim$100% of pairs with $\Delta v = 0$ km s^{-1} have $E_{min} < 0$, while more than 80% of pairs

Table 2.1: Free Parameters Fitted for SMH Relationship

	log (M_1)	$(M_S/M_D)_0$	β	γ
Best Fit	11.899	0.02817	1.068	0.611
σ^+	0.026	0.00063	0.051	0.012
σ^-	0.024	0.00057	0.044	0.010

with $\Delta v > 900$ km s^{-1} have $E_{min} < 0$. Patton et al. (2013) showed that the effects from pair interactions on SFR diminishes at a separation of $\sim 150\ h_{70}^{-1}$ kpc; therefore, for the purpose of displaying the data in a meaningful manner, a limit on r_p is set at $r_p \leq 300\ h_{70}^{-1}$ kpc, which leaves 112,807 galaxies in the sample that have $E < 0$ and $r_p \leq 300\ h_{70}^{-1}$ kpc.

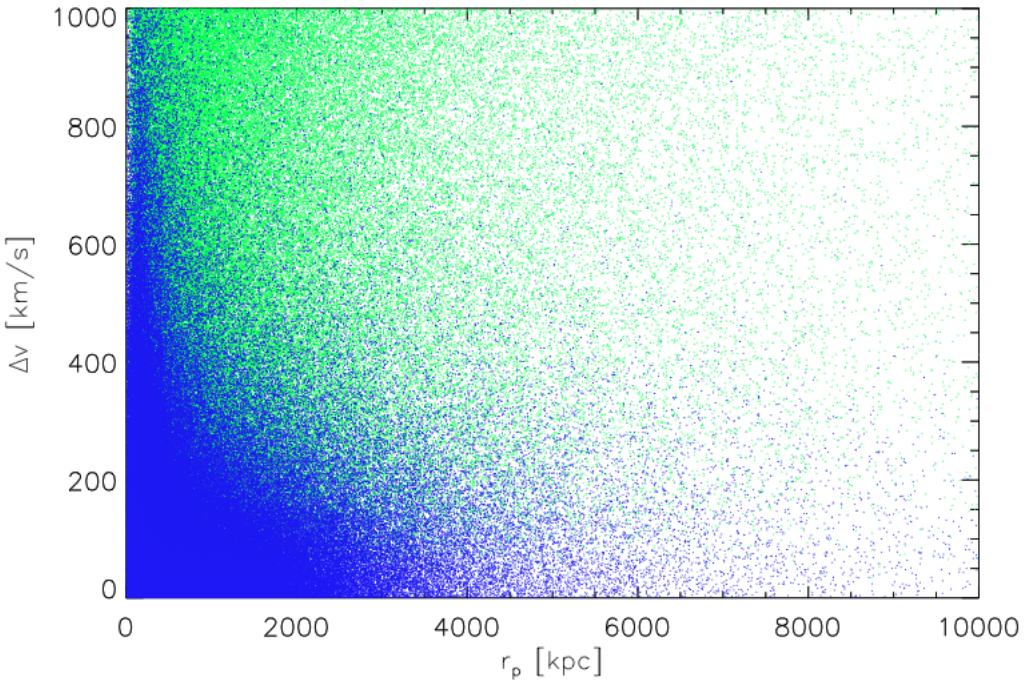

Figure 2.2: A scatter plot of Δv vs. r_p of the entire sample of pairs showing accepted pairs with $E_{min} < 0$ as blue points, and rejected pairs with $E_{min} > 0$ in green. 64% of the population was identified with $E_{min} < 0$, with 112,807 galaxies having both $E_{min} < 0$ and $r_p < 300\ h_{70}^{-1}$ kpc.

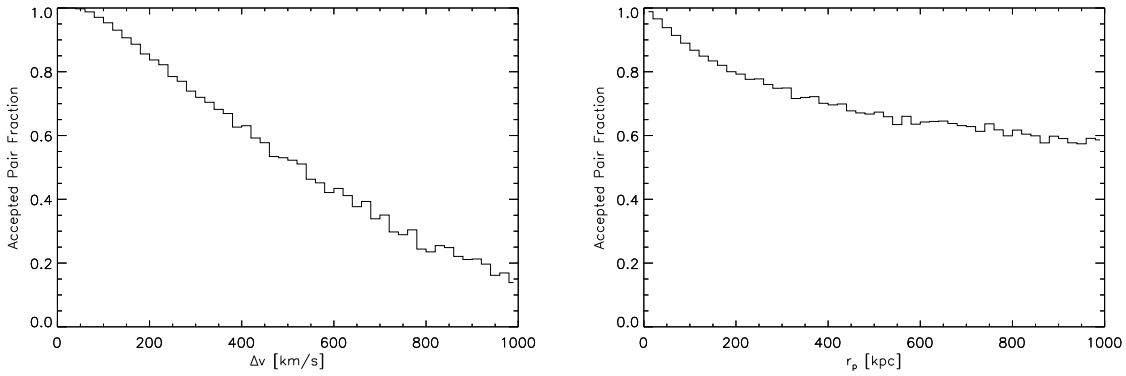

Figure 2.3: Plots of the fraction of galaxies designated under the given criteria as paired as functions of (a) Δv on the left, and (b) r_p on the right.

2.2 Environmental Classification

There are many different methods used in the literature to determine the environment in which galaxies reside. Many of those methods involve either counting the number of neighbouring galaxies within a specific distance surrounding a galaxy or measuring the distances to a specific close neighbour. The aim of this thesis is to find the effects of the membership to a specific environment (field, groups, or clusters) on interacting galaxy pairs; therefore, defining appropriate and accurate environment classes is crucial. In order to test and find the most appropriate method of classifying environmental membership, the catalogue of Yang et al. (2007) was used. In their paper, Yang et al. (2007) published a catalogue of galaxy groups for the SDSS DR4 galaxies using a modified halo-based group finder. What makes their catalogue unique is that their halo-based group finder was iterative, based on adaptive filters modeled after the properties of the dark matter halos of the groups, and capable of assigning single isolated galaxies to groups of one rather than removing them from the sample.

Using the catalogue of Yang et al. (2007) with updates to include DR7, we obtain the ID and properties of the group to which each galaxy in the sample belongs. This allows for the use of two methods to determine environmental membership of the SDSS galaxies: Number of Members and Halo Mass. For each group, the number of members identified in each group are counted, and from the number of members the environments are defined as seen in Table 2.2. It is agreed upon in the literature that the mean dark matter halo mass of a galaxy group is $\sim 10^{13} M_{\odot}$ (e.g., Parker et al. 2005), and since the largest halo mass in the sample is $\sim 10^{16} M_{\odot}$, and the smallest is $\sim 10^{11} M_{\odot}$, the environmental definition is set using the halo mass given by Yang et al. (2007) as seen in Table 2.3.

Table 2.2: Number of Members Environmental Definition

Environment	Definition
Field	3 or fewer members
Poor Group	4 - 10 members
Rich Group	11 - 20 members
Cluster	more than 20 members

Table 2.3: Halo Mass Environmental Definition

Environment	Definition
Field	$\log(\text{halo mass}/M_{\odot}) \leq 12.0$
Poor Group	$12.0 < \log(\text{halo mass}/M_{\odot}) \leq 13.0$
Rich Group	$13.0 < \log(\text{halo mass}/M_{\odot}) \leq 14.0$
Cluster	$14.0 < \log(\text{halo mass}/M_{\odot})$

Figure 2.4 shows the average number of members in halos and the average halo mass as functions of redshift. It is quite evident that there is a significant bias when looking at the number of members in halos at increasing redshifts; at $z < 0.03$ the average number of members is consistently in the cluster range, while at $z > 0.1$ it is consistent with 1 - 2 galaxies per halo. This significant dependence on redshift indicates that many galaxies are being missed by the survey at higher redshifts, making the number of galaxies in a halo a significantly flawed metric to use as an environment definition. Furthermore, Table 2.4 clearly shows that using the number of members of a halo as a proxy for the type of environment leaves the sample with $\sim 86\%$ of the galaxies being classified as isolated in the field, which is inconsistent with our knowledge that the majority of galaxies reside in groups. In comparison, in Figure 2.4, the average halo mass seems to show a relatively smaller dependence on redshift, and retains average values within the group environment at all redshifts. The distribution of galaxies by their environment in Table 2.4 shows results that are comparable to expectations where the majority of galaxies are classified to be in the group environments. However, there remains a significant increase of a factor of ~ 40 between the average halo mass at low z and at high z. Yang et al. (2007) use an extensive reiterative method for determining halos and their masses, where their group finder is based on an adaptive filter modeled after the general properties of dark matter halos. Therefore, the trend of increased mean halo mass with increased redshift is caused mainly by biases in the SDSS data, whereby denser environments can be observed to large redshifts due to their increased apparent magnitudes, while lower density environments tend to have lower magnitudes and therefore are more difficult to observe at higher redshifts.

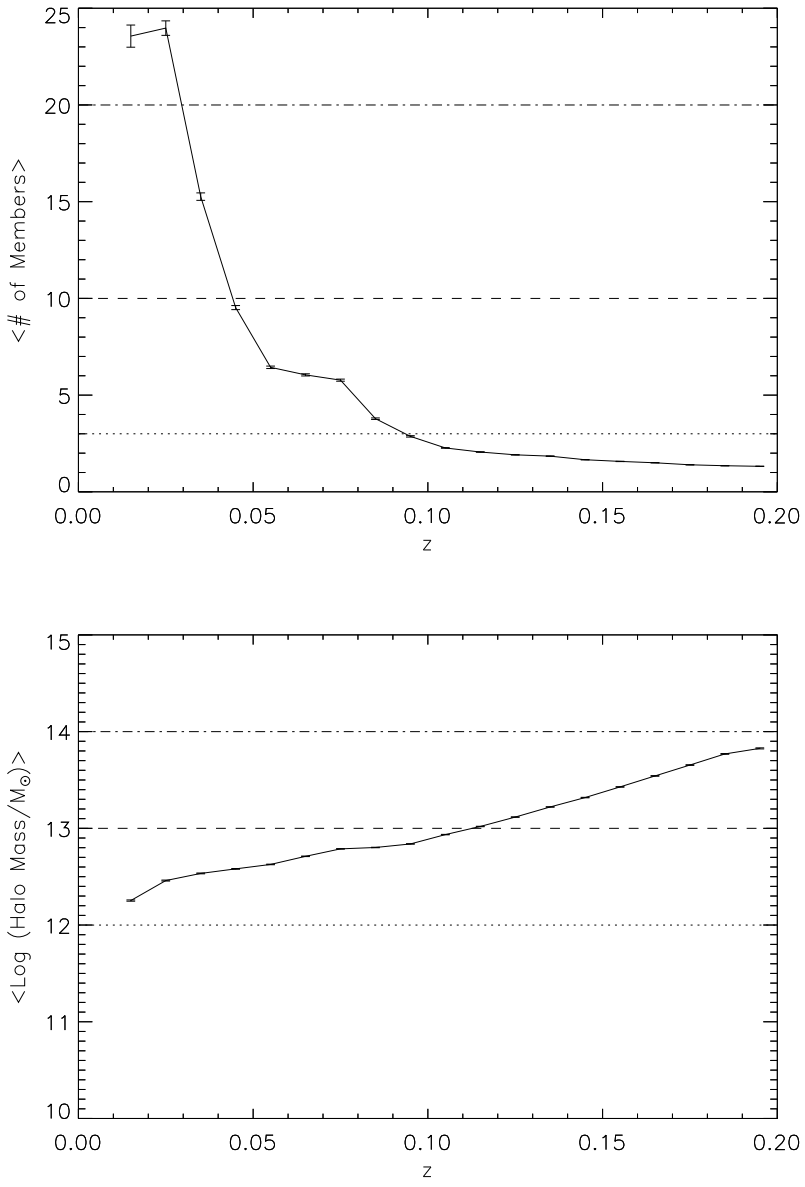

Figure 2.4: (a) Plot on top shows the average number of members in halos as a function of redshift. (b) Plot on the bottom shows the average halo mass of dark matter halos as a function of redshift. In both plots: values below the dotted line are identified as field galaxies, between the dotted and dashed lines are poor groups, between the dashed and dot-dashed lines are rich groups, and above the dot-dashed lines are clusters.

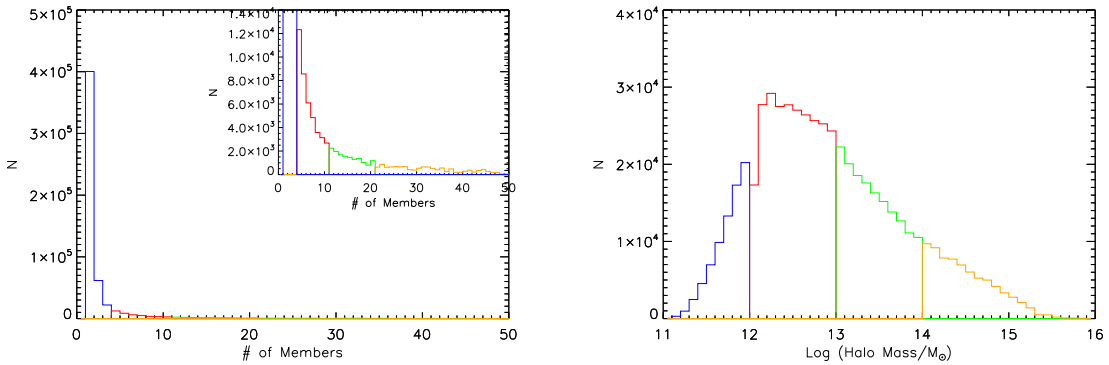

Figure 2.5: Histograms of (a) the number of members in each halo on the left, and (b) the halo mass on the right. Blue corresponds to the isolated field, red to poor groups, green to rich groups, and orange to clusters. The subplot inside (a) is a zoom-in of (a) for clarity.

Table 2.4: Distribution of Galaxies by Environment

Environment	Number of Members Method	Halo Mass Method
Field	85.7%	13.4%
Poor Group	7.3%	45.7%
Rich Group	2.6%	28.0%
Cluster	4.4%	12.9%

For the purpose of this thesis, halo mass is used as the defining metric for the environment due to all the evidence pointing to it being the more reliable metric on which to base the environmental definition. With the environment classes defined as seen in Table 2.3, the distributions of the properties of galaxies by environment in the sample are plotted in Figures 2.6, 2.7, and 2.8, which show the distributions of r_p and redshift, Δv and stellar mass, and N_2 and r_2, respectively. It is immediately apparent from these histograms that the populations of galaxies in each environmental class are significantly different. The distributions of r_p, r_2, and N_2 provide assurance for

the use of halo mass to define the environments. It is expected that higher density environments would contain more paired galaxies that have smaller r_p and r_2 values, and larger N_2 values than lower density environments; therefore, their presence in Figures. 2.6 and 2.8 provides support for the environmental selection technique used in this sample.

Together with the difference in the distributions of properties that reflect the environmental densities, it can also be seen that the distributions of redshifts, total stellar masses, and relative velocities significantly vary between environments. In terms of redshift, the distribution in Figure 2.6 shows that field paired galaxies peak at $z \sim 0.05$ with no field galaxies seen beyond $z \sim 0.11$, while rich group and cluster paired galaxies' redshift distributions peak at $z \sim 0.13$. These significantly varied distributions in redshift are mainly the product of field galaxies being more difficult to detect at higher redshifts due to their low apparent magnitude in comparison with galaxies in denser environments. This phenomenon is also reflected in the stellar mass distributions which show a peak at $\log(M_*/M_\odot) < 10$ for field paired galaxies, while cluster and rich group paired galaxies show a peak in their stellar mass distributions at $\log(M_*/M_\odot) < 11.5$. It is important to note that these varied distributions of properties between the paired galaxies in different environments significantly complicates the analysis of results later in the thesis. The comparison between paired galaxies and their controls in an environment can be made robust by the selection of a well-matched control sample (as will be described in more detail in the following section), resulting in any differences seen between the paired galaxies and their respective controls to be the result of interaction effects in the paired galaxies alone.

However, differences between the effects of interactions in one environment versus another cannot be attributed entirely to environmental effects alone, as they could also be caused by selection bias due to the varied distributions of properties in different environments.

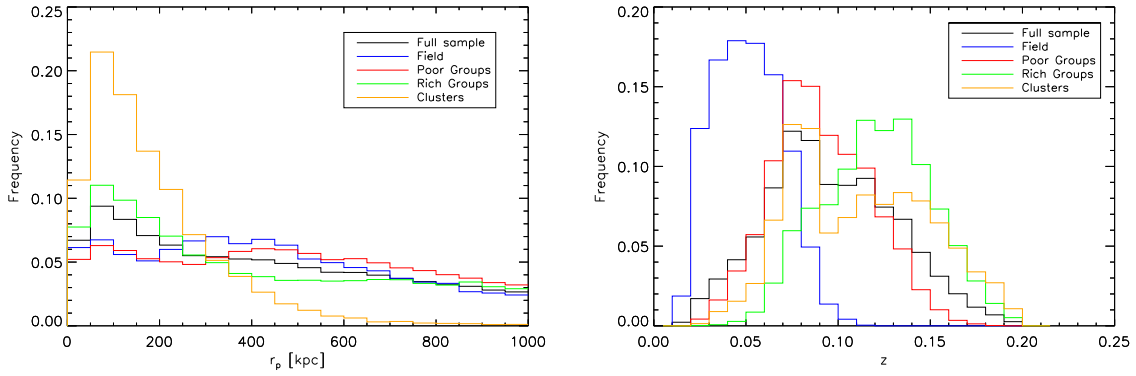

Figure 2.6: Histograms of (a) r_p on the left, and (b) redshift on the right. Blue corresponds to the isolated field, red to poor groups, green to rich groups, orange to clusters, and black shows the distribution of the entire sample together.

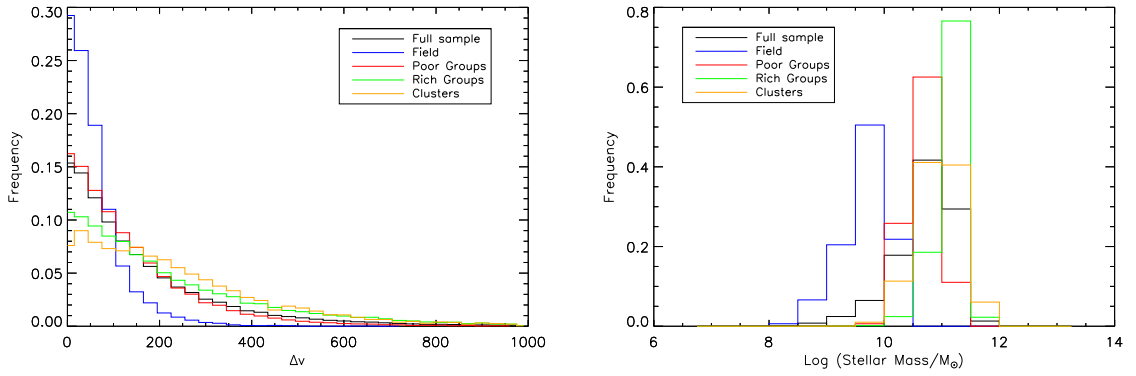

Figure 2.7: Histograms of (a) Δv on the left, and (b) M_* on the right. Colour scheme follows that of Figure 2.6.

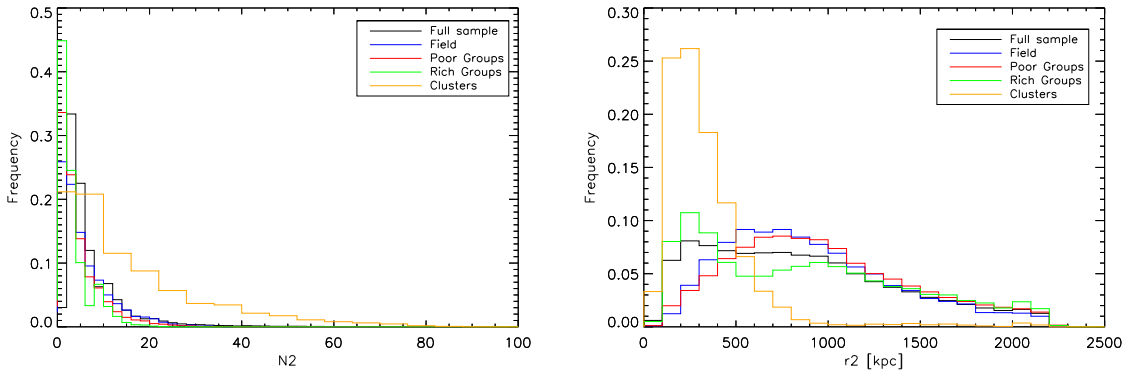

Figure 2.8: Histograms of (a) N_2 on the left, (b) r_2 on the right. Colour scheme follows that of Figure 2.6.

2.3 Control Sample

In order to test for the effect of the environment on interacting pairs, we must compare the interacting pairs at different separations to carefully chosen controls for each environment. Many studies concerning close galaxy pairs have used this approach, where their control sample had similar selection criteria to the pairs but just without a close companion (e.g., Ellison et al. 2008; Patton et al. 2011). This approach is quite robust, but only works for relatively close pairs. When looking at a sample with pair separation extending to $\sim 300\ h_{70}^{-1}$ kpc, the control sample galaxies become substantially more isolated than the paired galaxies that they are being compared with. This is due to the use of a control sample that is completely separate from the paired galaxies sample, where a galaxy can only be either a control for a paired galaxy, or a paired galaxy but not a control. In the case of the sample having paired galaxies separated by as much as $300\ h_{70}^{-1}$ kpc to within a Δv limit, then all the control galaxies have no companions closer than $300\ h_{70}^{-1}$ kpc. Therefore, a paired

galaxy separated by 20 h_{70}^{-1} kpc from its closest companion and 40 h_{70}^{-1} kpc from its second closest companion can only be compared with a galaxy separated by a minimum of 300 h_{70}^{-1} kpc from its closest companion and even further so from any other companions. Therefore, when one extends the pair selection criteria to larger r_p limits, this control finding method causes the control sample to become significantly more isolated than the paired galaxies sample, and the comparison between pairs and controls becomes meaningless when one needs to account for environmental effects.

An approach used by Barton et al. (2007) required both pairs and control galaxies to be isolated on larger scales, which works well for field galaxies, but since most galaxies reside in groups and clusters, as seen in Table 2.4, this method may remove the majority of our sample. Therefore instead, Patton et al. (2013) introduced a new methodology with which they matched the control sample in both local density and isolation, which they describe in more detail in Patton et al. (*in prep*).

A different approach to deal with this issue is to match paired and control galaxies on a local density estimator based on the distance to the fourth and fifth closest neighbours within 1000 km s^{-1}(e.g., Ellison et al. 2010; Scudder et al. 2012) together with matching on isolation on larger scales (e.g., Barton et al. 2007). Local density is typically measured within a few Mpc, which is far greater than the separation between paired galaxies. Therefore, if an environment contains small scale structure, such as compact groups embedded in loose groups (Mendel et al., 2011), matching solely on local density does not account for such structures. Requiring paired galaxies and controls to be isolated on larger scales would work well for field galaxies; however, this thesis requires the use of galaxy samples in all environments including the field, groups, and clusters. Therefore instead, combining both methods, where the control

sample and the paired galaxies are matched in both local density and isolation, fixes these problems and provides an adequately matched control sample (Patton et al., 2013).

In this thesis, the local density is quantified by N_2 (the number of galaxies observed within 2 Mpc of the galaxy) as well as the dark matter halo mass. As for isolation, r_2 provides the distance to the second closest neighbour. Since the only difference between the control galaxy and the paired galaxy it is being matched with is having a close companion at a separation of r_p, then the second closest companion of the paired galaxy ($r_{2,pair}$) should be at approximately the same distance as the closest companion to the control galaxy ($r_{p,control}$). Therefore, to match for isolation, the paired galaxy's r_2 is matched with the control galaxy's r_p. Figure 2.9 is a plot of the fibre weighted and unweighted mean N_2 and r_2 as functions of r_p for the galaxy pairs in our sample. Both plots imply a significant dependence of pair separation on the environment in which they are found. N_2 is seen to constantly decrease as pair separation increases. This is due to the environment in which galaxy pairs are found, where in denser environments such as groups or clusters, it is more likely to find close galaxy pairs than wider separated ones with no galaxies in between. On the other hand, the r_2 increases as pair separation increases, which demonstrates the dependence of the isolation of galaxies based on their environment. In this case paired galaxies with wide separations are more likely to be in low density, field-like environments, therefore, the average distance to their second closest neighbour is larger than for closer galaxy pairs that are more likely found in denser environments with closer second neighbours. These two biases are then corrected for by choosing a control sample that is matched in both N_2 and r_2 such that the dependence of pair

separation on both environment and isolation is equal for the paired galaxies sample and their respective controls.

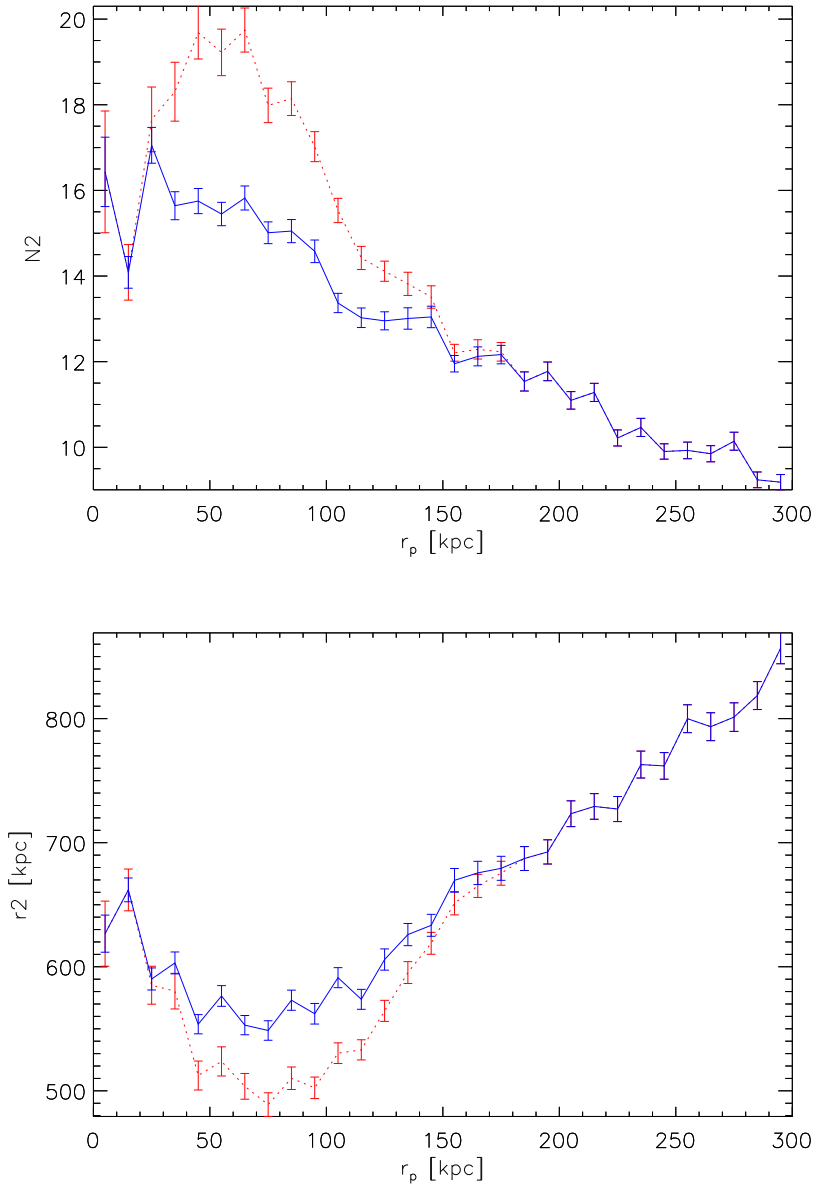

Figure 2.9: (a) The upper panel shows a plot of the mean N_2 of the paired galaxies as a function of r_p. (b) The lower panel shows a plot of the mean r_2 of the paired galaxies as a function of r_p. In both plots, the dashed red line shows the data before the corrective fibre weights, and the solid blue line shows the data after the weight correction. The error bars show the error in the mean.

In this thesis, I use a slightly modified version of the methodology for finding the control sample described in Patton et al. (2013). For every galaxy in the pair sample, a control sample is identified such that it is matched in stellar mass, redshift, local density, isolation, and environment class. Each control galaxy is required to have a redshift within 0.01 of the paired galaxy, and a stellar mass within 0.1 dex[1]. To match on local density, each control galaxy is also required to have N_2 within 10% of the paired galaxy's N_2. As for isolation, the r_p of the control galaxy's closest companion must be within 10% of the paired galaxy's r_2. Finally, the control galaxies are also required to be in dark matter halos that have masses within 0.1 dex of the halo mass of the paired galaxies. Each paired galaxy is required to have a minimum of 10 control galaxies, and in the case where this number is not met, the matching criteria (σ) are increased in the following manner:

$$\sigma(n) = \sigma(0) * \frac{2^{n+1} - 1}{2^n} \tag{2.5}$$

$\sigma(0)$ is the starting matching range (e.g., 0.1 dex for stellar mass), n is the number of times the iteration had to be done, and $\sigma(n)$ is the new matching range. As an example to clarify this method, if the matching range initially is $\sigma(0) = 0.1$ dex, and less than 10 control galaxies were found, then this range is increased to $\sigma(1) = 0.15$ dex and the matching algorithm is rerun. If 10 control galaxies were not found again, the range is increased to $\sigma(2) = 0.175$ dex, then $\sigma(3) = 0.1875$ dex, and so on until a minimum of 10 control galaxies are found, which guarantees that the matching limit never exceeds twice the initial range. For the sample used in this thesis, a

[1]dex is a contraction of decimal exponent. It is a logarithmic unit commonly used in astronomy, where 1 dex equals a factor of 10 and 0.1 dex means $10^{0.1}$.

minimum of 10 galaxies have been found for every paired galaxy, with an average of 106 controls per paired galaxy (and a median of 29 controls per paired galaxy). After the selection of the control galaxies, the mean is then determined for the properties of each galaxy's control sample to allow for a single "effective control" to be associated with every paired galaxy in the sample. This method yields excellent agreement between galaxies and their controls in the matched properties as seen in Figure 2.10.

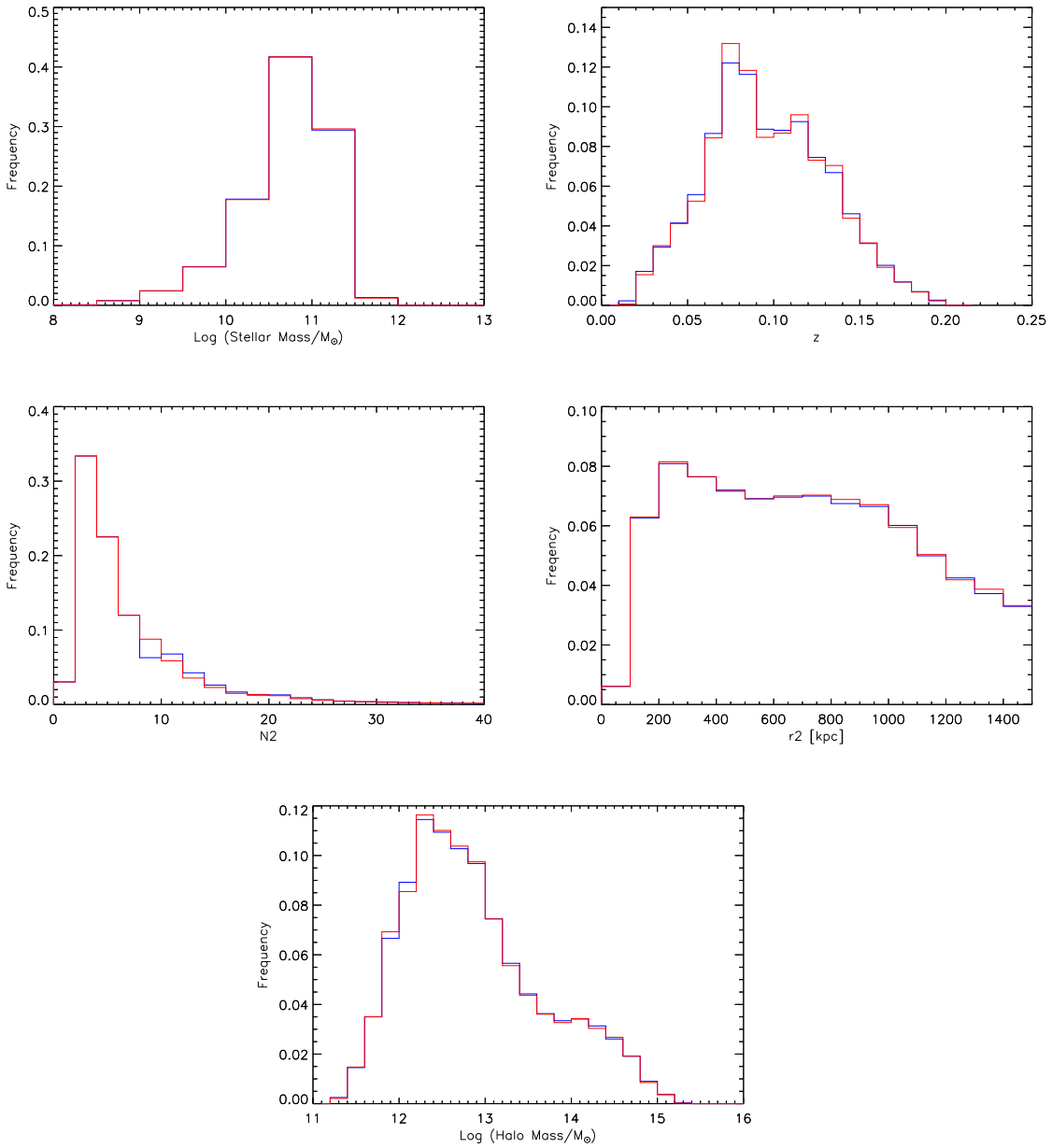

Figure 2.10: Histograms showing the distribution of: (a) stellar masses in the upper left plot, (b) redshift in the upper right plot, (c) N_2 in the center left plot, (d) r_2 in the center right plot, and (e) dark matter halo mass in the bottom plot, of paired (blue line) and their control (red line) galaxies.

Chapter 3

Star Formation Rates

3.1 Introduction

Star formation is crucial to the understanding of galaxy formation and evolution. In fact, star formation rates (SFRs) are considered to be one of the most important parameters to define galaxies and their evolution. By comparing the colours of morphologically peculiar galaxies to normal galaxies, Larson and Tinsley (1978) showed the first clear evidence of enhanced star formation in interacting galaxies. In recent years, it has been shown by numerous studies that galaxy-galaxy interactions and mergers contribute to the evolution of galaxies in several ways including triggering the formation of new stars, or quenching star formation in gas-rich galaxies (Schiminovich et al. 2007; Di Matteo et al. 2008; Wild et al. 2009). For example, many studies have shown that galaxy pairs in general exhibit enhanced SFR, and demonstrate an increase in the enhancement as pair separation decreases (e.g., Alonso et al. 2004; Ellison et al. 2008; Patton et al. 2011; Scudder et al. 2012). This enhancement has been reported to be sustained up to separations of $\sim 150\ h_{70}^{-1}$ kpc (Patton et al., 2013), which is far larger than what is often considered by merger rate studies.

In this chapter, I investigate the effect of environmental membership on the SFR and SFR enhancements of the paired galaxies. The different environment classes are defined using the dark matter halo masses. The control sample is matched in the number of galaxies within 2 Mpc (N_2), the distance to the second closest neighbour (r_2), and the dark matter halo mass where the galaxies reside, as well as in stellar mass and redshift. Therefore any differences seen between the paired galaxies and their controls should be caused by the interactions only. I then quantify the differences between the paired galaxies' SFRs and their controls' SFRs in the form of SFR enhancements. It is worth noting that the properties of galaxies in different environments do not have the same distributions (field paired galaxies generally have lower stellar masses and redshift values than group and cluster paired galaxies). Therefore, even though enhancements are likely to be the sole product of interactions, various levels of enhancements depending on the environment can be caused by selection bias in the samples.

As is mentioned in §1.4, in the past decade, a number of studies were concerned with determining the role of local environment in changing galaxy-galaxy interaction properties. For example, Lambas et al. (2003) and Alonso et al. (2004) studied the properties of the 2-degree field (2dFGRS) close galaxy pairs in the field and groups respectively. They concluded that there is a lower level of star formation activity in denser systems than in the field, with the enhancement in the SFR requiring smaller separations in groups than in the field. Their work was later extended by Alonso et al. (2006) to also include galaxy pairs from the Sloan Digital Sky Survey (SDSS). Low, intermediate, and high density environments were defined using an estimator based on the distance to the 5th nearest neighbour (Σ_5). Galaxy pairs were identified

by creating upper limits in r_p and Δv where the star formation activity became consistent with the average activity of their control galaxies, which are at $r_p < 100$ h_{70}^{-1} kpc and $\Delta v < 350$ km s^{-1}. Alonso et al. (2006) reported that enhanced star formation was evident in wider separation pairs for lower Σ_5. However, their control sample consisted of a single averaged value rather than a comparison on a galaxy-by-galaxy basis, where instead of comparing the SFR of paired galaxies in a specific r_p bin with the average SFR of the controls of those specific paired galaxies, the authors take the average of the SFR of all the controls in all r_p bins, and compare the SFR of pairs to that one value. With this method, the authors wind up comparing the galaxy pairs with a control sample that no longer matches the paired sample. Moreover, further bias is introduced by the lack of equal matching in Σ_5.

More recently, Perez et al. (2009) improved on this analysis by creating a control sample that is matched with the pair sample in redshift, stellar mass, Σ_5, and dark matter halo mass. However, they maintained the use of a single averaged value to describe the entire control sample for comparison with the paired galaxies. With this method, they found that even though pairs in the lowest environmental density have the highest absolute fraction of star forming galaxies, pairs with $r_p < 20$ h_{70}^{-1} kpc regardless of density have a fraction of high star forming galaxies almost twice that of their controls. Moreover, Ellison et al. (2010) used a sample of close galaxy pairs from the SDSS DR4 to examine in which environments galaxy mergers occur, and how the results of these mergers depend on differences in local galaxy density. They matched the pair and control samples in mass, redshift, and local projected density (defined by the average distances to the 4th and 5th neighbours within 1000 km s^{-1}), and concluded from the comparison of pairs and controls that galaxies in the

lowest density environments showed the largest changes in SFR enhancement, and triggered star formation was seen only in low-to-intermediate density environments. The suggested explanation for these results was that they are likely due to the typically higher gas fractions of galaxies in low density environments. Similar results have been obtained by many other works (Freedman Woods et al., 2010; Wong et al., 2011; Hwang et al., 2011; Ideue et al., 2012; Alonso et al., 2012).

It is clear that the environment does have an effect on the star formation of galaxy pairs. Previous works mostly agree that SFR enhancement is lower in higher densities than it is in lower density environments. In this thesis, I aim to extend the analysis to more widely separated pairs with a more rigorous and carefully obtained control sample to examine the true effect of environmental membership on the star formation of interacting pairs. Therefore, in this chapter, I explore the star formation rates (SFR) and specific star formation rates (sSFR; the SFR per unit galaxy stellar mass) of galaxy pairs and merging systems selected from the SDSS DR7 in different environments using a novel method to select the pairs as well as their controls. I perform a comparative study of galaxy pairs with their carefully chosen controls for each environment with the purpose of assessing the relative importance of the role of interactions over global environmental processes, while removing sources of possible biases. In the next section (§3.2) I briefly describe the sample used, and describe how the SFRs were obtained. In §3.3 I show the comparison between the SFR of pairs and their controls in different environments while focusing on the enhancement of SFR, and in §3.4 I do the same with sSFR, and discuss the results in each. In §3.5 the pair sample is extended to include paired galaxies at separations $r_p < 1000\ h_{70}^{-1}$ kpc and I focus on the SFR suppression in the paired galaxies. In §3.6 I provide a summary

of the results and discuss possible physical causes and consequences, and provide a conclusion in §3.6.2.

3.2 Sample Description

The sample used for this thesis is described in detail in Chapter 2. The galaxy pair sample is obtained from the SDSS DR7 with all the galaxies having redshifts in the range $0.01 < z < 0.20$. The photometric total stellar mass measurements are obtained from Mendel et al. (2014), which was estimated using the updated photometry in the $g-$ and $r-$bands of Simard et al. (2011) together with new $u-$ and $i-$bands. The pair sample was constructed in compliance with the method of Patton et al. (2013) (described in more detail in §2.1.2 and in Patton et al. (*in prep*)). The closest neighbour to a galaxy is defined as the galaxy with the smallest r_p with a stellar mass within a factor of 10 of the galaxy's stellar mass and 1000 km s^{-1} in Δv. The projected separation of the second closest neighbour (r_2) and number of galaxies within 2 Mpc (N_2) are then recorded. Using classical mechanics and minimum binding energies, pairs with energies greater than zero are excluded from the pair sample (but kept for the control sample).

In order to define the environment, the dark matter halo masses of the Yang et al. (2007) catalogue for the SDSS DR7 galaxies are used. The definition for each environment (field, poor groups, rich groups, and clusters) are given in Table 2.3. The control sample for the pairs is then constructed as seen in §2.3, by matching the pairs and controls in redshift, stellar mass, isolation, local density, and halo mass.

3.2.1 Star Formation Rate Measurements

The SFRs used in this thesis are obtained from Brinchmann et al. (2004), with updates using this method for the DR7. To obtain the SFR values for the SDSS galaxies, Brinchmann et al. (2004) begin by defining subsamples of galaxies based on their emission line properties. The subsamples are mainly divided using the signal-to-noise ratio (S/N) and strength of the emission lines of Baldwin, Phillips, and Terlevich (1981) (BPT hereafter): [NII], Hα, Hβ, and [OIII]. Galaxies with S/N $>$ 3 in each line are classified into star-forming, AGN, or composite galaxies. This is determined by using the Kauffmann et al. (2003) and Kewley et al. (2001) distinctions in terms of where the galaxies lie on the BPT diagram ([NII]/Hα vs. [OIII]/Hβ).

Of the galaxies that have S/N $>$ 3 for all four BPT lines, some are classified with confidence as star-forming galaxies. For these star-formers, the SFRs are determined by fitting their emission lines with the models of Charlot and Longhetti (2001). Galaxies that are classified as AGN or composite, as well as galaxies without BPT emission lines with S/N $>$ 3 have their SFRs determined by using an empirical relation between the sSFR of the galaxy and its 4000Å break strength (D_n4000, Balogh et al. 1999). Lastly, galaxies with S/N $>$ 2 in Hα flux that do not have this level of signal in the remaining BPT lines can have their SFRs determined using the relation of Kennicutt (1998). Even though the full modeling apparatus of Brinchmann et al. (2004) cannot be used in this case, they show that the SFRs can still be determined using the dust corrected emission luminosity of Hα.

Since the SDSS is a fibre-based survey, all these methods for assigning SFRs to galaxies are derived from the spectra of those galaxies. Therefore, they are restricted to the fibre aperture, and at median redshift and stellar mass of the survey, the spectra

only sample $\sim 1/3$ of the total galaxy light. Brinchmann et al. (2004) calculate the global (or total) SFR for galaxies in the SDSS using an aperture correction that uses the resolved colour information available for each galaxy in the $(g-r)$ and $(r-i)$ bands. This is done by constructing a likelihood distribution for the probability of a given SFR based on the i-band luminosity (L_i) outside of the fibre and the colour of this unsampled region. This correction is purely empirical and relies on the assumption that the distribution of L_i at fixed $(g-r)$ and $(r-i)$ colour should be the same for both the inside and outside of the fibre region, which could potentially cause a bias in the results. Therefore, for the purpose of this thesis, the measurements used are those of the fibre SFRs.

The sample also contains no cuts in SFR or sSFR. The reasoning behind a SFR cut is mostly due to the unreliability of the SFR data for the passive fraction. This unreliability stems from the method used to obtain the SFRs of passive systems, where a minimum value is set for the sSFR of passive systems that causes an overestimation in their values. Moreover, the errors in SFRs do not become vanishingly small as the SFRs decline, which causes less constraint on the exact values of the lower SFRs. The errors are also increased by the fact that unlike star-forming systems, passive systems' SFRs are obtained using indirect methods, where the SFR is assigned to the system based on the 4000 Å break - sSFR relation. This relation has an intrinsic scatter, and therefore, causes a larger error in the determination of the exact SFR values for passive systems (Brinchmann et al., 2004). Due to the overestimated SFR values, studies generally tend to cull the passive galaxies and only use the star formers. However, we argue that even though the SFR values of passive galaxies are overestimated, galaxies on the SF sequence on average have SFRs that are 45 times larger than passive

galaxies. The SFRs of passive galaxies are sufficiently low to be approximately zero and the overestimation in the SFR of the passive galaxies becomes insignificant and does not affect the mean SFR values. In fact, we tested the mean SFR values of paired galaxies by replacing all the passive galaxies' SFRs with a value of 0, and obtained results that are indistinguishable from those obtained using the passive galaxies' SFR from Brinchmann et al. (2004). Therefore, the need to investigate the full range of SFRs far outweighs any insignificant effects from the overestimation of passive galaxies' SFRs, and no cuts in SFR or sSFR are applied in this work.

Out of the original sample of ∼505,000 galaxies that have SFRs, ∼320,000 galaxies are considered paired galaxies, with ∼113,000 paired galaxies having $r_p < 300\ h_{70}^{-1}$ kpc, with an average of 106 controls per paired galaxy (and a median of 29 controls per paired galaxy).

3.3 Star Formation Rate Enhancements

With the SFR measurements for the pair and control galaxies in the sample at hand, the comparison of the enhancement in star formation in different environments can begin. In Figure 3.1, I plot the mean SFRs of paired galaxies and their associated controls as functions of r_p. The mean SFR values of the control sample show little dependence on r_p, which demonstrates the lack of a close companion that causes increased SFRs at close separations as seen in the paired galaxies' SFRs. Moreover, the difference between the paired galaxies' SFRs and those of their respective controls in every environment diminishes with increased projected separation. This is due to the small-scale interaction effects being overcome by the large-scale environmental effects due to the large separation between the paired galaxies.

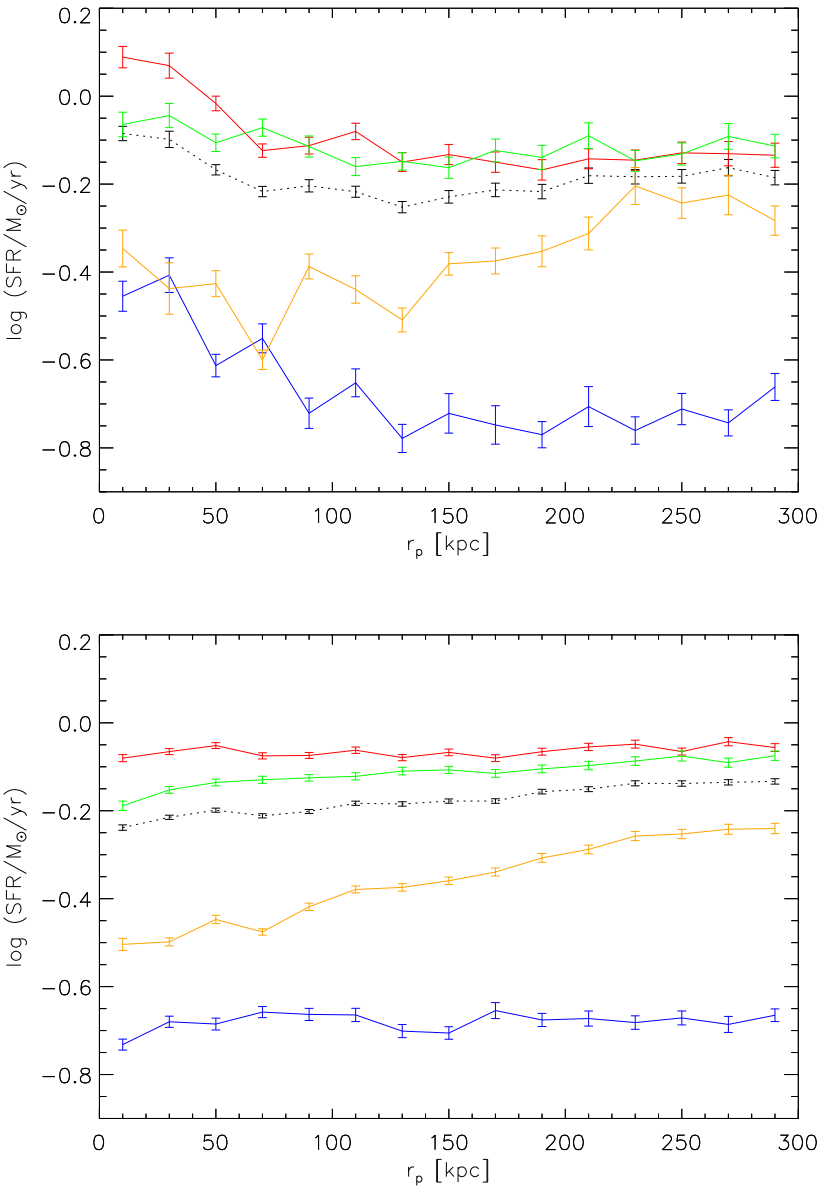

Figure 3.1: Plot showing the mean SFRs of paired galaxies (top plot) and their associated control galaxies (bottom plot) as function of projected separation r_p in different environments. The dotted black line shows the mean SFRs of the entire sample (not split into environments), the blue lines represent galaxies in the field, red represents galaxies in poor groups, green for galaxies in rich groups, and orange for galaxies in clusters. All error bars show the standard error in the mean.

In order to quantify the effect of the interaction on paired galaxies, I use the offset method of Patton et al. (2011) where the ratio of paired versus control SFRs can be interpreted as the enhancement of SFR due to interactions and is given by the following:

$$\Delta\mathrm{SFR} = \frac{\mathrm{SFR_{pairs}}}{\mathrm{SFR_{controls}}} \tag{3.1}$$

Here ΔSFR is the SFR enhancement, and $\mathrm{SFR_{pairs}}$ and $\mathrm{SFR_{controls}}$ are the mean SFRs of the paired and control galaxies respectively. In this formalism a ΔSFR of one means no enhancement and less than one means suppression. This can be seen in Figure 3.2, where at the small separations paired galaxies in all environments show an enhancement in SFR, with the strongest enhancement seen in field galaxy pairs. However, this enhancement quickly vanishes as pair separation starts to increase.

Table 3.1 shows a summary of some of the key features of Figure 3.2. It can be seen that unlike what can be found in the literature (e.g., Heiderman et al. 2009; Knapen and James 2009; Robaina et al. 2009), the enhancement in SFR is consistently less than 2. Conversely, Patton et al. (2013) reported enhancements up to a factor of 3 at the smallest separations, with moderate enhancements of $\sim 20\%$ over the range $50 < r_p < 120\ h_{70}^{-1}$ kpc, and no visible enhancements by $r_p \sim 150\ h_{70}^{-1}$ kpc. For the full sample used in this thesis, the maximum enhancement is seen reaching a factor of $\sim 45\%$ and the enhancement drops to zero for pairs with $r_p > 70\ h_{70}^{-1}$ kpc. Even though the sample used in this thesis is from the same source as that used in Patton et al. (2013), the differences in the results can be attributed to the criteria set on the SFRs in Patton et al. (2013) where they require every galaxy in their pair sample to be classified as star-forming according to the criteria of Kauffmann et al. (2003). No SFR restrictions are applied to my sample, resulting in it including star-formers

as well as non-star-formers, AGN, and composites, which drives the enhancement in the SFR down. Furthermore, Patton et al. (2013) used r_p bins that are 10 h_{70}^{-1} kpc wide, while in this work the width of the r_p bins is 20 h_{70}^{-1} kpc which dilutes the enhancement, and explains the difference between the two results.

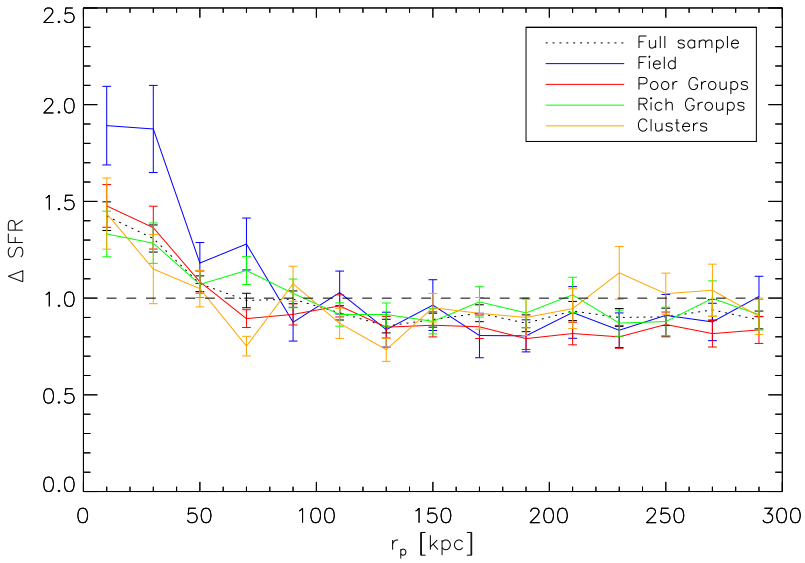

Figure 3.2: Mean SFR enhancement (ratio of pair SFR to control SFR) is plotted versus r_p for the pairs in different environments. The colour scheme follows that of Figure 3.1, with the dashed horizontal line denoting zero enhancement. All error bars show the standard error in the mean.

Table 3.1: SFR Enhancement

Environment	Enhancement for $r_p < 20\ h_{70}^{-1}$ kpc	r_p for zero enhancement
All	1.45 ± 0.07	$\sim 70\ h_{70}^{-1}$ kpc
Field	1.86 ± 0.20	$\sim 80\ h_{70}^{-1}$ kpc
Poor Group	1.49 ± 0.11	$\sim 60\ h_{70}^{-1}$ kpc
Rich Group	1.37 ± 0.12	$\sim 70\ h_{70}^{-1}$ kpc
Cluster	1.46 ± 0.19	$\sim 50\ h_{70}^{-1}$ kpc

From Table 3.1, it is clear that at the smallest separations ($r_p < 40\ h_{70}^{-1}$ kpc) the enhancement in field pairs is greater than the enhancements in denser regions, and it is visible up to separations $\sim 80\ h_{70}^{-1}$ kpc, which is larger than the denser environments. The SFR enhancements seen in groups and clusters are consistent with each other within the uncertainty. As noted previously, the differences in the enhancement levels seen in the different environments can be caused by environmental effects, but it is equally likely that it is also caused by the distribution of stellar masses and redshifts of the galaxies in each environment. Field galaxies have preferentially lower masses and redshifts than cluster galaxies, and both stellar mass and redshift are known to have a correlation with SFRs, which affects the SFR enhancement levels. The SFR enhancement seen in an environment can confidently be attributed to interaction effects alone due to the careful control matching that assures the only difference between paired galaxies and their controls is the one close neighbour. On the other hand, the differences in the levels of enhancements seen in different environments cannot be solely attributed to environmental effects due to the various differences in the samples in each environments. Moreover, one cannot certainly conclude whether the increased SFR enhancement in close field pairs is due to greater star formation activity in individual galaxies, or that interactions in the field produce a higher fraction of enhanced SFR paired galaxies than the denser environments, or a combination of both. In order to extract this information, the interacting galaxy pairs should be examined on an individual basis rather than in a statistical study where such information is lost or, alternatively, numerically simulate the galaxy interactions for identical pairs in different environments to test the enhancement of SFR in each case. Both of these proposed options are beyond the scope of this thesis.

From the available analysis, it can be concluded that close field paired galaxies show the greatest level of mean SFR enhancements, which is consistent with the findings of Alonso et al. (2006) and Ellison et al. (2010). On the other hand, we also report statistically significant SFR enhancements in close paired galaxies in all environments, including rich groups and clusters, while Ellison et al. (2010) using data from the SDSS DR4 reported that galaxies in the higher density environments show no enhancements in SFRs. These conflicting results can be caused by various differences in the methodology used to obtain the sample of paired galaxies and their controls. Ellison et al. (2010) used data from the DR4, which is now known to overestimate SFRs in specific galaxies (Salim et al., 2007), and corrected for fibre incompleteness by culling a fraction of the wide separation pairs rather than apply a statistical weight to pairs with $\theta < 55$ arcsec. Moreover, the control sample used in Ellison et al. (2010) is only matched on environment using a single parameter obtained from the distance to the 4th and 5th closest neighbours, together with a significantly different method of obtaining controls for each paired galaxy in comparison with the method used in this thesis. Furthermore, while Ellison et al. (2010) removed passive galaxies from their sample, the sample of galaxies used in thesis includes star forming galaxies as well as passive galaxies, which yields a substantially larger sample of cluster galaxies in particular. Therefore, all these differences in sample selection and methodology can account for the discrepancy in the SFR enhancements of close paired galaxies in denser environments.

3.4 Specific Star Formation Rate Enhancements

It is worth noting that in Figure 3.1 it is clear that every environment has a significant effect on the SFR of all galaxies within them. One would expect the field galaxies to have the highest SFRs followed by poor and rich groups and then clusters with the lowest SFRs (e.g., Lewis et al. 2002; Baldry et al. 2004; van den Bosch et al. 2008; Pasquali et al. 2009; Peng et al. 2010; Wijesinghe et al. 2012, etc.); however, this is not seen in Figure 3.1. The field has the lowest SFR for both pairs and their controls, followed by clusters, rich groups, and poor groups with the highest SFRs, which brings into question the reliability of the results obtained using the methods of this thesis. However, in Figure 2.7, it is clear that the distribution of stellar masses is different depending on the environment. Each environment has a unique stellar mass distribution, and SFRs and stellar masses are known to have a correlation with one another (e.g., Brinchmann et al. 2004; Peng et al. 2010; Whitaker et al. 2012). Lower mass galaxies produce lower levels of SFR, and field galaxies have preferentially lower masses than galaxies in higher density environments in our sample, which explains their lower mean SFRs. Therefore, in order to change the dependence on stellar mass, and verify that the results in the previous section are not simply an artifact due to the differing stellar mass distributions of the different environments, the specific star formation rates are calculated.

The specific star formation rate (sSFR) is simply defined as the star formation rate per unit stellar mass (SFR/M_*), or the fractional mass-growth per unit time. The sSFR is commonly regarded as a proxy for the efficiency of star formation in galaxies. Recently there have been several studies that have shown the relationship between the sSFRs of galaxies and their stellar mass. For the SDSS, Elbaz et al.

(2007) and Salim et al. (2007) showed that for the star forming galaxies there exists a tight "main sequence" where the sSFR is approximately constant for a wide range of stellar masses. More recently Peng et al. (2010) also showed that there is only a weak dependence of sSFR on mass, where sSFR $\propto M_*^{\beta}$ with $\beta = -0.1$. Therefore, in order to test the reliability of the SFR results obtained in the previous section, I calculate the sSFR of galaxy pairs and their associated controls using the fibre SFR data from the previous section, divided by their fibre stellar masses for the sake of consistency. For the sample used in this thesis, Figure 3.3 clearly shows that the dependence of the sSFRs on stellar mass for the SDSS galaxies is far lower than that of the SFRs, however the spread of SFR values in the main sequence is tighter than the spread of sSFRs. To quantify the dependence of the SFR and sSFR on stellar mass, first the active and passive populations were distinguished using the definition of Bluck et al. (2014), where a galaxy is passive if $\log(\Delta\text{SFR}) \leq -1$. A line of best fit is then fitted to the active population, and lowered to match the separating limit between passive and active galaxies. The slope of the line of best fit β indicates the dependence of the SFR or sSFR on the stellar mass, with $\beta = 1.0 \pm 0.6$ for the SFR-M_* relation, and $\beta = -0.14 \pm 0.08$ for the sSFR-M_* relation. These slopes are consistent with results from previous studies (e.g., Peng et al. 2010; Abramson et al. 2014), and demonstrate the significant decrease in the dependance on stellar mass for sSFRs ($\sim$ 10 times lower than SFR-M_* slope).

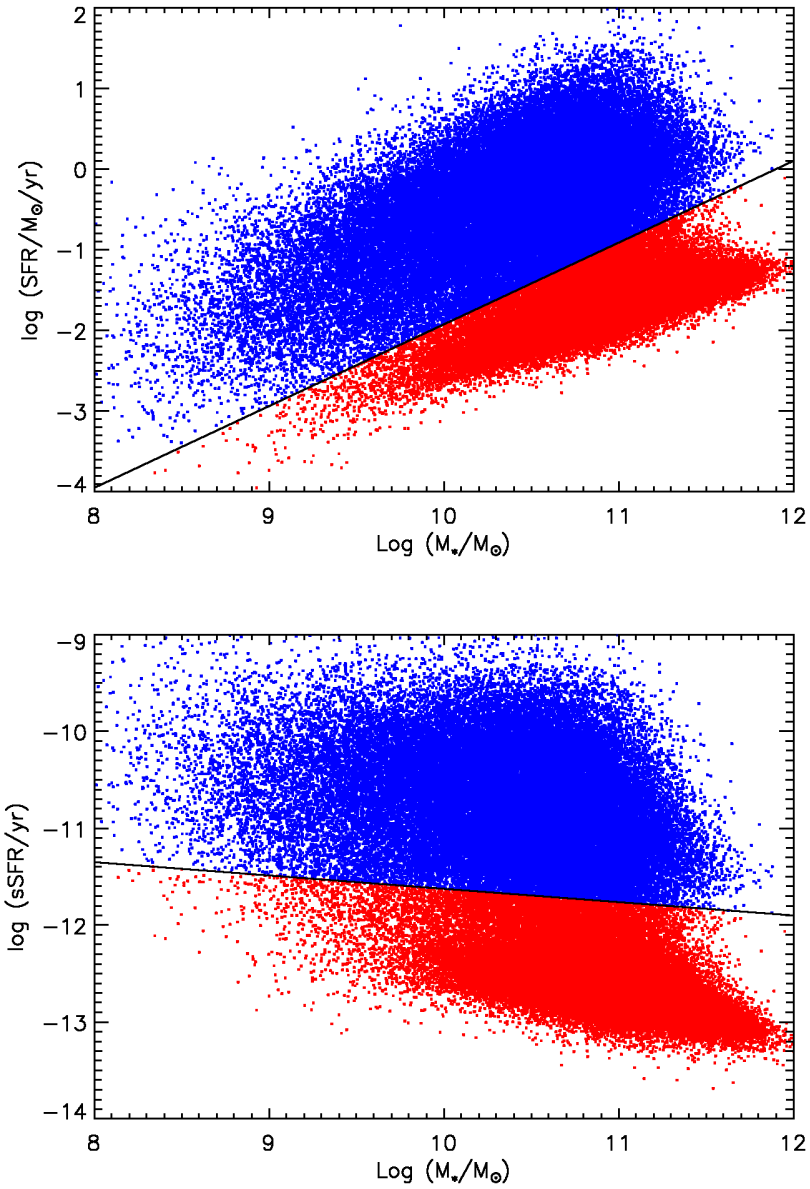

Figure 3.3: Scatter plots showing the dependence of SFR (top plot) and sSFR (bottom plot) on stellar mass. The solid line separates the star-forming main sequence from the red fraction, with its slope indicating the dependence of SFR or sSFR on stellar mass.

Figure 3.4 is a plot of the mean sSFRs of paired galaxies as well as their associated controls. It is immediately apparent that the expected order in terms of environments is produced, with the highest sSFR seen in field galaxies, followed by poor and rich group galaxies, and cluster galaxies showing the least sSFR for both pairs and controls. Just as with SFRs previously, the comparison between the pair and control sSFRs provides information on the enhancement in sSFR, which translates to information on the enhancement in the efficiency of forming stars. Therefore, with the sSFRs for the different environments in the predicted order, the SFR enhancement results can be justified by the existence of compatible results in the similar treatment of sSFRs.

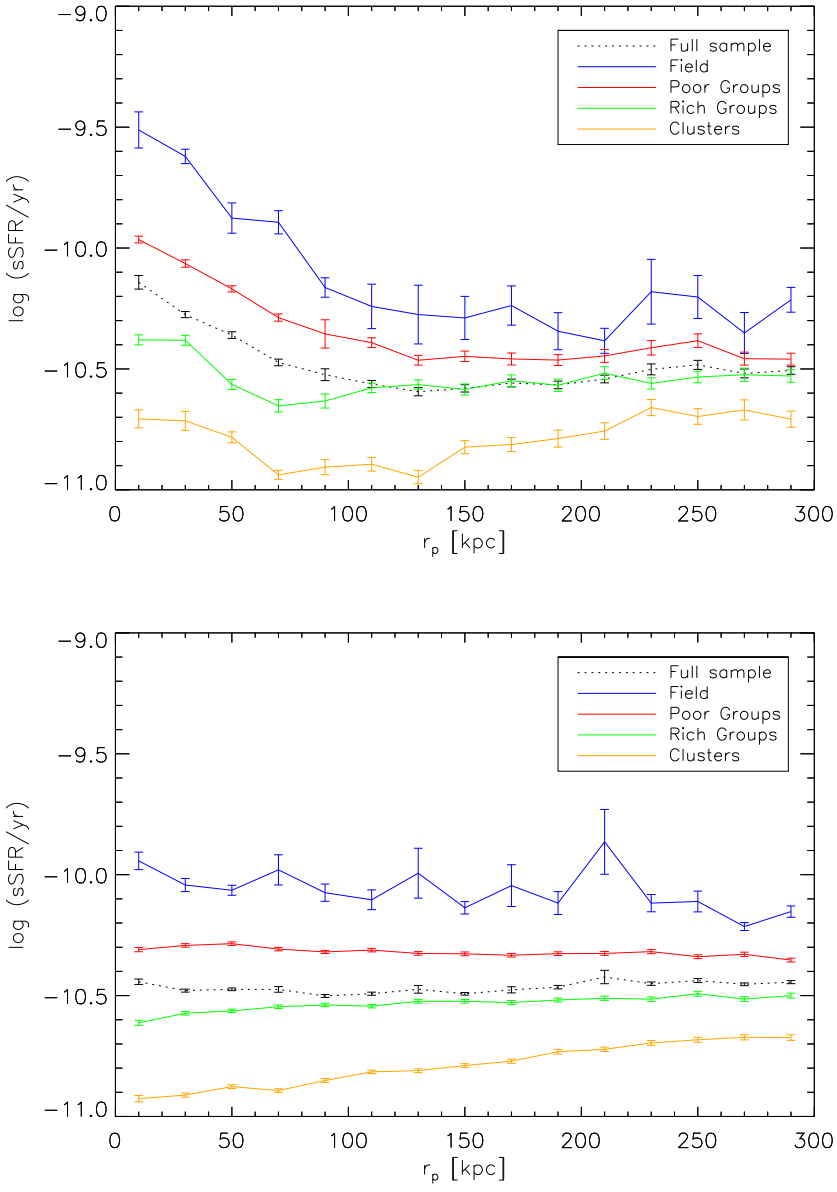

Figure 3.4: Plot showing the mean sSFRs of paired galaxies (top plot) and their associated control galaxies (bottom plot) as function of projected separation r_p in different environments. The colour scheme follows that of Figure 3.1. All error bars show the standard error in the mean.

The resulting sSFR enhancements are seen in Figure 3.5, with the key features summarized in Table 3.2. It is evident that the order of the strength of enhancements at smallest separations by environment is as expected from the enhancements of SFRs, with the field paired galaxies experiencing the largest enhancement, while the paired galaxies interacting at smallest separations in the higher density environments show lower levels of enhancement. However, comparing the enhancements in sSFRs with those of the SFRs in Figure 3.2 shows that the enhancements in sSFRs are higher than in SFRs for all environments. The discrepancy in levels of enhancements between SFRs and sSFRs may appear to be an error since the paired galaxies are matched with their controls in stellar mass and should have a constant ratio between pairs' and controls' properties when dividing by their respective stellar masses, as shown below:

$$\Delta\mathrm{SFR} = \frac{\mathrm{SFR_{pairs}}}{\mathrm{SFR_{control}}} \tag{3.2}$$

$$\begin{aligned}\Delta\mathrm{sSFR} &= \frac{\mathrm{sSFR_{pairs}}}{\mathrm{sSFR_{control}}} \\ &= \frac{\mathrm{SFR_{pairs}}/\mathrm{M_{*,pairs}}}{\mathrm{SFR_{control}}/\mathrm{M_{*,control}}}\end{aligned}$$

therefore, if $\mathrm{M_{*,pairs}} \simeq \mathrm{M_{*,controls}}$, then

$$\Delta\mathrm{sSFR} = \frac{\mathrm{SFR_{pairs}}}{\mathrm{SFR_{control}}} = \Delta\mathrm{SFR} \tag{3.3}$$

and this is not seen from comparing Figure 3.2 and Figure 3.5. However, the values shown in those figures are of the *average* SFR and sSFR enhancements. Even though the conclusion in eq. 3.3 holds for the individual paired galaxies' SFRs' and sSFRs'

enhancements, it does not hold for the mean enhancements in each r_p bin. This is due to the fact that when calculating the mean enhancement in SFRs, the galaxies with the highest SFR enhancements contribute more towards the mean enhancement in the bin than galaxies with low SFR enhancements. A galaxy with a high SFR enhancement and high mass would contribute more to the mean SFR enhancement than a galaxy with low SFR enhancement and low mass. However, as seen previously, since the SFRs and stellar masses are correlated, the ratios of SFR to masses (i.e., sSFRs) are often similar for both galaxies, resulting in the galaxies being weighted equally when contributing to the mean sSFR enhancement. This explains the discrepancy and validates the use of the sSFR enhancements as a verification for the results obtained in the previous section with the SFR enhancements.

The similar enhancements in both SFRs and sSFRs at smallest separations, combined with the similar limits in separation at which enhancements in SFR begin to appear for the paired galaxies in different environments, provides confidence in the results obtained in the previous section, as well as confidence in the SFRs used in this thesis. Just as with the SFR enhancements, field paired galaxies at the smallest separations ($r_p < 40\ h_{70}^{-1}$ kpc) are greater than the enhancements for paired galaxies in denser environments at similar separations, which is consistent with the results of Ellison et al. (2010). The existence of statistically significant enhancements in the mean SFR and sSFR of close paired galaxies in all higher density environments is inconsistent with the findings of Ellison et al. (2010). However, as was mentioned in the previous section, this could be caused by various differences in the sample selection and control finding methods utilized in this thesis as opposed to those used in Ellison et al. (2010).

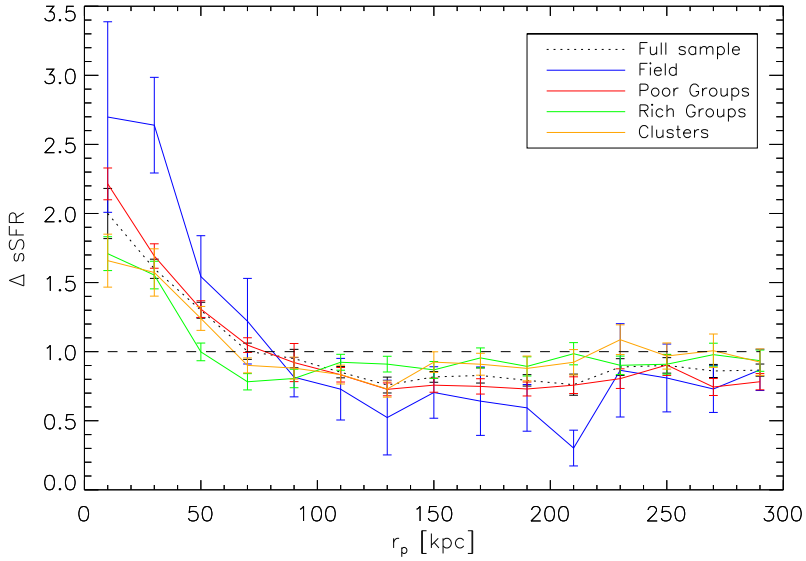

Figure 3.5: Mean sSFR enhancement (ratio of pair sSFR to control sSFR) is plotted versus r_p for the pairs in different environments. The colour scheme follows that of Figure 3.1, with the dashed horizontal line denoting zero enhancement. All error bars show the standard error in the mean.

Table 3.2: sSFR Enhancement

Environment	Enhancement for $r_p < 20\ h_{70}^{-1}$ kpc	r_p for zero enhancement
All	1.99 ± 0.18	$\sim 70\ h_{70}^{-1}$ kpc
Field	2.70 ± 0.69	$\sim 80\ h_{70}^{-1}$ kpc
Poor Group	2.21 ± 0.12	$\sim 70\ h_{70}^{-1}$ kpc
Rich Group	1.71 ± 0.12	$\sim 50\ h_{70}^{-1}$ kpc
Cluster	1.66 ± 0.19	$\sim 70\ h_{70}^{-1}$ kpc

3.5 Star Formation Rate Suppression

Figure 3.2 shows clear signs of SFR enhancements for paired galaxies at separations $r_p < 80\ h_{70}^{-1}$ kpc with varying levels of enhancement depending on the environment. However, looking past separations of $r_p > 120\ h_{70}^{-1}$ kpc, the entire sample's mean SFR is seen to be systematically suppressed. Even though this phenomenon is mostly evident for the lower density environments, when combining the environments to look at the full sample, the suppression seems to systematically persist for galaxies paired at separations of $r_p > 120\ h_{70}^{-1}$ kpc. This is also evident in sSFR with the paired galaxies showing systematic suppression at separations $r_p > 80\ h_{70}^{-1}$ kpc in Figure 3.5.

The mean SFR suppression in Figure 3.2 is seen to persist for pairs separated by up to $300\ h_{70}^{-1}$ kpc, therefore in order to further investigate the cause of the suppression, Figure 3.6 shows the SFR enhancements for paired galaxies with separations $r_p < 1000\ h_{70}^{-1}$ kpc in all the different environments. Separations as large as $1000\ h_{70}^{-1}$ kpc should show SFR results for paired galaxies indistinguishable from their controls since these distance probe the large scale environmental effects with no contribution from the relatively distant closest neighbour. Figure 3.6 contains three regions with varying behaviour, namely the SFR enhancements at smallest separations ($r_p < 80\ h_{70}^{-1}$ kpc), the suppression at intermediate separations ($80 < r_p < 400\ h_{70}^{-1}$ kpc), and the lack of activity relative to controls at the largest separations ($r_p > 400\ h_{70}^{-1}$ kpc). The first region, which exhibits SFR enhancements at separations $r_p < 80\ h_{70}^{-1}$ kpc, was shown in the previous two sections to be the product of close interacting pairs and varies in the level of enhancement due to the environments in which the interactions take place. As for the second region, the work of Geha et al. (2012) may provide insight into the cause of the observed suppression at those separations.

Dwarf galaxies in the NASA-Sloan Atlas (a re-analysis of the SDSS DR8) were found to exhibit a clear behaviour in terms of the quenched fraction which decreases with increased distance from the closest massive galaxy. The fraction of dwarf galaxies at closest separations (< 250 kpc) that are quenched was found to be between 21 - 32%, and drops to 0 - 5% for separations larger than 1.5 Mpc. By examining Figure 3.6 one can see a consistency between the separations where the quenching occurs and those given by Geha et al. (2012), namely that the cause of the suppression observed in Figure 3.6 may be attributed to suppression in lower mass galaxies due to interactions with a more massive galaxy.

This hypothesis is tested in Figure 3.7, where the paired galaxies are split into two categories: galaxies with a more massive companion(mass ratio > 1), and galaxies with a less massive companion (mass ratio < 1). By splitting the pairs by their mass ratios, a few differences in behaviour become apparent. Looking at the closest separations, it is quite clear that the enhancement in SFR for the higher mass galaxies in the pairs are far larger than those seen for the lower mass paired galaxies, and this is seen for all environments. Individually, the higher mass paired galaxies in the field show the highest rate of enhancement in SFR, while the higher mass pairs in clusters show the least enhancement at $r_p < 50\ h_{70}^{-1}$ kpc, which is consistent with the findings in the past section. As for the lower mass paired galaxies at $r_p < 50\ h_{70}^{-1}$ kpc, SFR enhancement is only seen in field paired galaxies and at almost half the enhancement seen for their higher mass counterparts. Within the uncertainty limits, there are no SFR enhancements seen for lower mass paired galaxies in the higher density environments at the smallest separations.

The second region in Figure 3.6 at separations of $100 < r_p < 400\ h_{70}^{-1}$ kpc, which

exhibits quenching in SF for paired galaxies in all environments, is seen in Figure 3.7 to behave differently for higher mass paired galaxies than their lower mass companions. The higher mass paired galaxies show no evidence for quenching in this region for all environments. In fact, they show no differing activity from their controls for all $r_p > 120\ h_{70}^{-1}$ kpc in all environments. On the other hand, the lower mass companions are consistently suppressed relative to their controls, with a higher rate of suppression for field and poor group galaxies than for rich group and cluster galaxies. The suppression seems to start at $r_p \sim 400\ h_{70}^{-1}$ kpc for all environments, and stops at where the majority of studies in this area define as the maximum projected separation for interacting galaxy pairs ($r_p \sim 100\ h_{70}^{-1}$ kpc). At separations greater than $400\ h_{70}^{-1}$ kpc, the lower mass companions show SFRs that are consistent with their controls (i.e., no enhancement or quenching) for all environments except for those in clusters. An enhanced SFR is seen in the lower mass companions that reside in cluster environments at separations greater than $400\ h_{70}^{-1}$ kpc relative to their controls. This phenomenon is most likely due to false pairs, where the individual galaxies in pairs at separations greater than $400\ h_{70}^{-1}$ kpc in a cluster environment are not individual but have other companions closer by that are too faint to pick up on. This explanation is justified by the fact that it is extremely unlikely for a galaxy to reside in the densest possible environment (i.e., the cluster) and be more than $400\ h_{70}^{-1}$ kpc from its closest companion without having any galaxies in between. Looking back at Figure 2.4 in §2.2, we see that even though the halo mass increases slightly with redshift, the number of members decreases dramatically from an average of ~ 25 galaxies at $z = 0.01$ to ~ 6 galaxies at $z = 0.05$ and then to $\sim 1 - 2$ at $z > 0.1$. This dramatic decrease in the number of galaxies observed combined with the lack of decrease in halo mass

shows that many galaxies are being missed in the catalogue due to either being too faint (low mass), too distant (high redshift), too close to another larger companion, or a combination of all factors. Therefore, the reliability of the information obtained for paired galaxies at those separations in dense environments decreases as the pair separation increases due to the increased likelihood of having undetected companions. This is less likely to happen in more isolated environments since it is quite possible to have galaxy pairs at those separations without any undetected companions in between due to the low environmental densities.

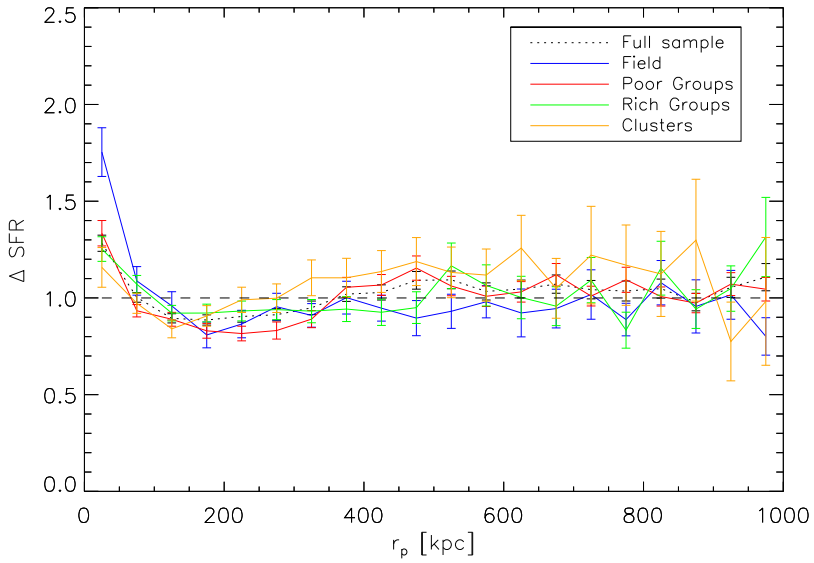

Figure 3.6: Mean SFR enhancement (ratio of pair SFR to control SFR) is plotted versus r_p for the pairs in different environments. The colour scheme follows that of Figure 3.1, with the dashed horizontal line denoting zero enhancement. All error bars show the standard error in the mean.

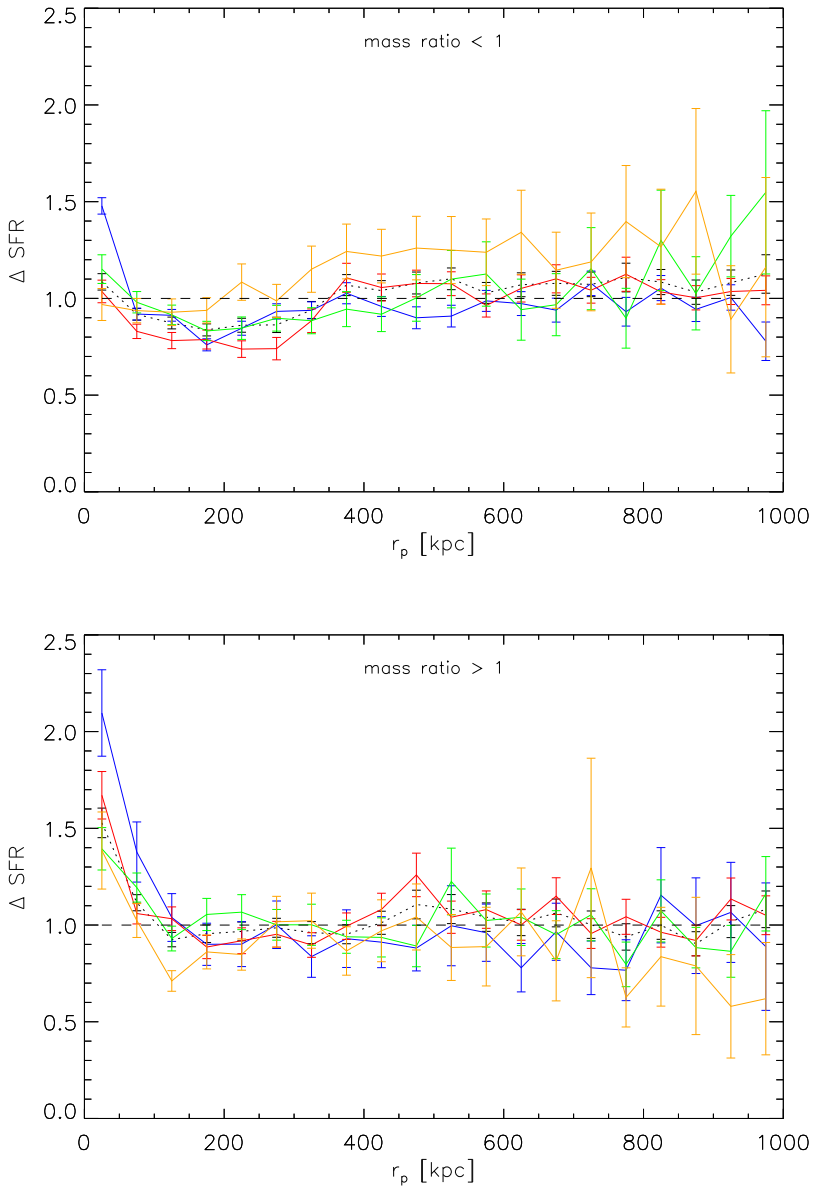

Figure 3.7: Mean SFR enhancement (ratio of pair SFR to control SFR) is plotted versus r_p for the pairs in different environments. The plot on top shows the lower mass paired galaxies, while the higher mass paired galaxies are plotted on the bottom. The colour scheme follows that of Figure 3.1, with the dashed horizontal line denoting zero enhancement. All error bars show the standard error in the mean.

3.6 Discussion & Conclusion

3.6.1 Discussion

Using a sample of galaxy pairs with wide separations selected from the SDSS DR7, together with their SFRs obtained from Brinchmann et al. (2004) and stellar masses from Mendel et al. (2014), I have examined the effects of interactions on star formation in different environments (field, poor and rich groups, and clusters). I found evidence of the dependence of the SFRs and sSFRs of galaxies on the environment in which they reside. However, due to the differences in stellar mass and redshift distributions between the different environments, where the lower density environments have a higher fraction of low mass and low redshift galaxies than denser environments, the comparison of the samples in each environment becomes nontrivial. Any differences in enhancements observed between two environments could be due to environmental effects, sample selection bias, or a combination of both. SFR and sSFR values are correlated with stellar mass, but with different degrees of dependence. Therefore, seeing similar enhancements in all environments in SFR and sSFR, as well as the expected behaviour of mean sSFRs for galaxies in different environments (e.g, Kauffmann et al. 2004; McGee et al. 2011; Scudder et al. 2012) provides confidence in the SFR values used in this thesis as well as the environment selection criteria and control matching.

As for the galaxy interaction effects in different environments, it is found that enhancements in SFR and sSFR for galaxy pairs can be found in all environments, but to varying degrees. The largest boost in star formation and star formation efficiency is found in galaxy pairs in the field with $r_p < 40\ h_{70}^{-1}$ kpc. Paired galaxies in rich groups and clusters are found to have the lowest levels of enhancement, while poor group pairs show moderate enhancements between those of the field and denser

environments. Therefore, it can be concluded that paired galaxies show statistically significant enhancements in SFR and higher star forming efficiency than controls in all environments. Moreover, the maximum separation at which enhancements can be seen is found in this study to be largest for field paired galaxies (at $r_p \sim 80\ h_{70}^{-1}$ kpc), and lower for paired galaxies in groups and clusters. Patton et al. (2013) showed that the SFR enhancement in their wide separation sample extends to $r_p \sim 150\ h_{70}^{-1}$ kpc. The findings in this study do not necessarily point towards an inconsistency, especially when the restrictions on the SFRs in Patton et al. (2013) are taken into account. In this thesis, there are no restrictions applied to the SFR of the pairs or controls, while Patton et al. (2013) only considered star-forming galaxies in their sample. The lack of a SFR cut is motivated by the need to investigate the full range in star forming properties, with the overestimation of low SFRs posing an insignificant effect on the mean SFRs in the sample. This means that there are more low SFR galaxies in the sample used in this thesis, which causes the average star formation rate enhancement to balance out due to this population of passive galaxy pairs lowering the mean enhancements.

In order to explain the differences in enhancement factors together with the differences in maximum separation at which enhancements are visible one must consider whether the effects are due to mechanisms affecting the identical galaxies in different environments due to overdensities (e.g., ISM-ICM interactions, and Galaxy-Cluster interactions), or whether the galaxy populations in the different environments are inherently different. In the latter case, the galaxies in both isolation and overdensities are reacting to the same set of mechanisms and evolutionary processes, and the only reason their enhancements are different is due to their populations reacting

differently to the same processes. One such mechanism is known as assembly bias (e.g., Croton et al. 2007; Cooper et al. 2010), which states that galaxies in high mass halos tend to be older as a result of merging and clustering at an earlier epoch and with greater frequency that more isolated galaxies. Therefore, in rich groups and clusters, one might expect to find a larger fraction of old, 'red and dead' galaxies, which have encountered many mergers and interactions, and have been affected by the quenching mechanisms described previously for a longer period of time. If galaxies in rich groups and clusters are simply older than their more isolated counterparts in poor groups and the field, then they would be further along in their evolution and gas consumption. Therefore, when galaxies interact in dense environments, due to their age and the extent of all the environmental effects acting on them, they are preferentially gas poor, which causes the triggering of SFR enhancement to become more difficult. On the other hand, galaxies in the field contain a larger fraction of gas due to the lack of interactions and environmental effects during their lifetimes in comparison with cluster galaxies, and therefore have a far easier task of triggering SFR during interactions. This mechanism does not require the star formation rates to be triggered differently in different environments, but rather the efficiency of the formation is changed due to the lack of gas in denser environments. Since the star formation enhancement mechanism can be identical for all environments under this formalism, then the triggering of it is essentially the same in all environments but at varying rates depending on the gas fraction.

This case was tested by extending the pair sample from $r_p < 300\ h_{70}^{-1}$ kpc to include paired galaxies with $r_p < 1000\ h_{70}^{-1}$ kpc, and splitting the paired galaxies sample into two categories: galaxies with a more massive companion, and galaxies with a less

massive companion. At separations greater than 400 h_{70}^{-1} kpc, the paired galaxies are unaffected by their companions in all environments. The behaviour of both the low mass and the high mass galaxies at the largest separations matches that of their controls. For paired galaxies at intermediate separations, at $100 \lesssim r_p \lesssim 400\ h_{70}^{-1}$ kpc the paired galaxies with the lower mass exhibit signs of suppression, which are more apparent for lower density environments (field and poor groups) than higher density environments (rich groups and clusters). The suppression can be possibly explained by Geha et al. (2012) who show that dwarf galaxies experience quenching when in the proximity of a more massive galaxy at those separations. This quenching can be due to the reservoirs of gas in the smaller galaxy being depleted by the gravitational effects of the incoming more massive galaxy companion, or it could also be caused by a previous encounter with the more massive galaxy that consumed the star forming gas, leaving the lower mass galaxy with suppressed SFR. The more massive galaxy in the pair exhibits no suppression or enhancement until the smaller companion is within $\sim 100\ h_{70}^{-1}$ kpc. The rate of suppression in the lower mass companions is seen to be larger for lower density environments than higher density environments. A justification for this phenomenon is seen in Figure 3.4, where it is evident that all the galaxies residing in higher density environments such as rich groups and clusters have, on average, significantly lower sSFRs than lower density environments. Therefore, the lower mass paired galaxies in higher density environments exhibit lower levels of quenching in comparison with their controls at intermediate separations than lower mass galaxies in the field and poor groups because in denser environments the galaxies are "pre-quenched". Since higher density environments cause galaxies residing within them to have inherent lower SFRs per unit mass then the suppression due

to a close massive companion is not expected to be dramatic since the galaxies are already stripped of their star forming gas reservoirs. As the companions approach one another, at smallest separations ($r_p < 100\ h_{70}^{-1}$ kpc), the interaction boosts the galaxies' SFRs. However, since the lower massed companions have a suppressed SFR, the enhancement in their SFRs is far lower than the enhancements seen in their more massive companions. The SFR enhancements seen in field pairs are higher than those in denser environments, which can also be attributed to the initial increased suppression of all galaxies in denser environments relative to those in isolation. By maintaining their star forming gas reservoirs before the close encounter takes place, the more massive field paired galaxies experience the largest SFR enhancement of all the other paired galaxies.

3.6.2 Conclusion

The differences in the levels of enhancement in SFRs of paired galaxies at separations $r_p < 40\ h_{70}^{-1}$ kpc appear to be the result of assembly bias rather than differing interaction mechanisms in the different environments. As expected from previous works, the SFR enhancement for closest separations was seen to be largest for field paired galaxies, and smallest for cluster paired galaxies. To be able to differentiate whether this result is driven by interaction mechanisms differing by environment, or simply the consequence of having different galaxy populations in different environments, the average suppression seen in all environments at separations between $100 < r_p < 400$ h_{70}^{-1} kpc is investigated. Following the work of Geha et al. (2012), by splitting the paired galaxy by mass ratio, the behaviour of paired galaxies with a more massive companion can be compared to that of paired galaxies with a less massive companion

of the same environment. The lower mass companions show systematic mean suppression in SFRs in all environments, while their higher mass companions show no evidence of suppression at $100 < r_p < 400$ h_{70}^{-1} kpc. This result is also accompanied by significantly decreased SFR enhancements at $r_p < 40$ h_{70}^{-1} kpc for lower massed companions in comparison with their more massive closest neighbours in all environments. In fact, lower mass paired galaxies in groups and clusters show enhancements consistent with zero at $r_p < 40$ h_{70}^{-1} kpc, while the more massive cluster paired galaxies show similar average levels of enhancement as the lower mass field paired galaxies.

Clusters contain galaxies that are redder than field galaxies and are generally more gas poor due to the effects of ISM-ICM and galaxy-cluster interactions on galaxies residing in those dense environments as discussed in more detail in §1.2. Lower mass cluster paired galaxies experience another mechanism of gas depletion from their more massive counterpart, which is shown in the suppression experienced at $100 < r_p < 400$ h_{70}^{-1} kpc, and is likely the cause of the lack of SFR enhancement at $r_p < 40$ h_{70}^{-1} kpc. Since field galaxies are generally more gas rich than galaxies in denser environments, the mean SFR enhancements are greater in comparison. However, lower mass field paired galaxies show mean SFR enhancements that are consistent with those seen in the higher mass cluster paired galaxies at smallest separations. Since lower mass field galaxies experience suppression prior to the interaction, and show similar mean enhancements to cluster paired galaxies that experience quenching from their environment but no suppression from their lower mass companion, it can be deduced that the interaction mechanism affecting both populations in the different environments is producing galaxies with similar properties. This result points towards identical

interaction mechanisms producing galaxies with varying properties in different environments mainly due to the initial galaxy populations being inherently different due to environmental effects.

Chapter 4

Asymmetry

4.1 Introduction

Galaxy morphology is a classical subject with a rich history in astronomy. Morphology and classification were the first steps in the study of galaxies and their evolution, and as eloquently noted by Peng et al. (2002): "clues to galaxy formation lay hidden in the fine details of galaxy structure". Edwin Hubble (1889 - 1953) first observed that the majority of galaxies can be classified into two main categories: ellipticals and spirals (Hubble, 1936). Due to the intrinsic simplicity of this system, Hubble's classification with modifications remains in use to this day as the standard morphological classification of galaxies.

The definition for what constitutes an "environment" in an extra-galactic sense is not clearly defined and may seem arbitrary, however it has been long recognized that galaxy morphology is dependent on the environment (Hubble and Humason, 1931). One of the earliest quantitative measurements of systematic differences in morphology with local environment was shown in the morphology-density relation in nearby clusters (Dressler, 1980; Postman and Geller, 1984). The relation is defined as

the observed variation of the proportion of different Hubble types with local density, with ellipticals being more common in high-density environments, and spirals being more common in low-density regions. As explained in greater depth in Ch. 1, the morphology-density relation can be produced through many different mechanisms ranging from ISM-ICM interactions such as ram pressure stripping (Gunn and Gott, 1972; Nulsen, 1982), thermal evaporation (Cowie and Songaila, 1977; Nipoti and Binney, 2007), and starvation (Larson et al., 1980; Balogh et al., 2000; van den Bosch et al., 2008), to galaxy-cluster interactions such as tidal interactions (Byrd and Valtonen, 1990; Bekki et al., 2001; Gnedin, 2003; Coziol and Plauchu-Frayn, 2007), as well as galaxy-galaxy harassment (Moore et al., 1996; Fujita, 1998; Moore et al., 1999; Gnedin, 2003; Park and Hwang, 2009). Since ellipticals are generally more symmetrical than spirals, the morphology-density relation points towards having lower asymmetries in denser environments than in isolated systems.

Morphological differences are not just the product of environment. Hubble also noticed that $\sim 3\%$ of the extra-galactic nebulae cannot be classified as either ellipticals or spirals due to a lack in rotational symmetry and dominating nuclei. Therefore, he created a new category for those outliers and called them "irregular". Some of those irregular galaxies showed signs of long bridges and tails, and were often distorted. It was not until the 1950's that Fritz Zwicky described those filaments connecting the galaxies as tides and countertides and guessed correctly that the light emanating from them comes from stars. Zwicky also proposed a sequence of events leading to the creation of those "intergalactic bridges" (Zwicky, 1956, 1959). However, it took another couple of decades for a real breakthrough in understanding the possible impact of galaxy interactions on galaxy morphology to take place. This was achieved in 1972

by brothers Alar and Juri Toomre who correctly reproduced available observations of four interacting local galaxy pairs with their numerical models (Toomre and Toomre, 1972). They also made predictions that two strongly interacting disc galaxies would merge and produce a remnant that would become an elliptical galaxy. This discovery led to a new understanding of galaxy mergers and interactions and their impact on the global galaxy populations, especially on the effects of mergers and interactions in changing the galaxy morphologies. It is now known that the efficiency of galaxy-galaxy harassments (Moore et al., 1996) and mergers (Barnes and Hernquist, 1991) correlates with local density but decreases significantly with increasing relative velocities that lead to low interaction cross sections. Therefore, both mergers and interactions are considered very likely to contribute significantly to the morphology-density relation found in low to intermediate local density (e.g., Goto et al. 2003; Ma and Ebeling 2011).

Using the Galaxy Zoo 2 (Lintott et al., 2008) visual classification, Casteels et al. (2013) studied the morphological signatures of interactions for galaxy pairs in the SDSS. They show that many observable features in interacting galaxy pairs correlate with the projected separation between the pairs. The features included the obvious indicators of merging, such as disturbance and tidal tails, as well as regular features, such as spiral arms and bars. They report an enhancement in spiral features for galaxy pairs with $r_p \lesssim 70\ h_{70}^{-1}$ kpc, together with a decrease in the likelihood of identifying a bar at $r_p \lesssim 30\ h_{70}^{-1}$ kpc. Moreover, they show that loosely wound spiral arms can be used as a reliable signal of an interaction for pairs with r_p up to $\sim 100\ h_{70}^{-1}$ kpc. In terms of asymmetry, De Propris et al. (2007) used a volume limited sample of galaxies drawn from the Millennium Galaxy Catalogue (MGC; Liske et al., 2003) in

order to compare the use of galaxy asymmetry and pair proximity for measuring the galaxy merging fraction. They defined dynamically close pairs in their sample as galaxy pairs with projected separation $r_p < 100\ h_{70}^{-1}$ kpc and relative velocity difference $\Delta v < 500$ km s^{-1} and showed that galaxies in close pairs are generally more asymmetric than their isolated counterparts, with the degree of asymmetry in the pairs increasing for closer pairs. For pairs with $r_p < 20\ h_{70}^{-1}$ kpc, at least 35% showed significant asymmetry, and among asymmetric galaxies, 80% were found to be either interacting systems or merger remnants.

Therefore, it is clear that the large-scale environment in which galaxies reside has a substantial effect on their morphologies, and at the same time, the small-scale interactions also have a significant effect on the interacting galaxy pairs' morphologies. Plauchu-Frayn and Coziol (2010a,b) studied the influence of environment on the formation and evolution of galaxies in the nearby universe. In their work they used three different density environments: galaxies in compact groups, galaxies in isolated pairs, and isolated galaxies. They found no evidence of asymmetry in isolated galaxies, but significant asymmetries in isolated pairs and compact group galaxies. The key difference between the compact group galaxies and the isolated pairs was found in the lack of star formation in compact group galaxies, as opposed to the intense star formation produced in the isolated paired galaxies. This was also independently shown in Ellison et al. (2010), where paired galaxies in the lowest density environments showed the largest changes in SFR and asymmetry, while the closest pairs in the highest local densities only showed enhancements in asymmetry. These results indicate that even though interactions and mergers occur in all environments, the difference in the properties of the interacting galaxies can be attributed to the higher

density environments containing a larger fraction of gas poor galaxies. This causes higher density environments to contain a larger fraction of dry mergers and interactions than lower density environments. This is partially seen in the previous chapter in Figures 3.6 and 3.7, where the enhancement in SFR is largest for field galaxy pairs and non-existent for galaxies in denser environments with a more massive companion.

In order to establish that the results obtained in Ch. 3 are physically meaningful, this chapter deals with the difference in asymmetries between paired galaxies and their controls in each environment. The asymmetric residuals of Simard et al. (2011), based on the definitions of Simard et al. (2002) (which will be discussed in more detail in §4.2.1) are used to quantify the asymmetry of galaxies. By using carefully chosen controls, the effect of the interactions on the asymmetry of the paired galaxies can be observed independent of the effect of the environment. This allows for the comparison of the effect of the interaction on the paired galaxies in different environments to probe the differences in interactions within the various environments. In this chapter, I start with describing the sample in §4.2, and describing the properties used to quantify the asymmetry and morphology of the galaxies in the literature in general, and in this thesis in particular. In §4.3 I show the comparison between the paired galaxies' asymmetries and their controls for the different environments, and as was done in the previous chapter, split the sample into the paired galaxies with mass ratio > 1, and paired galaxies with mass ratio < 1 in order to provide further indications that the results obtained in the previous chapter are indeed physical. In §4.4 I provide a summary of the results and discuss possible physical causes and consequences, and provide a conclusion in §4.4.2.

4.2 Sample Description

The sample used in this chapter is obtained from the SDSS DR7, with the pair selection, environment definitions, and control sample finding described in detail in Chapter 2. The galaxies in the sample have redshifts within $0.01 < z < 0.20$, with total stellar masses obtained from the catalogue of Mendel et al. (2014). The paired and control galaxies are chosen using an adapted version of the method of Patton et al. (2013). The various environments in which galaxies reside are defined using the dark matter halo masses of Yang et al. (2007), with the definitions given in Table 2.3. In the end the sample contains $\sim$ 113,000 paired galaxies, with an average of 106 controls per paired galaxy (and a median of 29 controls per paired galaxy) that are matched in redshift, stellar mass, isolation, local density, and dark matter halo mass.

4.2.1 Morphology and Asymmetry Measurements

Describing galaxy structure has been a topic of debate since the discovery of galaxies. Currently the methods for measuring and quantifying galaxy structure can be split into two main categories: visual methods and quantitative methods. The apparent visual morphology classification is the classical approach towards understanding the structures of galaxies. The system of classification in use today has been developed using the works of Hubble (1926), de Vaucouleurs (1959), and Sandage (1961, 1975). Visual methods has had a recent resurgence due to citizen science projects such as Galaxy Zoo (Lintott et al., 2008), and Galaxy Zoo 2 (Willett et al., 2013), which provide online tools for non-scientists to visually classify over a million galaxies.

Visual morphology is a qualitative method for describing galaxy structure. One of the first quantitative approaches was done through the use of integrated light profiles.

These profiles are determined simply by measuring the average intensity of light at a given radius in a galaxy, and then finding how this intensity changes as a function of radius. The first detailed description of this was done by de Vaucouleurs (1948) using the measurements of light from photometry at different apertures for elliptical galaxies. Later, Sérsic (1963) found a more general form that better explains surface brightness profiles for different galaxy types, as seen in the following equation:

$$I(R) = I_0 \times \exp(-b(n) \times R/R_e^{1/n} - 1) \tag{4.1}$$

where $I(R)$ is the intensity at a projected distance R from the center of the galaxy, I_0 is the intensity at $R = 0$, and $b(n)$ is a constant whose value is determined such that the effective radius, R_e, contains half of the light within the galaxy and depends on the value of n. The shape of this profile is described generally by the Sérsic index, n, where the de Vaucouleurs profile is given by $n = 4$, and exponential disks by $n = 1$. With the advent of large galaxy surveys, codes such as GALFIT by Peng et al. (2002), and GIM2D by Simard et al. (2011) allow for a quick method of measuring the light profiles of many galaxies. Moreover, these codes are able to fit two dimensional profiles of galaxies with various forms such as the Sérsic, exponential, and de Vaucouleurs profile.

Fitting profiles is a parametric measurement of structure, however more recent measurement techniques involve non-parametric methods of measuring light distributions in galaxies. The first attempt at quantifying light concentration was done by Morgan (1962), although extensive and generally accepted quantitative measures were not done until the mid-1990s. The first deep images of the Hubble Space Telescope were the driver behind the earnest development of the non-parametric methods

(Schade et al., 1995; Abraham et al., 1996). Currently the most common methods for measuring galaxy structure in a non-parametric way are those designed to capture the major features of the underlying structures of galaxies. An example of some of the widely used non-parametric measurements are the CAS (concentration, asymmetry, clumpiness) system and the Gini/M_{20} parameters (see Bershady et al. (2000); Conselice et al. (2000); Conselice (2003), and Lotz et al. (2008) for more detail). The following is a brief description of some of these parameters:

- Concentration

  Defined as the ratio of two circular radii which contain 20% and 80% of the total galaxy flux. Concentration is then a measure of the intensity of light contained within a central region in comparison to a larger region in the outer-parts of a galaxy. Higher values of concentration indicate that larger amounts of light are contained in the central regions.

- Asymmetry

  Defined as the measure of how asymmetric a galaxy is after rotating along the center of the galaxy by 180 degrees (Conselice, 1997). It is one of the most commonly used indices among non-parametric methods, and can be thought of as an indicator of the fraction of the light in a galaxy that is emanating from non-symmetric components. The asymmetry is calculated using the following formula:

  $$A = \min\left(\frac{\Sigma|I_0 - I_{180}|}{\Sigma|I_0|}\right) - \min\left(\frac{\Sigma|B_0 - B_{180}|}{\Sigma|I_0|}\right) \tag{4.2}$$

  where I_0 represents the original galaxy image, and I_{180} represents the rotated image. The second term in this equation is used to correct for any background

noise.

- Clumpiness

  Clumpiness (or smoothness) is a parameter that describes the fraction of light in a galaxy which is contained in clumpy distributions. Conselice (2003) calculate it by blurring the original image of the galaxy, then subtracting the blurred image from the original, leaving a residual map that contains only the high frequency structures in the galaxy.

- Gini coefficient

  The Gini coefficient (G) is a statistical tool that is a measure of the evenness of the distribution of light in a galaxy. G is calculated by ordering the pixels of a galaxy based on their brightness and then counting them as part of the cumulative distribution. A high Gini value indicates a very unequal distribution (G = 1 indicates all the light is in 1 pixel), while low Gini values indicate a more equal distribution of light in the galaxy (G = 0 indicates that all pixels have equal brightness). A galaxy is then considered as a collection of n pixels, where each pixel has the flux f_i (where i ranges from 0 to n), whose Gini coefficient is calculated using the following equation

$$G = \frac{1}{|\overline{f}|n(n-1)} \sum_{i}^{n} (2i - n - 1)|f_i| \tag{4.3}$$

  where $\overline{f}$ is the average pixel flux value.

- M_{20}

  The M_{20} parameter is similar in concept to the concentration parameter, but

calculated differently. The value of M_{20} is the moment of the fluxes of the brightest 20% of light in a galaxy normalized by the total light moment of all pixels. A very negative M_{20} value indicates high concentration but, unlike the Concentration parameter, it does not imply a central concentration as the light could be concentrated anywhere in the galaxy.

The most appropriate measure of galaxy structure for the use of this thesis is the asymmetry of galaxies due to its sensitivity to the most common structural features of interacting galaxies (e.g, tidal tails and bridges). Therefore, in order to quantify the asymmetries of galaxies in the sample, the residuals (introduced by Schade et al. (1995) and expanded on by Simard et al. (2002) using GIM2D) are used. The calculation of the residuals of a galaxy are done by first constructing a symmetric model of the galaxy. A best-fit model of the galaxy is created using GIM2D, which uses the properties and parameters obtained from the symmetrical image of the galaxy. This best-fit model is then subtracted from the original image to obtain the residual R_{ij}, which is repeated again but with the image rotated by 180 degrees about the galaxy center to obtain the residual R_{ij}^{180}. The total and asymmetric residuals (R_T and R_A respectively) are then defined as:

$$R_T = \frac{\Sigma_{ij}(1/2)|R_{ij} + R_{ij}^{180}|}{\Sigma_{ij} I_{ij}} - \frac{\Sigma_{ij}(1/2)|B_{ij} + B_{ij}^{180}|}{\Sigma_{ij} I_{ij}} \tag{4.4}$$

$$R_A = \frac{\Sigma_{ij}(1/2)|R_{ij} - R_{ij}^{180}|}{\Sigma_{ij} I_{ij}} - \frac{\Sigma_{ij}(1/2)|B_{ij} - B_{ij}^{180}|}{\Sigma_{ij} I_{ij}} \tag{4.5}$$

where, I_{ij} is the original image, and B_{ij} and B_{ij}^{180} are the background residuals used to correct for the background noise. Figure 4.1 shows a sample of galaxies from the

SDSS together with their bulge+disk GIM2D model, and the residual image as seen in Simard et al. (2011).

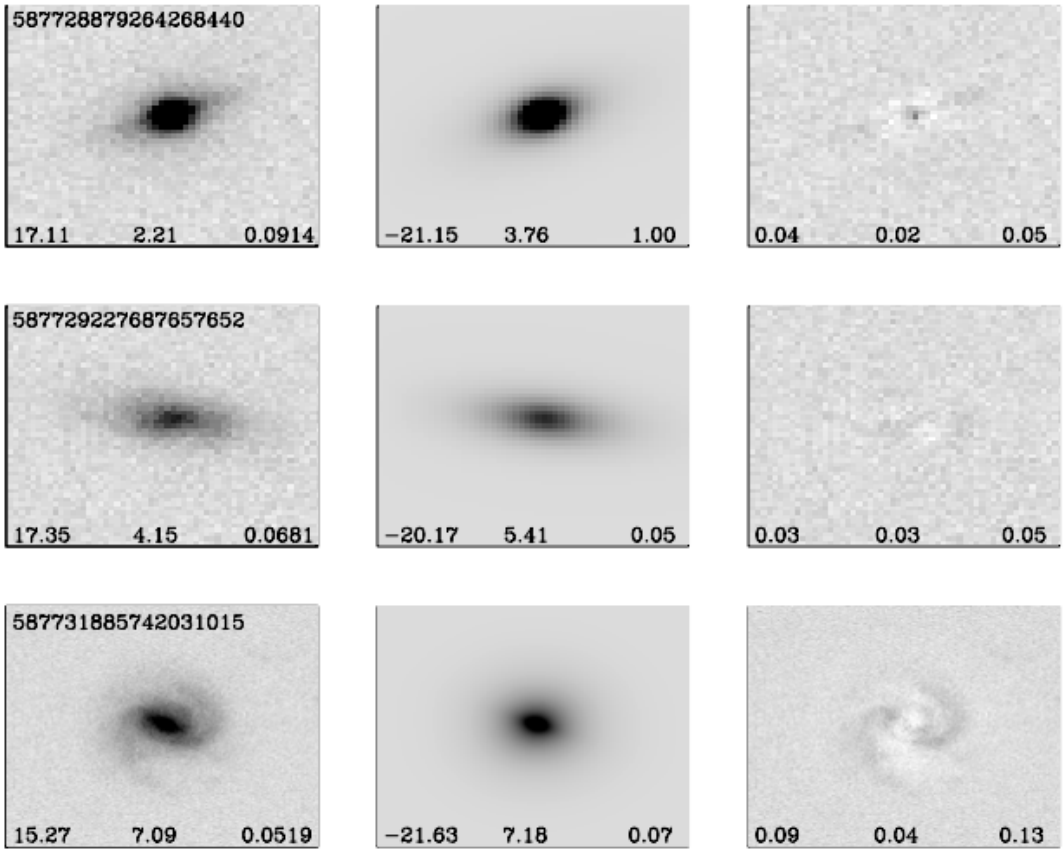

Figure 4.1: Mosaic of r-band GIM2D bulge+disk decompositions obtained from Simard et al. (2011). Three images are shown for each galaxy from left to right: galaxy cutout from SDSS corrected image, galaxy bulge+disk GIM2D model convolved with its point-spread function, and the GIM2D residual image. Each corrected image cutout is labeled by objID, apparent GIM2D model magnitude, GIM2D model half-light radius in arcsecs, and its SDSS redshift. Each GIM2D model image is labeled by GIM2D model rest-frame absolute magnitude, GIM2D model half-light radius in kiloparcsecs, and GIM2D model bulge fraction. Each GIM2D residual image is labeled by three asymmetry indices: R_T, R_A, and $R_T + R_A$.

Therefore, the total (R_T) and the asymmetric (R_A) residuals are the total and residual fluxes respectively, expressed as fractions of the total galaxy flux. The formalism used in equations 4.4 and 4.5 indicates that R_T represents the fraction of all structures in a galaxy that deviate from its GIM2D symmetric model, including features such as enhanced spiral arms and bars, as well as tidal tails and bridges. On the other hand R_A represents the fraction of asymmetric structures in a galaxy, which are more indicative of an interaction. Therefore, the R_A values obtained from the Simard et al. (2011) catalogue are used to quantify the asymmetry of galaxies for the remainder of this thesis.

4.3 R_A Enhancement

With the asymmetry of galaxies quantified using the asymmetric residuals (hereafter, R_A) of Simard et al. (2011), the comparison between the asymmetries of paired galaxies and their controls in the various environments can begin. Figure 4.2 shows the mean asymmetries of paired galaxies and their respective controls as functions of the paired galaxies' projected separations r_p (up to $r_p < 300\ h_{70}^{-1}$ kpc). It is worth noting that at large separations ($r_p > 150\ h_{70}^{-1}$ kpc) the average values of asymmetry in the paired sample should be similar to those in the control sample for each environment. This is seen in both plots in Figure 4.2, where at large separations the mean asymmetry in pairs in all environments is consistent with the mean asymmetry of their respective controls. This is due to the fact that at large separations the paired and control samples are both probing similar large-scale environmental effects, while at small separations, the small-scale interactions become evident as seen in the deviation between the mean asymmetries of paired galaxies and their controls. Moreover, it is

clear from both plots that the environment does indeed have a significant effect on the asymmetry of its residing galaxies, namely that lower density environments contain on average more asymmetric galaxies than higher density environments. This can be attributed to the morphology-density relation (Dressler, 1980), where the more symmetric ellipticals are more common in high-density environments, whereas lower density environments contain more spirals with larger R_A values.

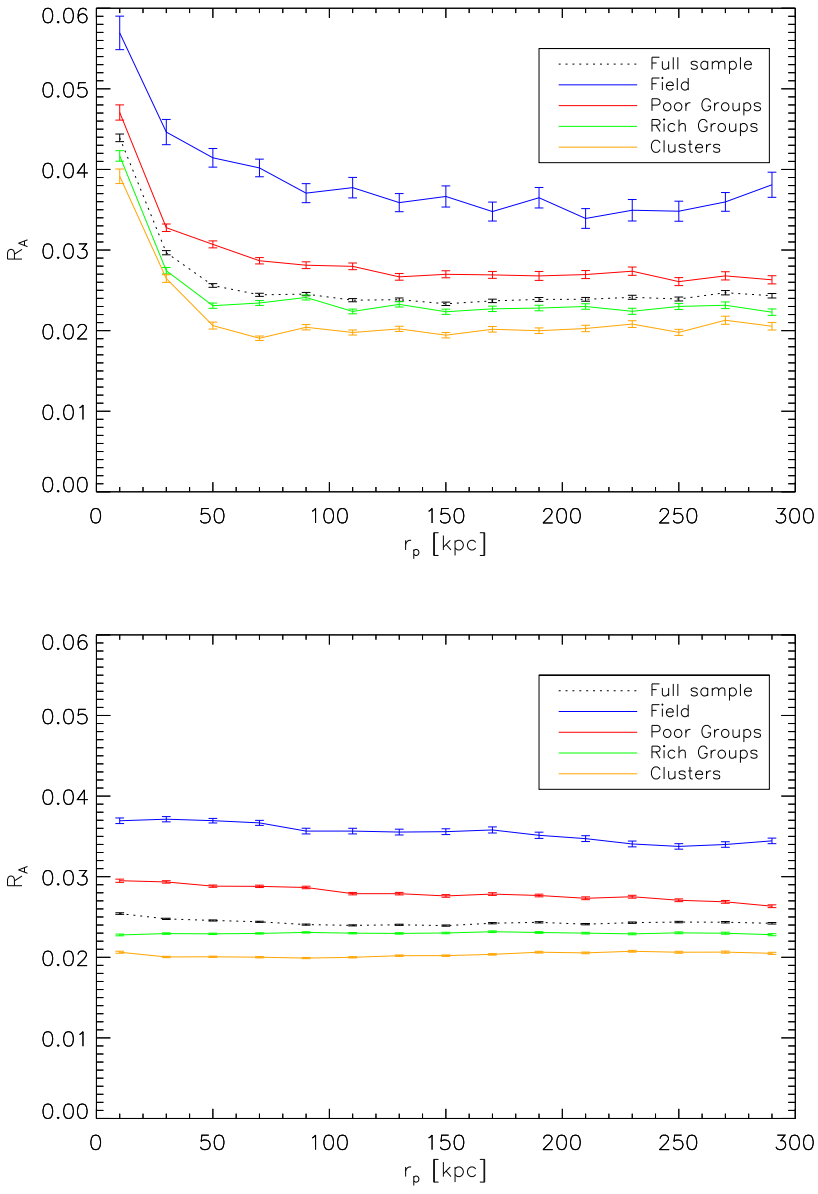

Figure 4.2: Plot showing the mean R_A of paired galaxies (top plot) and their associated control galaxies (bottom plot) as function of projected separation r_p in different environments. The colour scheme follows that of Figure 3.1. All error bars show the standard error in the mean.

In order to compare the paired galaxies' asymmetries to their respective controls, a similar procedure is used as with Ch. 3, in which the offset in the asymmetry is defined as the ratio of the paired galaxy' asymmetry to its controls' average asymmetry. This ratio can then be seen as:

$$\Delta R_A = \frac{R_{A,pairs}}{R_{A,controls}} \tag{4.6}$$

The enhancement in asymmetry is then plotted for paired galaxies in all environments in Figure 4.3, with the results summarized in Table 4.1. Unlike what was seen in the previous chapter with SFR enhancement, it can be clearly seen that the close pairs ($r_p < 20\ h_{70}^{-1}$ kpc) in clusters and rich groups experience a larger asymmetry enhancement than close pairs in poor groups and the field. Galaxies in denser environments tend to be exposed to a larger array of mechanisms that strip their gas reservoirs off prior to any interaction, which results in suppressed star formation during the interactions as opposed to field galaxies that maintain their gas reservoirs and thus experience a larger SFR enhancement during interactions. Therefore, even though SFR enhancements are generally accompanied by asymmetry enhancements since both are the products of galaxy interactions, if a galaxy's gas reservoirs were depleted prior to an interaction, it is expected that the galaxy may not exhibit a large SFR enhancement, while its asymmetry enhancement would remain significantly visible. Therefore, this could explain the fact that the SFR enhancements seen in the previous chapter are not translated into asymmetry enhancements as seen in Figure 4.3. Interactions cause the galaxies to develop asymmetrical features thus increasing their R_A values. Considering the morphology-density relation, denser environments tend to have a larger fraction of more elliptical galaxies, which have low R_A

values, while the field contains more spirals which have higher R_A values. Moreover, as seen in Figure 2.7, cluster galaxies have higher masses than field galaxies, and higher mass galaxies tend to be ellipticals rather than spirals, which indicates that there is a selection bias towards more symmetrical galaxies in clusters. Figure 2.6 also shows that clusters have preferentially higher redshifts than field galaxies, and the more distant galaxies tend to appear more symmetrical due to the lower resolution at greater distances, which also provides another source of bias in the sample towards lower asymmetry values in higher density environments. Therefore, the relative change from elliptical (low R_A) to interacting asymmetrical (higher R_A) is larger than a change from spirals with inherently higher R_A to interacting asymmetrical. Figure 4.4 uses the difference in R_A values between the paired galaxies and their controls in order to quantify the offset in asymmetry. This difference is calculated in the following manner:

$$R_{A,diff} = R_{A,pairs} - R_{A,controls} \tag{4.7}$$

With this formalism, it is clear from Figure 4.4 that at closest separations ($r_p < 20\ h_{70}^{-1}$ kpc) the R_A differences are similar to within the uncertainty for paired galaxies in all environments. This indicates that the change in asymmetry caused by interactions at close separations may be independent of the environment for the closest paired galaxies.

In both Figures 4.3 and 4.4 and Table 4.1, it is clear that signs of asymmetry are evident in paired galaxies in the field with separations $r_p < 130\ h_{70}^{-1}$ kpc, while paired galaxies in rich groups and clusters only show an offset in asymmetry at separations $r_p < 50\ h_{70}^{-1}$ kpc with no evidence of enhancement for more widely separated paired

galaxies. This difference may be caused by environmental effects on the control galaxies rather than the paired galaxies. In dense environments such as rich groups and clusters, many mechanisms affect the morphology of the residing galaxies, some of which have similar consequences to interactions on the morphologies of galaxies. Due to the increased density of rich groups and clusters, harassment is a common occurrence. Paired galaxies in dense environments have r_2 values that are only slightly larger than their r_p values since denser environments are by definition more crowded. Since control galaxies' r_p values are matched with the r_2 values of the paired galaxies, the controls' r_p values are similar to the paired galaxies' r_p values, and therefore, are susceptible to the same mechanisms that alter their morphologies causing the asymmetries of pairs and controls to be similar. However, as the paired galaxies' separation decreases, the influence of the interaction on the asymmetry of the interacting galaxies starts to overcome the effects from the larger-scale environment, and the difference between the paired and control galaxies' asymmetries becomes apparent.

All-in-all, the results obtained in this chapter are compatible with those from the previous chapter. The difference in the enhancements may be attributed to the gas fractions left in the galaxies prior to the interactions, where galaxies in denser environments had their gas reservoirs depleted and therefore experienced little SFR enhancement relative to galaxies in the field. In this section the asymmetry enhancement in close paired galaxies is seen to be independent of the environment, with the only difference occurring in the maximum separation at which an enhancement is visible and this can be attributed to the difference in the galaxy populations for different environments rather than a difference in the mechanism of the interactions.

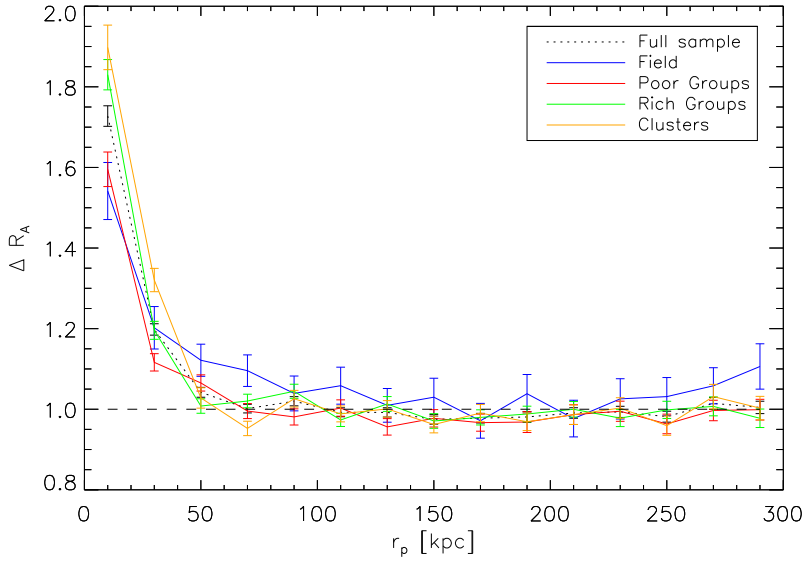

Figure 4.3: Mean R_A enhancement (ratio of pair R_A to control R_A) is plotted versus r_p for the pairs in different environments. The colour scheme follows that of Figure 3.1, with the dashed horizontal line denoting zero enhancement. All error bars show the standard error in the mean.

Table 4.1: R_A Enhancement

Environment	Enhancement for $r_p < 20\ h_{70}^{-1}$ kpc	r_p for zero enhancement
All	1.73 ± 0.03	$\sim 70\ h_{70}^{-1}$ kpc
Field	1.54 ± 0.07	$\sim 130\ h_{70}^{-1}$ kpc
Poor Group	1.60 ± 0.04	$\sim 70\ h_{70}^{-1}$ kpc
Rich Group	1.83 ± 0.04	$\sim 50\ h_{70}^{-1}$ kpc
Cluster	1.90 ± 0.06	$\sim 50\ h_{70}^{-1}$ kpc

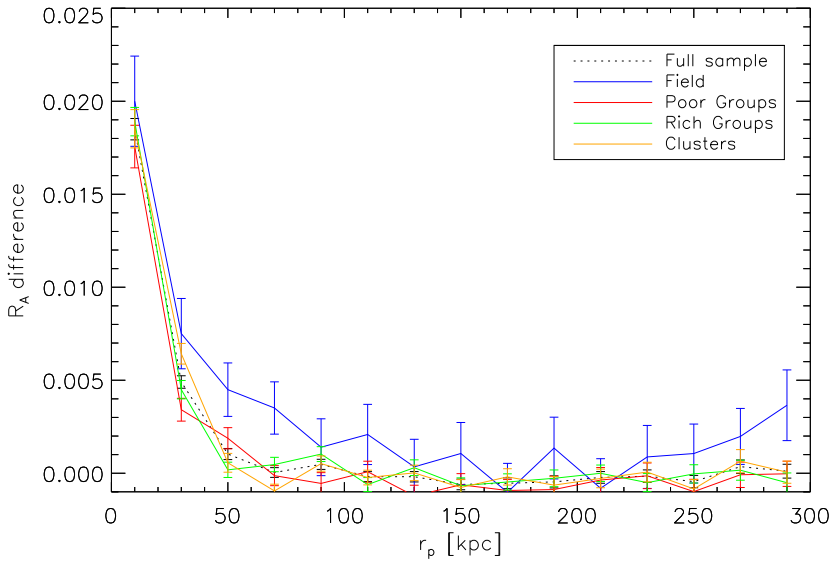

Figure 4.4: Mean R_A difference (difference between pair R_A and control R_A) is plotted versus r_p for the pairs in different environments. The colour scheme follows that of Figure 3.1, with the dashed horizontal line denoting zero enhancement. All error bars show the standard error in the mean.

4.4 Mass Ratio Dependence

In §3.5 we find evidence of interactions affecting the lower mass galaxy in a pair differently than the higher mass galaxy. Specifically, it is apparent that on average the lower mass galaxy in an interacting pair begins exhibiting signs of SFR suppression at separations of $r_p < 400\ h_{70}^{-1}$ kpc, while the higher mass galaxy shows no sign of interaction until closer separations ($r_p < 100\ h_{70}^{-1}$ kpc) where SFR enhancements are evident. At close separations, galaxies in interacting pairs (high and low mass) on average show signs of enhanced SFRs with varying degrees of enhancement that seem to be dependent on the amount of suppression experienced prior to the close interaction. Even though this SFR enhancement and suppression in paired galaxies provides

crucial information about the interaction, one cannot determine the physical mechanism driving those changes using the SFR information alone. Asymmetry probes a different set of parameters than SFRs; therefore, it provides a complimentary set of information that, combined with the SFR information, can provide evidence for the mechanism driving the changes in the interacting galaxies.

Just as was done in §3.5, the paired galaxy population is split into two categories: the lower mass paired galaxies with mass ratios < 1 (i.e., the paired galaxies with stellar masses that are lower than their companions' stellar masses) and the higher mass paired galaxies with mass ratios > 1. Figure 4.5 shows the asymmetry enhancement for the lower mass and higher mass paired galaxies separately as functions of projected pair separation r_p. It is clear that the two populations exhibit different behaviour in comparison with each other, as well as in comparison with Figure 3.7. The following list draws attention to the important results obtained from Figure 4.5:

- Rich group and cluster paired galaxies show more enhancement in asymmetry for the lower mass than the higher mass companions at closest separations ($r_p < 20\ h_{70}^{-1}$ kpc). This result is the opposite of what is seen with SFR enhancements, where the lower mass companions show almost no SFR enhancements, while the higher mass companions exhibit significant SFR enhancements. As previously noted, the significant enhancement in asymmetry for denser environments may be mostly driven by the larger change in asymmetry when low R_A elliptical galaxies interact, as opposed to the lower density environments containing a larger fraction of higher R_A spirals that show a relatively lower asymmetry change when interacting. The increased enhancement in asymmetry for the lower mass close companions accompanied by a lack in SFR enhancement can be

interpreted as the result of the removal of gas reservoirs prior to the interaction. During the interaction, even though the lower mass companion experiences larger forces from its more massive companion, no SFR enhancement is present, which may be due to a depleted gas reservoir in the lower mass companion.

- Field and poor group paired galaxies exhibit approximately similar asymmetry enhancements at closest separations ($r_p < 20\ h_{70}^{-1}$ kpc) for both high and low mass paired galaxies. Since this lack of difference in asymmetry enhancement is accompanied by greater SFR enhancements in higher mass paired galaxies than their lower mass closest neighbours, this result can also be seen as compatible with the previous interpretation that the lower SFR enhancements seen in the lower mass companions in the field are likely the consequence of the removal of the gas reservoirs prior to the interactions.

- Asymmetry enhancement in higher mass paired galaxies in all environments is on average the same for the closest separations ($r_p < 20\ h_{70}^{-1}$ kpc), while lower mass paired galaxies exhibit higher rates of enhancement with increased local density.

- No enhancement in asymmetry is seen for all paired galaxies (higher and lower mass) in all environments at separations $r_p > 150\ h_{70}^{-1}$ kpc, and at further inspection of the asymmetry in pairs extending to $r_p < 1000\ h_{70}^{-1}$ kpc, the mean asymmetry enhancement is found to be consistent with zero for all paired galaxies with $r_p > 150\ h_{70}^{-1}$ kpc. Therefore, the suppression in SFRs seen in paired galaxies with separations $100 < r_p < 400\ h_{70}^{-1}$ kpc is not accompanied by enhancement or suppression in the asymmetry. This further indicates that the

suppression is not caused by the removal of gas from within the galaxies since this mechanism would affect the morphology of the galaxies, but rather the removal of the gas reservoirs feeding into the galaxies that maintain their SFRs, which has no effect on the asymmetry of those galaxies. However, it could also indicate that the mechanism causing the suppression seen at $100 < r_p < 400\ h_{70}^{-1}$ kpc has occurred far enough in the past that any enhanced asymmetries are no longer detectable. This suppression could then be due to a past interaction with the more massive galaxy that caused starbursts to deplete the gas content of the lower mass galaxies, and given sufficient time any asymmetrical features caused by the interaction would have settled. The duration and timing of the various steps in an interaction that cause observed morphological changes depend heavily on the various properties of the interaction including galaxy orientations, orbital parameters, gas properties of the initial galaxies, and the presence of dust. However, it is generally agreed upon that the duration between the various interaction steps is of the order of 0.5 - 1.0 Gyr (Lotz et al., 2008). Given this time, and an average relative velocity between 200 - 800 km s^{-1}, the galaxies would be expected to have a separation between 100 - 400 h_{70}^{-1} kpc, which is the same separation where SFR suppression is observed.

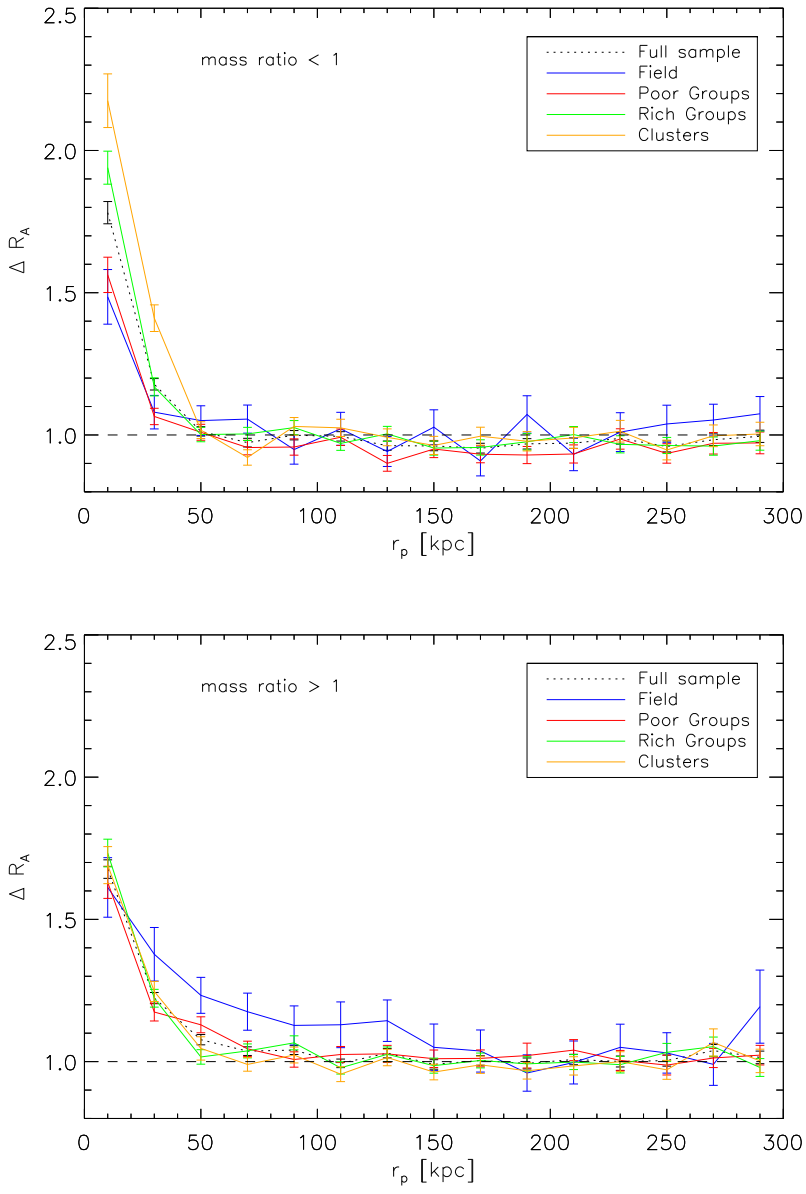

Figure 4.5: Mean R_A enhancement (ratio of pair R_A to control R_A) is plotted versus r_p for the pairs in different environments. The plot on top shows the lower mass paired galaxies, while the higher mass paired galaxies are plotted on the bottom. The colour scheme follows that of Figure 3.1, with the dashed horizontal line denoting zero enhancement. All error bars show the standard error in the mean.

4.5 Discussion & Conclusion

4.5.1 Discussion

To further probe the effects of interactions in different environments, a sample of galaxy pairs with wide separations from the SDSS DR7 was used in this chapter. The sample included a carefully chosen control sample and asymmetries quantified using the GIM2D R_A values described in Simard et al. (2002) and summarized in §4.2.1. Similar to the results obtained in the previous chapter with star formation rates, the environments seem to have a visible effect on the average asymmetry values of their residing galaxies. Namely, galaxies in denser environments are on average less asymmetrical than galaxies in lower density environments. This is expected from the morphology-density relation, where spirals are more common in the field, while ellipticals are more common in rich groups and clusters. It is also the product of the higher density environments containing galaxies with higher redshifts and stellar masses than the field environment. This bias causes higher density galaxies to appear more symmetrical than galaxies in lower densities.

It is evident that for close interacting galaxies in all environments, signs of asymmetry enhancement are visible with varying degrees. Unlike SFR enhancement, the largest difference in asymmetry between paired galaxies and their controls is seen in close paired galaxies in clusters, followed by paired galaxies in rich groups, poor groups, and lastly in the field. This difference in the rate of enhancement can be attributed to the inherent low asymmetry of galaxies in higher densities without a close neighbour versus the inherently higher asymmetry of galaxies in the field. The low asymmetry of ellipticals causes any changes in shape due to an interaction to be more easily distinguished and to have a greater difference relative to the control than with

spirals. Since spirals are more abundant in the field environment, control galaxies will tend to contain more spirals with higher R_A values than the control galaxies for clusters that contain more ellipticals. Therefore, when comparing the asymmetry of interacting galaxies with $r_p < 20\ h_{70}^{-1}$ kpc to their respective average control R_A, the difference is expected to be larger for cluster than for field paired galaxies. In fact, when the enhancement in asymmetry is defined as the absolute difference between the paired galaxies' R_A values and those of their controls, close paired galaxies in all environments showed the same level of enhancement regardless of the environment in which they reside.

Looking at field galaxies, it is clear that paired galaxies in this environment exhibit signs of enhanced asymmetry in comparison with their controls at separations much larger than for paired galaxies in denser environments. Evidence of enhanced asymmetry is visible in field paired galaxies at $r_p < 130\ h_{70}^{-1}$ kpc, while denser environments only exhibit enhanced asymmetry at $r_p < 50\ h_{70}^{-1}$ kpc. This difference between interactions is not necessarily the product of different mechanisms of interactions depending on the environment, but can rather be the product of the choice of controls for the paired galaxies in different environments. Among other properties, control galaxies are matched in local density, isolation, and environment class (N_2, r_2, and halo mass) with their respective paired galaxy. Therefore, the control galaxies chosen for field paired galaxies are far more isolated than the control galaxies selected for cluster paired galaxies. It is then safe to assume that the control galaxies of denser environments are continuously encountering various mechanisms that affect their morphologies and causes them to have asymmetry values similar to paired galaxies at wide separations ($r_p > 80\ h_{70}^{-1}$ kpc). On the other hand, control galaxies

in the field encounter far less harassment and gravitational pulls since they are more isolated, therefore small changes in the asymmetry of interacting galaxies even at wide separations can be visible since their controls do not show similar changes.

These results support the interpretation of the previous chapter where the differences in the properties of interacting galaxies in different environments are attributed to assembly bias, where the galaxy populations in the different environments are what drives the differences in interactions rather than an interaction mechanism affecting identical galaxies in different environments differently. Evidence that supports this conclusion in the previous chapter was found by investigating the SFR enhancement in paired galaxies with a stellar mass greater than their companion's (referred to here as higher mass galaxies), and comparing it to the SFR enhancements in paired galaxies with stellar mass lower than their companion's (lower mass galaxies). Therefore, in this chapter, the sample is also divided by mass ratio and the enhancements in asymmetry is investigated. It is found that the lower mass paired galaxies exhibited larger asymmetry enhancements together with lower SFR enhancements in comparison with their higher mass companions at closest separations. Moreover, no evidence for asymmetry enhancement is seen for paired galaxies in all environments at wide separations, while star formation suppression is seen at separations $100 < r_p < 400\ h_{70}^{-1}$ kpc. The lack of asymmetry enhancement at wide separations indicates that the mechanism driving the suppression in star formation is either affecting the gas reservoir outside the galaxy rather than the gas content of the galaxy itself, or has occurred at a sufficiently earlier time such that any asymmetries caused by the interaction would have settled. The depletion of the gas that feeds the star formation in the galaxy can cause starvation to occur and reduce the SFR of the

lower mass galaxy without affecting its asymmetry. At closer separations, little to no SFR enhancements together with substantial asymmetry enhancements are seen for the lower mass paired galaxies while the higher mass companions exhibit greater SFR enhancements and lower asymmetry enhancements at $r_p < 50\ h_{70}^{-1}$ kpc. This goes to further support the interpretation that the interaction mechanisms are independent of the environment, and the differences in galaxy populations are what is causing the various degrees of enhancements in interactions in different environments.

4.5.2 Conclusion

The comparison of the asymmetry enhancements of paired galaxies in different environments provides further support for the findings of the previous chapter, as well as an indication to the physical mechanism that causes the SFR suppression at $100 < r_p < 400\ h_{70}^{-1}$ kpc. As expected from the morphology-density relation, galaxies in denser environments are found to have lower average asymmetry values than galaxies in lower density environments, which provides confidence in the environmental classification criteria as well as the asymmetry values used.

When comparing the asymmetry enhancements in paired galaxies in different environments, it is evident that paired galaxies in denser environments have on average higher asymmetry enhancements than paired galaxies in less dense environments at closest separations. However, when comparing the asymmetry offset (absolute difference) between the paired and control galaxies' asymmetries, it is evident that the asymmetry offset is independent of the environment since the mean asymmetry offset for paired galaxies in all environments is the same to within the uncertainty. This result points towards a common interaction mechanism for all environments with

the difference in asymmetry enhancement possibly explained by the difference in the populations of galaxies in different environments. Therefore, the findings in this chapter are compatible with those from the SFR enhancements obtained in the previous chapter, where it is found that assembly bias may be the most important contributing factor in the difference in enhancements seen at the smallest separations in different environments.

Suppression in SFRs was found in the previous chapter in the separation range of $100 < r_p < 400\ h_{70}^{-1}$ kpc; however, no difference in asymmetry between paired and control galaxies was observed in this range of projected separations in all environments. The lack of asymmetry enhancement or suppression at those separations combined with a suppression in SFRs points towards a mechanism of interaction that affects the gas content of the galaxy. This is also supported by the fact that at closest separations ($r_p < 20\ h_{70}^{-1}$ kpc) paired galaxies with stellar mass lower than their closest neighbours have on average higher asymmetry enhancements and lower SFR enhancements than their more massive companion. This result supports the conclusions of the previous chapter, whereby either a lower mass galaxy has its gas reservoirs depleted by the more massive galaxy or that the lower mass galaxy had an earlier interaction that caused its gas content to be consumed in early starbursts.

Chapter 5

Summary and Conclusions

5.1 Summary of Results

In this thesis we examined the effects of interactions on the SFR and asymmetry of paired galaxies in different environments. The aim of this research is to separate the small-scale interaction effects from the large-scale environmental effects on galaxies. This allowed us to determine whether varying interaction outcomes in different environments are caused by differing interaction mechanisms or whether they are due to different galaxy populations inhabiting different environments. This question was addressed in this thesis statistically by extending the pair selection to larger separations, adequately defining the environments, and carefully matching controls. The sample used here was extracted from the SDSS DR7 ($0.01 < z < 0.20$), where galaxies were required to have secure redshifts and be classified both photometrically and spectroscopically as galaxies. Steps were taken to minimize the effects of biases and incompleteness in the sample including limits on the extinction-corrected Petrosian apparent magnitudes, a minimum limit on the distance to the boundary of the survey, and statistical weights to correct for fibre incompleteness.

The paired galaxies sample was selected by defining the closest neighbour to every galaxy as the closest galaxy with a relative velocity of 1000 km s^{-1} in order to avoid projected pairs, and a mass ratio between 0.1 and 10 in order to avoid minor mergers. In order to clean the sample of some of the projected paired galaxies, we developed a method that utilizes the minimum binding energy of paired galaxies, calculated using the projected separations, stellar masses, and relative velocities of paired galaxies. This method allows for the removal of some of the projected paired galaxies that are not interacting and contaminate the sample. The different environmental classes (field, poor groups, rich groups, and clusters) were defined using the dark matter halo masses. The control sample was matched with the paired galaxies in stellar mass (within 0.1 dex), redshift (within 0.01), local density (N_2, within 10%), isolation (r_2, within 10%), and environmental class (dark matter halo mass, within 0.1 dex). A minimum of 10 controls were required for each paired galaxy, and if 10 were not found the limits were increased in a manner that never let them exceed twice the original limits until 10 control galaxies were found. These methods result in finding $\sim 321,000$ paired galaxies (out of an original sample of $\sim 506,000$ galaxies), with an average of 106 control galaxies per paired galaxy (and a median of 29).

The environmental definition and controls finding were tested by observing the mean SFR and asymmetry of the paired and control galaxies as function of pair separation in the different environments. The sSFR of field galaxies was found to be the highest while cluster galaxies had the least mean sSFR, which is consistent with previous findings. Moreover, as the morphology-density relation predicts, field galaxies are found to be on average the most asymmetrical while cluster galaxies were the most symmetrical. The similarity in the distributions of the various properties

between the paired and control sample, together with the flatness of mean SFR and R_A of the control sample when plotted as functions of r_p, and the similarity in the properties of the paired sample and control sample at large r_p provides confidence in the control selection and the ability to distinguish the small-scale interaction effects from the large-scale environmental effects.

The enhancements in SFRs and asymmetries at close separations ($r_p < 40\ h_{70}^{-1}$ kpc) were mostly consistent with previous findings. Namely, field paired galaxies showed the largest enhancement in SFR and the smallest in asymmetry, while cluster paired galaxies showed the greatest enhancement in asymmetry and the lowest in SFR (but still showed a statistically significant enhancement) at $r_p < 40\ h_{70}^{-1}$ kpc. However, when considering asymmetry offsets rather than enhancements, paired galaxies at $r_p < 40\ h_{70}^{-1}$ kpc showed similar differences in R_A in all environments in comparison with the mean R_A values of their respective controls. Moreover, suppression in mean SFRs were observed in all environments at separation $r_p > 100\ h_{70}^{-1}$ kpc, and when the plots were extended to include paired galaxies at $r_p < 1000\ h_{70}^{-1}$ kpc rather than $r_p < 300\ h_{70}^{-1}$ kpc, it was found that the suppression is visible in paired galaxies with $100 < r_p < 400\ h_{70}^{-1}$ kpc in all environments. Splitting the sample into the low mass paired galaxies whose closest neighbour is more massive than they are (i.e., have mass ratio < 1), and high mass paired galaxies whose closest neighbour is less massive than they are (i.e., have mass ratio > 1), revealed that the suppression at $100 < r_p < 400\ h_{70}^{-1}$ kpc is only visible in lower mass companions in all environments, but not in their higher mass companions. Furthermore, this suppression is not seen in the mean asymmetries of those galaxies.

Together with the SFR suppression at $100 < r_p < 400\ h_{70}^{-1}$ kpc, the lower mass

paired galaxies showed reduced SFR enhancements at closest separations ($r_p < 40$ h_{70}^{-1} kpc) in comparison with higher mass paired galaxies in the same environment. In fact, lower mass paired galaxies in dense environments show enhancements consistent with zero at $r_p < 40$ h_{70}^{-1} kpc, indicating the possibility of having the effects of the interactions cancel out due to both more enhancement and more suppression in close paired galaxies in dense environments. Moreover, unlike SFR enhancements, lower mass paired galaxies showed larger R_A enhancements than higher mass paired galaxies in the same environment classes.

5.2 Conclusions

The results of this thesis support a few possible interaction scenarios. The first possibility would be that in which galaxies interacting with more massive galaxies experience the effects of the interaction at large separations, which result in the depletion of their gas reservoirs prior to the separation required for bursts of star formation to occur. The SFR suppression experienced by lower mass paired galaxies is not accompanied by deviations in asymmetry at the same separations. This result indicates that the gas outside the lower mass galaxies (i.e, the gas that is responsible for maintaining the SFR in the galaxy, but is not considered when measuring the asymmetry of the galaxy) is possibly removed by the interaction with the more massive galaxy at large separations. This scenario results in decreased SFR enhancements at closer separations due to the depleted gas reservoirs in comparison with the higher mass galaxies that maintain their gas reservoirs prior to the close encounter. The results obtained in this thesis support such a framework, which can be used to determine the cause of varying interaction results in different environments.

Another possible explanation for the results would be galaxies experiencing suppression following bursts of star formation during a previous encounter with the more massive companion at a time sufficiently distant in the past to allow the resultant shape asymmetries to have settled out. Following an interaction with a massive galaxy, the lower mass companion experiences intense bursts of star formation that consume its star forming gas. As the galaxies separate after pericentre passage, the lower mass galaxy at intermediate separations ($100 < r_p < 400\ h_{70}^{-1}$ kpc) would exhibit signs of suppression in star formation due to the lack of star forming gas from the previous encounter, but would show no signs of asymmetry enhancements as enough time would have passed for the galaxy to settle into a symmetric shape. In fact, using a reasonable range for the duration between the various stages of observed morphological changes in an interaction of 0.5 - 1.0 Gyr, and average relative velocities between 200 - 800 km s^{-1}, such galaxies would be expected to be found at separations between 100 - 400 h_{70}^{-1} kpc.

Both scenarios allude to the assembly bias being the more likely driver behind the varying enhancements at small separations in different environments rather than interaction mechanisms being different. This conclusion is mainly motivated by the difference in SFR enhancements of the lower mass field paired galaxies in comparison with their more massive companions at smallest separations, together with the similarity in enhancements with the higher mass cluster paired galaxies. Namely, lower mass field paired galaxies experience suppression from their higher mass companions due to a possible loss of gas from their reservoirs, while higher mass cluster galaxies are suppressed by interactions with their dense environment which results in

them being gas poor. Both of these populations produce similar levels of enhancements during small-scale interactions. Therefore, it can be concluded that interaction mechanisms are the same for all environments, and the various populations of galaxies in different environments are likely what causes the interactions between galaxies in those environments to produce different results.

5.3 Future work

In this thesis, contamination of the sample due to projection effects are one of the major causes of error. In an attempt to reduce this contamination while maintaining the ability to select paired galaxies at large separations, we developed the method of using the minimum binding energy of pairs to remove some of those that are not bound. This method suffers from a few downfalls that can be corrected for given more time and resources. One such problem is the fact that some pairs are removed from the sample due to their E_{min} being greater than 0, but can still be bound due to dynamical friction. This is beyond the scope of this thesis, but given more time can be included in the calculation of the binding energy for better results. Moreover, the removal of some projected pairs does not guarantee that the sample is free of them. Many projected pairs remain selected as bound due to our inability to measure tangential velocities, however this can be rectified with better future technology. Furthermore, our inability to differentiate peculiar velocities from redshift velocities cause us to lose information on the depth separation between galaxies. This can also be corrected by more accurate measures of galaxy distances given better technology in the distant future. It is worth mentioning that technology remains a significantly long way from being able to achieve such goals. Currently with the

most accurate technology available (i.e., the GAIA Mission), the positions of objects brighter than magnitude 15 can be measured to an accuracy of 24 micro arc seconds (Eyer et al., 2013). An object of magnitude 15 that is at redshift 0.1, would cover 24 micro arcsec in $\sim$ 410 years if it had a tangential velocity of 1000 km s^{-1}, or $\sim$ 820 years if its tangential velocity is 500 km s^{-1}. Therefore, significant improvements in technology are required before measuring tangential velocities becomes a reality.

This thesis only dealt with the SFRs and asymmetries of the interacting galaxies; however there is a broad list of properties of galaxies that can also be studied such as colours, AGN fraction, metallicities, etc. The examination of those properties can provide further information on the difference between paired galaxies and their controls in different environments. This would allow for more confidence in the conclusion that we arrived at in this thesis, as well as possible other details that might be of interest.

We have only attempted to answer the main question of this thesis using a statistical approach to a large sample of galaxies. However, the results obtained in such a manner will always be questionable due to biases and contamination of the sample that are difficult to account for, as well as errors in the measurement of the properties being tested due to technological limitations. This is usually rectified by the use of numerical simulations of interacting galaxies in different situations that can then support or confirm the conclusion obtained from the results. In this thesis, since the environment is a variable that cannot be ignored, simulations need to account for all the different interactions and mechanisms that affect galaxies in different environments. Therefore, to truly separate the small-scale interaction effects from the large-scale environmental effects, simulations need to include the large scale

environment with enough accuracy to simulate the small-scale interactions between the galaxies. This is extremely computationally expensive, and was quite difficult to accomplish even with the availability of large simulations such as the Millennium Run (Springel et al., 2005). However, new technology is making it possible to simulate large-scale environments with the needed resolution to produce accurate small-scale interaction simulations. As an example, the Illustris Project (Vogelsberger et al., 2014) provides an unprecedented combination of high resolution, total volume, and physical fidelity. Moreover, unlike previous large simulations that included only dark matter particles, the Illustris simulation is hydrodynamical and, as a result, directly traces star formation. Therefore, given the advancement in technology, it is possible to test the conclusion of this thesis and arrive at more robust and physically supported conclusions.

Bibliography

M. G. Abadi, B. Moore, and R. G. Bower. Ram pressure stripping of spiral galaxies in clusters. *MNRAS*, 308:947–954, October 1999. doi: 10.1046/j.1365-8711.1999.02715.x.

K. N. Abazajian, J. K. Adelman-McCarthy, M. A. Agüeros, S. S. Allam, C. Allende Prieto, D. An, K. S. J. Anderson, S. F. Anderson, J. Annis, N. A. Bahcall, and et al. The Seventh Data Release of the Sloan Digital Sky Survey. *ApJS*, 182:543, June 2009. doi: 10.1088/0067-0049/182/2/543.

R. G. Abraham, S. van den Bergh, K. Glazebrook, R. S. Ellis, B. X. Santiago, P. Surma, and R. E. Griffiths. The Morphologies of Distant Galaxies. II. Classifications from the Hubble Space Telescope Medium Deep Survey. *ApJS*, 107:1, November 1996. doi: 10.1086/192352.

L. E. Abramson, D. D. Kelson, A. Dressler, B. Poggianti, M. D. Gladders, A. Oemler, Jr., and B. Vulcani. The Mass-independence of Specific Star Formation Rates in Galactic Disks. *ApJL*, 785:L36, April 2014. doi: 10.1088/2041-8205/785/2/L36.

M. S. Alonso, P. B. Tissera, G. Coldwell, and D. G. Lambas. Galaxy pairs in the 2dF survey - II. Effects of interactions on star formation in groups and clusters. *MNRAS*, 352:1081–1088, August 2004. doi: 10.1111/j.1365-2966.2004.08002.x.

M. Sol Alonso, D. G. Lambas, P. Tissera, and G. Coldwell. Effects of galaxy interactions in different environments. *MNRAS*, 367:1029–1038, April 2006. doi: 10.1111/j.1365-2966.2006.10020.x.

S. Alonso, V. Mesa, N. Padilla, and D. G. Lambas. Galaxy interactions. II. High density environments. *A&A*, 539:A46, March 2012. doi: 10.1051/0004-6361/201117901.

H. Arp. *Atlas of peculiar galaxies*. Pasadena: California Inst. Technology, 1966.

I. K. Baldry, K. Glazebrook, J. Brinkmann, Ž. Ivezić, R. H. Lupton, R. C. Nichol, and A. S. Szalay. Quantifying the Bimodal Color-Magnitude Distribution of Galaxies. *ApJ*, 600:681–694, January 2004. doi: 10.1086/380092.

J. A. Baldwin, M. M. Phillips, and R. Terlevich. Classification parameters for the emission-line spectra of extragalactic objects. *PASP*, 93:5–19, February 1981. doi: 10.1086/130766.

M. L. Balogh, S. L. Morris, H. K. C. Yee, R. G. Carlberg, and E. Ellingson. Differential Galaxy Evolution in Cluster and Field Galaxies at z $\sim$ 0.3. *ApJ*, 527:54–79, December 1999. doi: 10.1086/308056.

M. L. Balogh, J. F. Navarro, and S. L. Morris. The Origin of Star Formation Gradients in Rich Galaxy Clusters. *ApJ*, 540:113–121, September 2000. doi: 10.1086/309323.

M. L. Balogh, S. L. McGee, D. J. Wilman, A. Finoguenov, L. C. Parker, J. L. Connelly, J. S. Mulchaey, R. G. Bower, M. Tanaka, and S. Giodini. Direct observational evidence for a large transient galaxy population in groups at $0.85 < z < 1$. *MNRAS*, 412:2303–2317, April 2011. doi: 10.1111/j.1365-2966.2010.18052.x.

J. Barnes, L. Hernquist, and F. Schweizer. Colliding galaxies. *Scientific American*, 265:40–47, August 1991. doi: 10.1038/scientificamerican0891-40.

J. E. Barnes. Encounters of disk/halo galaxies. *ApJ*, 331:699–717, August 1988. doi: 10.1086/166593.

J. E. Barnes and L. E. Hernquist. Fueling starburst galaxies with gas-rich mergers. *ApJL*, 370:L65–L68, April 1991. doi: 10.1086/185978.

E. J. Barton, J. A. Arnold, A. R. Zentner, J. S. Bullock, and R. H. Wechsler. Isolating Triggered Star Formation. *ApJ*, 671:1538–1549, December 2007. doi: 10.1086/522620.

K. Bekki and W. J. Couch. Starbursts from the Strong Compression of Galactic Molecular Clouds due to the High Pressure of the Intracluster Medium. *ApJL*, 596: L13–L16, October 2003. doi: 10.1086/379054.

K. Bekki, W. J. Couch, and Y. Shioya. Tidal Truncation of Gas Replenishment and Global Suppression of Galactic Star Formation in Distant Clusters. *PASJ*, 53: 395–400, June 2001. doi: 10.1093/pasj/53.3.395.

E. F. Bell, D. H. McIntosh, N. Katz, and M. D. Weinberg. The Optical and Near-Infrared Properties of Galaxies. I. Luminosity and Stellar Mass Functions. *ApJS*, 149:289–312, December 2003. doi: 10.1086/378847.

E. F. Bell, C. Wolf, K. Meisenheimer, H.-W. Rix, A. Borch, S. Dye, M. Kleinheinrich, L. Wisotzki, and D. H. McIntosh. Nearly 5000 Distant Early-Type Galaxies in COMBO-17: A Red Sequence and Its Evolution since z $\sim$ 1. *ApJ*, 608:752–767, June 2004. doi: 10.1086/420778.

M. A. Bershady, A. Jangren, and C. J. Conselice. Structural and Photometric Classification of Galaxies. I. Calibration Based on a Nearby Galaxy Sample. *AJ*, 119: 2645–2663, June 2000. doi: 10.1086/301386.

E. Bertin and S. Arnouts. SExtractor: Software for source extraction. *A&AS*, 117: 393–404, June 1996.

J. Binney and S. Tremaine. *Galactic dynamics*. Princeton, NJ, Princeton University Press, 1987.

M. R. Blanton and J. Moustakas. Physical Properties and Environments of Nearby Galaxies. *ARA&A*, 47:159–210, September 2009. doi: 10.1146/annurev-astro-082708-101734.

A. F. L. Bluck, J. T. Mendel, S. L. Ellison, J. Moreno, L. Simard, D. R. Patton, and E. Starkenburg. Bulge mass is king: the dominant role of the bulge in determining the fraction of passive galaxies in the Sloan Digital Sky Survey. *MNRAS*, 441: 599–629, June 2014. doi: 10.1093/mnras/stu594.

F. Bournaud, C. J. Jog, and F. Combes. Galaxy mergers with various mass ratios: Properties of remnants. *A&A*, 437:69–85, July 2005. doi: 10.1051/0004-6361:20042036.

G. B. Brammer, K. E. Whitaker, P. G. van Dokkum, D. Marchesini, I. Labbé, M. Franx, M. Kriek, R. F. Quadri, G. Illingworth, K.-S. Lee, A. Muzzin, and G. Rudnick. The Dead Sequence: A Clear Bimodality in Galaxy Colors from z = 0 to z = 2.5. *ApJL*, 706:L173–L177, November 2009. doi: 10.1088/0004-637X/706/1/L173.

J. Brinchmann, S. Charlot, S. D. M. White, C. Tremonti, G. Kauffmann, T. Heckman, and J. Brinkmann. The physical properties of star-forming galaxies in the low-redshift Universe. *MNRAS*, 351:1151–1179, July 2004. doi: 10.1111/j.1365-2966.2004.07881.x.

H. Butcher and A. Oemler, Jr. The evolution of galaxies in clusters. I - ISIT photometry of C1 0024+1654 and 3C 295. *ApJ*, 219:18–30, January 1978. doi: 10.1086/155751.

G. Byrd and M. Valtonen. Tidal generation of active spirals and S0 galaxies by rich clusters. *ApJ*, 350:89–94, February 1990. doi: 10.1086/168362.

K. R. V. Casteels, S. P. Bamford, R. A. Skibba, K. L. Masters, C. J. Lintott, W. C. Keel, K. Schawinski, R. C. Nichol, and A. M. Smith. Galaxy Zoo: quantifying morphological indicators of galaxy interaction. *MNRAS*, 429:1051–1065, February 2013. doi: 10.1093/mnras/sts391.

S. Chandrasekhar. Dynamical Friction. I. General Considerations: the Coefficient of Dynamical Friction. *ApJ*, 97:255, March 1943. doi: 10.1086/144517.

S. Charlot and M. Longhetti. Nebular emission from star-forming galaxies. *MNRAS*, 323:887–903, May 2001. doi: 10.1046/j.1365-8711.2001.04260.x.

C. J. Conselice. The Symmetry, Color, and Morphology of Galaxies. *PASP*, 109:1251–1255, November 1997. doi: 10.1086/134004.

C. J. Conselice. The Relationship between Stellar Light Distributions of Galaxies and Their Formation Histories. *ApJS*, 147:1–28, July 2003. doi: 10.1086/375001.

C. J. Conselice, M. A. Bershady, and J. S. Gallagher, III. Physical morphology and triggers of starburst galaxies. *A&A*, 354:L21–L24, February 2000.

M. C. Cooper, A. Gallazzi, J. A. Newman, and R. Yan. Galaxy assembly bias on the red sequence. *MNRAS*, 402:1942–1958, March 2010. doi: 10.1111/j.1365-2966.2009.16020.x.

L. L. Cowie and A. Songaila. Thermal evaporation of gas within galaxies by a hot intergalactic medium. *Nature*, 266:501–503, April 1977. doi: 10.1038/266501a0.

T. J. Cox, P. Jonsson, R. S. Somerville, J. R. Primack, and A. Dekel. The effect of galaxy mass ratio on merger-driven starbursts. *MNRAS*, 384:386–409, February 2008. doi: 10.1111/j.1365-2966.2007.12730.x.

R. Coziol and I. Plauchu-Frayn. Evidence for Tidal Interactions and Mergers as the Origin of Galaxy Morphology Evolution in Compact Groups. *AJ*, 133:2630–2642, June 2007. doi: 10.1086/513514.

D. J. Croton, L. Gao, and S. D. M. White. Halo assembly bias and its effects on galaxy clustering. *MNRAS*, 374:1303–1309, February 2007. doi: 10.1111/j.1365-2966.2006.11230.x.

O. Cucciati, L. Tresse, O. Ilbert, O. Le Fèvre, B. Garilli, V. Le Brun, P. Cassata, P. Franzetti, D. Maccagni, M. Scodeggio, E. Zucca, G. Zamorani, S. Bardelli, M. Bolzonella, R. M. Bielby, H. J. McCracken, A. Zanichelli, and D. Vergani. The star formation rate density and dust attenuation evolution over 12 Gyr with the VVDS surveys. *A&A*, 539:A31, March 2012. doi: 10.1051/0004-6361/201118010.

R. De Propris, C. J. Conselice, J. Liske, S. P. Driver, D. R. Patton, A. W. Graham, and P. D. Allen. The Millennium Galaxy Catalogue: The Connection between Close Pairs and Asymmetry; Implications for the Galaxy Merger Rate. *ApJ*, 666: 212–221, September 2007. doi: 10.1086/520488.

G. de Vaucouleurs. Recherches sur les Nebuleuses Extragalactiques. *Annales d'Astrophysique*, 11:247, January 1948.

G. de Vaucouleurs. Classification and Morphology of External Galaxies. *Handbuch der Physik*, 53:275, 1959.

P. Di Matteo, F. Combes, A.-L. Melchior, and B. Semelin. Star formation efficiency in galaxy interactions and mergers: a statistical study. *A&A*, 468:61–81, June 2007. doi: 10.1051/0004-6361:20066959.

P. Di Matteo, F. Bournaud, M. Martig, F. Combes, A.-L. Melchior, and B. Semelin. On the frequency, intensity, and duration of starburst episodes triggered by galaxy interactions and mergers. *A&A*, 492:31–49, December 2008. doi: 10.1051/0004-6361:200809480.

A. Dressler. Galaxy morphology in rich clusters - Implications for the formation and evolution of galaxies. *ApJ*, 236:351–365, March 1980. doi: 10.1086/157753.

D. Elbaz, E. Daddi, D. Le Borgne, M. Dickinson, D. M. Alexander, R.-R. Chary, J.-L. Starck, W. N. Brandt, M. Kitzbichler, E. MacDonald, M. Nonino, P. Popesso, D. Stern, and E. Vanzella. The reversal of the star formation-density relation in the distant universe. *A&A*, 468:33–48, June 2007. doi: 10.1051/0004-6361:20077525.

S. L. Ellison, D. R. Patton, L. Simard, and A. W. McConnachie. Galaxy Pairs in the Sloan Digital Sky Survey. I. Star Formation, Active Galactic Nucleus Fraction, and the Mass-Metallicity Relation. *AJ*, 135:1877–1899, May 2008. doi: 10.1088/0004-6256/135/5/1877.

S. L. Ellison, D. R. Patton, L. Simard, A. W. McConnachie, I. K. Baldry, and J. T. Mendel. Galaxy pairs in the Sloan Digital Sky Survey - II. The effect of environment on interactions. *MNRAS*, 407:1514–1528, September 2010. doi: 10.1111/j.1365-2966.2010.17076.x.

S. L. Ellison, J. T. Mendel, D. R. Patton, and J. M. Scudder. Galaxy pairs in the Sloan Digital Sky Survey - VIII. The observational properties of post-merger galaxies. *MNRAS*, 435:3627–3638, November 2013. doi: 10.1093/mnras/stt1562.

L. Eyer, B. Holl, D. Pourbaix, N. Mowlavi, C. Siopis, F. Barblan, D. W. Evans, and P. North. The Gaia Mission. *Central European Astrophysical Bulletin*, 37:115–126, 2013.

S. M. Faber, C. N. A. Willmer, C. Wolf, D. C. Koo, B. J. Weiner, J. A. Newman, M. Im, A. L. Coil, C. Conroy, M. C. Cooper, M. Davis, D. P. Finkbeiner, B. F. Gerke, K. Gebhardt, E. J. Groth, P. Guhathakurta, J. Harker, N. Kaiser, S. Kassin, M. Kleinheinrich, N. P. Konidaris, R. G. Kron, L. Lin, G. Luppino, D. S. Madgwick, K. Meisenheimer, K. G. Noeske, A. C. Phillips, V. L. Sarajedini, R. P. Schiavon, L. Simard, A. S. Szalay, N. P. Vogt, and R. Yan. Galaxy Luminosity Functions to z$\sim$1 from DEEP2 and COMBO-17: Implications for Red Galaxy Formation. *ApJ*, 665:265–294, August 2007. doi: 10.1086/519294.

D. Freedman Woods, M. J. Geller, M. J. Kurtz, E. Westra, D. G. Fabricant, and

I. Dell'Antonio. Triggered Star Formation in Galaxy Pairs at z = 0.08-0.38. *AJ*, 139:1857–1870, May 2010. doi: 10.1088/0004-6256/139/5/1857.

Y. Fujita. Quantitative Estimates of Environmental Effects on the Star Formation Rate of Disk Galaxies in Clusters of Galaxies. *ApJ*, 509:587–594, December 1998. doi: 10.1086/306518.

M. Geha, M. R. Blanton, R. Yan, and J. L. Tinker. A Stellar Mass Threshold for Quenching of Field Galaxies. *ApJ*, 757:85, September 2012. doi: 10.1088/0004-637X/757/1/85.

M. J. Geller and J. P. Huchra. Mapping the universe. *Science*, 246:897–903, November 1989. doi: 10.1126/science.246.4932.897.

M. R. George, A. Leauthaud, K. Bundy, A. Finoguenov, J. Tinker, Y.-T. Lin, S. Mei, J.-P. Kneib, H. Aussel, P. S. Behroozi, M. T. Busha, P. Capak, L. Coccato, G. Covone, C. Faure, S. L. Fiorenza, O. Ilbert, E. Le Floc'h, A. M. Koekemoer, M. Tanaka, R. H. Wechsler, and M. Wolk. Galaxies in X-Ray Groups. I. Robust Membership Assignment and the Impact of Group Environments on Quenching. *ApJ*, 742:125, December 2011. doi: 10.1088/0004-637X/742/2/125.

S. Giodini, A. Finoguenov, D. Pierini, G. Zamorani, O. Ilbert, S. Lilly, Y. Peng, N. Scoville, and M. Tanaka. The galaxy stellar mass function of X-ray detected groups. Environmental dependence of galaxy evolution in the COSMOS survey. *A&A*, 538:A104, February 2012. doi: 10.1051/0004-6361/201117696.

O. Y. Gnedin. Tidal Effects in Clusters of Galaxies. *ApJ*, 582:141–161, January 2003. doi: 10.1086/344636.

P. L. Gómez, R. C. Nichol, C. J. Miller, M. L. Balogh, T. Goto, A. I. Zabludoff, A. K. Romer, M. Bernardi, R. Sheth, A. M. Hopkins, F. J. Castander, A. J. Connolly, D. P. Schneider, J. Brinkmann, D. Q. Lamb, M. SubbaRao, and D. G. York. Galaxy Star Formation as a Function of Environment in the Early Data Release of the Sloan Digital Sky Survey. *ApJ*, 584:210–227, February 2003. doi: 10.1086/345593.

T. Goto, C. Yamauchi, Y. Fujita, S. Okamura, M. Sekiguchi, I. Smail, M. Bernardi, and P. L. Gomez. The morphology-density relation in the Sloan Digital Sky Survey. *MNRAS*, 346:601–614, December 2003. doi: 10.1046/j.1365-2966.2003.07114.x.

J. E. Gunn and J. R. Gott, III. On the Infall of Matter Into Clusters of Galaxies and Some Effects on Their Evolution. *ApJ*, 176:1, August 1972. doi: 10.1086/151605.

J. E. Gunn, M. Carr, C. Rockosi, M. Sekiguchi, K. Berry, B. Elms, E. de Haas, Ž. Ivezić, G. Knapp, R. Lupton, G. Pauls, R. Simcoe, R. Hirsch, D. Sanford, S. Wang, D. York, F. Harris, J. Annis, L. Bartozek, W. Boroski, J. Bakken, M. Haldeman, S. Kent, S. Holm, D. Holmgren, D. Petravick, A. Prosapio, R. Rechenmacher, M. Doi, M. Fukugita, K. Shimasaku, N. Okada, C. Hull, W. Siegmund, E. Mannery, M. Blouke, D. Heidtman, D. Schneider, R. Lucinio, and J. Brinkman. The Sloan Digital Sky Survey Photometric Camera. *AJ*, 116:3040–3081, December 1998. doi: 10.1086/300645.

C. P. Haines, G. P. Smith, E. Egami, R. S. Ellis, S. M. Moran, A. J. R. Sanderson, P. Merluzzi, G. Busarello, and R. J. Smith. LOCUSS: The Mid-Infrared Butcher-Oemler Effect. *ApJ*, 704:126–136, October 2009. doi: 10.1088/0004-637X/704/1/126.

A. Heiderman, S. Jogee, I. Marinova, E. van Kampen, M. Barden, C. Y. Peng, C. Heymans, M. E. Gray, E. F. Bell, D. Bacon, M. Balogh, F. D. Barazza, A. Böhm, J. A. R. Caldwell, B. Häußler, K. Jahnke, K. Lane, D. H. McIntosh, K. Meisenheimer, S. F. Sánchez, R. S. Somerville, A. Taylor, L. Wisotzki, C. Wolf, and X. Zheng. Interacting Galaxies in the A901/902 Supercluster with Stages. *ApJ*, 705:1433–1455, November 2009. doi: 10.1088/0004-637X/705/2/1433.

E. Holmberg. A study of double and multiple galaxies. *Annals of the Observatory of Lund*, 6:1, 1937.

E. Holmberg. A photographic photometry of extragalactic nebulae. *Meddelanden fran Lunds Astronomiska Observatorium Serie II*, 136:1, 1958.

E. Hubble and M. L. Humason. The Velocity-Distance Relation among Extra-Galactic Nebulae. *ApJ*, 74:43, July 1931. doi: 10.1086/143323.

E. P. Hubble. Extragalactic nebulae. *ApJ*, 64:321–369, December 1926. doi: 10.1086/143018.

E. P. Hubble. *Realm of the Nebulae*. New Haven: Yale University Press, 1936. ISBN 9780300025002.

H. S. Hwang, D. Elbaz, M. Dickinson, V. Charmandaris, E. Daddi, D. Le Borgne, V. Buat, G. E. Magdis, B. Altieri, H. Aussel, D. Coia, H. Dannerbauer, K. Dasyra, J. Kartaltepe, R. Leiton, B. Magnelli, P. Popesso, and I. Valtchanov. GOODS-Herschel: the impact of galaxy-galaxy interactions on the far-infrared properties of galaxies. *A&A*, 535:A60, November 2011. doi: 10.1051/0004-6361/201117476.

Y. Ideue, Y. Taniguchi, T. Nagao, Y. Shioya, M. Kajisawa, J. R. Trump, D. Vergani, A. Iovino, A. M. Koekemoer, O. Le Fèvre, O. Ilbert, and N. Z. Scoville. The Role of Galaxy Interaction in Environmental Dependence of the Star Formation Activity at z $\cong$ 1.2. *ApJ*, 747:42, March 2012. doi: 10.1088/0004-637X/747/1/42.

T. E. Jeltema, B. F. Gerke, E. S. Laird, C. N. A. Willmer, A. L. Coil, M. C. Cooper, M. Davis, K. Nandra, and J. A. Newman. Groups of galaxies in AEGIS: the 200-ks Chandra extended X-ray source catalogue. *MNRAS*, 399:715–727, October 2009. doi: 10.1111/j.1365-2966.2009.15377.x.

H.-Y. Jian, L. Lin, and T. Chiueh. Environmental Dependence of the Galaxy Merger Rate in a ΛCDM Universe. *ApJ*, 754:26, July 2012. doi: 10.1088/0004-637X/754/1/26.

G. Kauffmann, T. M. Heckman, S. D. M. White, S. Charlot, C. Tremonti, J. Brinchmann, G. Bruzual, E. W. Peng, M. Seibert, M. Bernardi, M. Blanton, J. Brinkmann, F. Castander, I. Csábai, M. Fukugita, Z. Ivezic, J. A. Munn, R. C. Nichol, N. Padmanabhan, A. R. Thakar, D. H. Weinberg, and D. York. Stellar masses and star formation histories for 10^5 galaxies from the Sloan Digital Sky Survey. *MNRAS*, 341:33–53, May 2003. doi: 10.1046/j.1365-8711.2003.06291.x.

G. Kauffmann, S. D. M. White, T. M. Heckman, B. Ménard, J. Brinchmann, S. Charlot, C. Tremonti, and J. Brinkmann. The environmental dependence of the relations between stellar mass, structure, star formation and nuclear activity in galaxies. *MNRAS*, 353:713–731, September 2004. doi: 10.1111/j.1365-2966.2004.08117.x.

R. C. Kennicutt, Jr. Star Formation in Galaxies Along the Hubble Sequence. *ARA&A*, 36:189–232, 1998. doi: 10.1146/annurev.astro.36.1.189.

L. J. Kewley, M. A. Dopita, R. S. Sutherland, C. A. Heisler, and J. Trevena. Theoretical Modeling of Starburst Galaxies. *ApJ*, 556:121–140, July 2001. doi: 10.1086/321545.

J. H. Knapen and P. A. James. The Hα Galaxy Survey. VIII. Close Companions and Interactions, and the Definition of Starbursts. *ApJ*, 698:1437–1455, June 2009. doi: 10.1088/0004-637X/698/2/1437.

D. G. Lambas, P. B. Tissera, M. S. Alonso, and G. Coldwell. Galaxy pairs in the 2dF survey - I. Effects of interactions on star formation in the field. *MNRAS*, 346: 1189–1196, December 2003. doi: 10.1111/j.1365-2966.2003.07179.x.

R. B. Larson and B. M. Tinsley. Star formation rates in normal and peculiar galaxies. *ApJ*, 219:46–59, January 1978. doi: 10.1086/155753.

R. B. Larson, B. M. Tinsley, and C. N. Caldwell. The evolution of disk galaxies and the origin of S0 galaxies. *ApJ*, 237:692–707, May 1980. doi: 10.1086/157917.

A. Leauthaud, M. R. George, P. S. Behroozi, K. Bundy, J. Tinker, R. H. Wechsler, C. Conroy, A. Finoguenov, and M. Tanaka. The Integrated Stellar Content of Dark Matter Halos. *ApJ*, 746:95, February 2012. doi: 10.1088/0004-637X/746/1/95.

I. Lewis, M. Balogh, R. De Propris, W. Couch, R. Bower, A. Offer, J. Bland-Hawthorn, I. K. Baldry, C. Baugh, T. Bridges, R. Cannon, S. Cole, M. Colless, C. Collins, N. Cross, G. Dalton, S. P. Driver, G. Efstathiou, R. S. Ellis, C. S. Frenk, K. Glazebrook, E. Hawkins, C. Jackson, O. Lahav, S. Lumsden, S. Maddox,

D. Madgwick, P. Norberg, J. A. Peacock, W. Percival, B. A. Peterson, W. Sutherland, and K. Taylor. The 2dF Galaxy Redshift Survey: the environmental dependence of galaxy star formation rates near clusters. *MNRAS*, 334:673–683, August 2002. doi: 10.1046/j.1365-8711.2002.05558.x.

I. H. Li, K. Glazebrook, D. Gilbank, M. Balogh, R. Bower, I. Baldry, G. Davies, G. Hau, and P. McCarthy. Dependence of star formation activity on stellar mass and environment from the Redshift One LDSS-3 Emission line Survey. *MNRAS*, 411:1869–1879, March 2011. doi: 10.1111/j.1365-2966.2010.17816.x.

I. H. Li, H. K. C. Yee, B. C. Hsieh, and M. Gladders. Evolution of Group Galaxies from the First Red-Sequence Cluster Survey. *ApJ*, 749:150, April 2012. doi: 10.1088/0004-637X/749/2/150.

C. J. Lintott, K. Schawinski, A. Slosar, K. Land, S. Bamford, D. Thomas, M. J. Raddick, R. C. Nichol, A. Szalay, D. Andreescu, P. Murray, and J. Vandenberg. Galaxy Zoo: morphologies derived from visual inspection of galaxies from the Sloan Digital Sky Survey. *MNRAS*, 389:1179–1189, September 2008. doi: 10.1111/j.1365-2966.2008.13689.x.

J. Liske, D. J. Lemon, S. P. Driver, N. J. G. Cross, and W. J. Couch. The Millennium Galaxy Catalogue: $16 \leq \mathrm{B}_{MGC} < 24$ galaxy counts and the calibration of the local galaxy luminosity function. *MNRAS*, 344:307–324, September 2003. doi: 10.1046/j.1365-8711.2003.06826.x.

J. M. Lotz, P. Jonsson, T. J. Cox, and J. R. Primack. Galaxy merger morphologies and time-scales from simulations of equal-mass gas-rich disc mergers. *MNRAS*, 391:1137–1162, December 2008. doi: 10.1111/j.1365-2966.2008.14004.x.

J. M. Lotz, P. Jonsson, T. J. Cox, D. Croton, J. R. Primack, R. S. Somerville, and K. Stewart. The Major and Minor Galaxy Merger Rates at z < 1.5. *ApJ*, 742:103, December 2011. doi: 10.1088/0004-637X/742/2/103.

K. Lundmark and F. Ark. *Arkiv for Matematik, Astronomi och Fysik*, 20:B3, 1927.

C.-J. Ma and H. Ebeling. The morphology-density relation of galaxies around MACS J0717.5+3745. *MNRAS*, 410:2593–2601, February 2011. doi: 10.1111/j.1365-2966.2010.17633.x.

D. S. Madgwick, O. Lahav, I. K. Baldry, C. M. Baugh, J. Bland-Hawthorn, T. Bridges, R. Cannon, S. Cole, M. Colless, C. Collins, W. Couch, G. Dalton, R. De Propris, S. P. Driver, G. Efstathiou, R. S. Ellis, C. S. Frenk, K. Glazebrook, C. Jackson, I. Lewis, S. Lumsden, S. Maddox, P. Norberg, J. A. Peacock, B. A. Peterson, W. Sutherland, and K. Taylor. The 2dF Galaxy Redshift Survey: galaxy luminosity functions per spectral type. *MNRAS*, 333:133–144, June 2002. doi: 10.1046/j.1365-8711.2002.05393.x.

B. E. Markarian. Galaxies with an Ultraviolet Continuum. *Astrofizika*, 3:55–68, 1967.

I. G. McCarthy, C. S. Frenk, A. S. Font, C. G. Lacey, R. G. Bower, N. L. Mitchell, M. L. Balogh, and T. Theuns. Ram pressure stripping the hot gaseous haloes of galaxies in groups and clusters. *MNRAS*, 383:593–605, January 2008. doi: 10.1111/j.1365-2966.2007.12577.x.

S. L. McGee, M. L. Balogh, D. J. Wilman, R. G. Bower, J. S. Mulchaey, L. C. Parker, and A. Oemler. The Dawn of the Red: star formation histories of group

galaxies over the past 5 billion years. *MNRAS*, 413:996–1012, May 2011. doi: 10.1111/j.1365-2966.2010.18189.x.

J. T. Mendel, S. L. Ellison, L. Simard, D. R. Patton, and A. W. McConnachie. Compact groups in theory and practice - IV. The connection to large-scale structure. *MNRAS*, 418:1409–1422, December 2011. doi: 10.1111/j.1365-2966.2011.19159.x.

J. T. Mendel, L. Simard, M. Palmer, S. L. Ellison, and D. R. Patton. A Catalog of Bulge, Disk, and Total Stellar Mass Estimates for the Sloan Digital Sky Survey. *ApJS*, 210:3, January 2014. doi: 10.1088/0067-0049/210/1/3.

D. Merritt. Relaxation and tidal stripping in rich clusters of galaxies. II. Evolution of the luminosity distribution. *ApJ*, 276:26–37, January 1984. doi: 10.1086/161590.

R. H. Miller. Flyby - Numerical experiments on a galaxy orbiting within a galaxy cluster. *A&A*, 167:41–52, October 1986.

B. Moore, N. Katz, G. Lake, A. Dressler, and A. Oemler. Galaxy harassment and the evolution of clusters of galaxies. *Nature*, 379:613–616, February 1996. doi: 10.1038/379613a0.

B. Moore, G. Lake, T. Quinn, and J. Stadel. On the survival and destruction of spiral galaxies in clusters. *MNRAS*, 304:465–474, April 1999. doi: 10.1046/j.1365-8711.1999.02345.x.

W. W. Morgan. Some Characteristics of Galaxies. *ApJ*, 135:1, January 1962. doi: 10.1086/147243.

B. P. Moster, R. S. Somerville, C. Maulbetsch, F. C. van den Bosch, A. V. Macciò, T. Naab, and L. Oser. Constraints on the Relationship between Stellar Mass and

Halo Mass at Low and High Redshift. *ApJ*, 710:903–923, February 2010. doi: 10.1088/0004-637X/710/2/903.

S. I. Muldrew, D. J. Croton, R. A. Skibba, F. R. Pearce, H. B. Ann, I. K. Baldry, S. Brough, Y.-Y. Choi, C. J. Conselice, N. B. Cowan, A. Gallazzi, M. E. Gray, R. Grützbauch, I.-H. Li, C. Park, S. V. Pilipenko, B. J. Podgorzec, A. S. G. Robotham, D. J. Wilman, X. Yang, Y. Zhang, and S. Zibetti. Measures of galaxy environment - I. What is 'environment'? *MNRAS*, 419:2670–2682, January 2012. doi: 10.1111/j.1365-2966.2011.19922.x.

A. Muzzin, G. Wilson, H. K. C. Yee, D. Gilbank, H. Hoekstra, R. Demarco, M. Balogh, P. van Dokkum, M. Franx, E. Ellingson, A. Hicks, J. Nantais, A. Noble, M. Lacy, C. Lidman, A. Rettura, J. Surace, and T. Webb. The Gemini Cluster Astrophysics Spectroscopic Survey (GCLASS): The Role of Environment and Self-regulation in Galaxy Evolution at z $\sim$ 1. *ApJ*, 746:188, February 2012. doi: 10.1088/0004-637X/746/2/188.

C. Nipoti and J. Binney. The role of thermal evaporation in galaxy formation. *MNRAS*, 382:1481–1493, December 2007. doi: 10.1111/j.1365-2966.2007.12505.x.

P. E. J. Nulsen. Transport processes and the stripping of cluster galaxies. *MNRAS*, 198:1007–1016, March 1982.

A. Oemler, Jr. The Systematic Properties of Clusters of Galaxies. Photometry of 15 Clusters. *ApJ*, 194:1–20, November 1974. doi: 10.1086/153216.

C. Park and H. S. Hwang. Interactions of Galaxies in the Galaxy Cluster Environment. *ApJ*, 699:1595–1609, July 2009. doi: 10.1088/0004-637X/699/2/1595.

L. C. Parker, M. J. Hudson, R. G. Carlberg, and H. Hoekstra. Mass-to-Light Ratios of Galaxy Groups from Weak Lensing. *ApJ*, 634:806–812, December 2005. doi: 10.1086/497117.

A. Pasquali, F. C. van den Bosch, H. J. Mo, X. Yang, and R. Somerville. The rise and fall of galaxy activity in dark matter haloes. *MNRAS*, 394:38–50, March 2009. doi: 10.1111/j.1365-2966.2008.14233.x.

D. R. Patton and J. E. Atfield. The Luminosity Dependence of the Galaxy Merger Rate. *ApJ*, 685:235–246, September 2008. doi: 10.1086/590542.

D. R. Patton, R. G. Carlberg, R. O. Marzke, C. J. Pritchet, L. N. da Costa, and P. S. Pellegrini. New Techniques for Relating Dynamically Close Galaxy Pairs to Merger and Accretion Rates: Application to the Second Southern Sky Redshift Survey. *ApJ*, 536:153–172, June 2000. doi: 10.1086/308907.

D. R. Patton, J. K. Grant, L. Simard, C. J. Pritchet, R. G. Carlberg, and K. D. Borne. A Hubble Space Telescope Snapshot Survey of Dynamically Close Galaxy Pairs in the CNOC2 Redshift Survey. *AJ*, 130:2043–2057, November 2005. doi: 10.1086/491672.

D. R. Patton, S. L. Ellison, L. Simard, A. W. McConnachie, and J. T. Mendel. Galaxy pairs in the Sloan Digital Sky Survey - III. Evidence of induced star formation from optical colours. *MNRAS*, 412:591–606, March 2011. doi: 10.1111/j.1365-2966.2010.17932.x.

D. R. Patton, P. Torrey, S. L. Ellison, J. T. Mendel, and J. M. Scudder. Galaxy pairs in the Sloan Digital Sky Survey - VI. The orbital extent of enhanced star formation

in interacting galaxies. *MNRAS*, 433:L59–L63, June 2013. doi: 10.1093/mnrasl/slt058.

R. Pelló, G. Rudnick, G. De Lucia, L. Simard, D. I. Clowe, P. Jablonka, B. Milvang-Jensen, R. P. Saglia, S. D. M. White, A. Aragón-Salamanca, C. Halliday, B. Poggianti, P. Best, J. Dalcanton, M. Dantel-Fort, B. Fort, A. von der Linden, Y. Mellier, H. Rottgering, and D. Zaritsky. Photometric redshifts and cluster tomography in the ESO Distant Cluster Survey. *A&A*, 508:1173–1191, December 2009. doi: 10.1051/0004-6361/200810644.

C. Y. Peng, L. C. Ho, C. D. Impey, and H.-W. Rix. Detailed Structural Decomposition of Galaxy Images. *AJ*, 124:266–293, July 2002. doi: 10.1086/340952.

Y.-j. Peng, S. J. Lilly, K. Kovač, M. Bolzonella, L. Pozzetti, A. Renzini, G. Zamorani, O. Ilbert, C. Knobel, A. Iovino, C. Maier, O. Cucciati, L. Tasca, C. M. Carollo, J. Silverman, P. Kampczyk, L. de Ravel, D. Sanders, N. Scoville, T. Contini, V. Mainieri, M. Scodeggio, J.-P. Kneib, O. Le Fèvre, S. Bardelli, A. Bongiorno, K. Caputi, G. Coppa, S. de la Torre, P. Franzetti, B. Garilli, F. Lamareille, J.-F. Le Borgne, V. Le Brun, M. Mignoli, E. Perez Montero, R. Pello, E. Ricciardelli, M. Tanaka, L. Tresse, D. Vergani, N. Welikala, E. Zucca, P. Oesch, U. Abbas, L. Barnes, R. Bordoloi, D. Bottini, A. Cappi, P. Cassata, A. Cimatti, M. Fumana, G. Hasinger, A. Koekemoer, A. Leauthaud, D. Maccagni, C. Marinoni, H. McCracken, P. Memeo, B. Meneux, P. Nair, C. Porciani, V. Presotto, and R. Scaramella. Mass and Environment as Drivers of Galaxy Evolution in SDSS and zCOSMOS and the Origin of the Schechter Function. *ApJ*, 721:193–221, September 2010. doi: 10.1088/0004-637X/721/1/193.

J. Perez, P. Tissera, N. Padilla, M. S. Alonso, and D. G. Lambas. Global environmental effects versus galaxy interactions. *MNRAS*, 399:1157–1166, November 2009. doi: 10.1111/j.1365-2966.2009.15358.x.

I. Plauchu-Frayn and R. Coziol. Comparative Study of Asymmetry Origin of Galaxies in Different Environments. I. Optical Observations. *AJ*, 139:2643–2668, June 2010a. doi: 10.1088/0004-6256/139/6/2643.

I. Plauchu-Frayn and R. Coziol. Comparative Study of Asymmetry Origin of Galaxies in Different Environments. II. Near-infrared Observations. *AJ*, 140:612–627, August 2010b. doi: 10.1088/0004-6256/140/2/612.

M. Postman and M. J. Geller. The morphology-density relation - The group connection. *ApJ*, 281:95–99, June 1984. doi: 10.1086/162078.

V. Presotto, A. Iovino, M. Scodeggio, O. Cucciati, C. Knobel, M. Bolzonella, P. Oesch, A. Finoguenov, M. Tanaka, K. Kovač, Y. Peng, G. Zamorani, S. Bardelli, L. Pozzetti, P. Kampczyk, C. López-Sanjuan, D. Vergani, E. Zucca, L. A. M. Tasca, C. M. Carollo, T. Contini, J.-P. Kneib, O. Le Fèvre, S. Lilly, V. Mainieri, A. Renzini, A. Bongiorno, K. Caputi, S. de la Torre, L. de Ravel, P. Franzetti, B. Garilli, F. Lamareille, J.-F. Le Borgne, V. Le Brun, C. Maier, M. Mignoli, R. Pellò, E. Perez-Montero, E. Ricciardelli, J. D. Silverman, L. Tresse, L. Barnes, R. Bordoloi, A. Cappi, A. Cimatti, G. Coppa, A. M. Koekemoer, H. J. McCracken, M. Moresco, P. Nair, and N. Welikala. A journey from the outskirts to the cores of groups. I. Color- and mass-segregation in 20K-zCOSMOS groups. *A&A*, 539:A55, March 2012. doi: 10.1051/0004-6361/201118293.

V. Quilis, B. Moore, and R. Bower. Gone with the Wind: The Origin of S0 Galaxies in Clusters. *Science*, 288:1617–1620, June 2000. doi: 10.1126/science.288.5471.1617.

A. R. Robaina, E. F. Bell, R. E. Skelton, D. H. McIntosh, R. S. Somerville, X. Zheng, H.-W. Rix, D. Bacon, M. Balogh, F. D. Barazza, M. Barden, A. Böhm, J. A. R. Caldwell, A. Gallazzi, M. E. Gray, B. Häussler, C. Heymans, K. Jahnke, S. Jogee, E. van Kampen, K. Lane, K. Meisenheimer, C. Papovich, C. Y. Peng, S. F. Sánchez, R. Skibba, A. Taylor, L. Wisotzki, and C. Wolf. Less Than 10 Percent of Star Formation in z $\sim$ 0.6 Massive Galaxies is Triggered by Major Interactions. *ApJ*, 704:324–340, October 2009. doi: 10.1088/0004-637X/704/1/324.

E. Roediger and M. Brüggen. Ram pressure stripping in a viscous intracluster medium. *MNRAS*, 388:L89–L93, July 2008. doi: 10.1111/j.1745-3933.2008.00506.x.

E. Roediger and G. Hensler. Ram pressure stripping of disk galaxies. From high to low density environments. *A&A*, 433:875–895, April 2005. doi: 10.1051/0004-6361:20042131.

S. Salim, R. M. Rich, S. Charlot, J. Brinchmann, B. D. Johnson, D. Schiminovich, M. Seibert, R. Mallery, T. M. Heckman, K. Forster, P. G. Friedman, D. C. Martin, P. Morrissey, S. G. Neff, T. Small, T. K. Wyder, L. Bianchi, J. Donas, Y.-W. Lee, B. F. Madore, B. Milliard, A. S. Szalay, B. Y. Welsh, and S. K. Yi. UV Star Formation Rates in the Local Universe. *ApJS*, 173:267–292, December 2007. doi: 10.1086/519218.

A. Sandage. *The Hubble atlas of galaxies*. Washington: Carnegie Institution, 1961.

A. Sandage. *Classification and Stellar Content of Galaxies Obtained from Direct Photography*, page 1. The University of Chicago Press, January 1975.

D. Schade, S. J. Lilly, D. Crampton, F. Hammer, O. Le Fevre, and L. Tresse. Canada-France Redshift Survey: Hubble Space Telescope Imaging of High-Redshift Field Galaxies. *ApJL*, 451:L1, September 1995. doi: 10.1086/309677.

K. Schawinski, C. M. Urry, B. D. Simmons, L. Fortson, S. Kaviraj, W. C. Keel, C. J. Lintott, K. L. Masters, R. C. Nichol, M. Sarzi, R. Skibba, E. Treister, K. W. Willett, O. I. Wong, and S. K. Yi. The green valley is a red herring: Galaxy Zoo reveals two evolutionary pathways towards quenching of star formation in early- and late-type galaxies. *MNRAS*, 440:889–907, May 2014. doi: 10.1093/mnras/stu327.

D. Schiminovich, T. K. Wyder, D. C. Martin, B. D. Johnson, S. Salim, M. Seibert, M. A. Treyer, T. Budavári, C. Hoopes, M. Zamojski, T. A. Barlow, K. G. Forster, P. G. Friedman, P. Morrissey, S. G. Neff, T. A. Small, L. Bianchi, J. Donas, T. M. Heckman, Y.-W. Lee, B. F. Madore, B. Milliard, R. M. Rich, A. S. Szalay, B. Y. Welsh, and S. Yi. The UV-Optical Color Magnitude Diagram. II. Physical Properties and Morphological Evolution On and Off of a Star-forming Sequence. *ApJS*, 173:315–341, December 2007. doi: 10.1086/524659.

S. Schulz and C. Struck. Multi stage three-dimensional sweeping and annealing of disc galaxies in clusters. *MNRAS*, 328:185–202, November 2001. doi: 10.1046/j.1365-8711.2001.04847.x.

C. Scott and S. Kaviraj. Star formation and AGN activity in interacting galaxies: a near-UV perspective. *MNRAS*, 437:2137–2145, January 2014. doi: 10.1093/mnras/stt2014.

N. Scoville, S. Arnouts, H. Aussel, A. Benson, A. Bongiorno, K. Bundy, M. A. A. Calvo, P. Capak, M. Carollo, F. Civano, J. Dunlop, M. Elvis, A. Faisst, A. Finoguenov, H. Fu, M. Giavalisco, Q. Guo, O. Ilbert, A. Iovino, M. Kajisawa, J. Kartaltepe, A. Leauthaud, O. Le Fèvre, E. LeFloch, S. J. Lilly, C. T.-C. Liu, S. Manohar, R. Massey, D. Masters, H. J. McCracken, B. Mobasher, Y.-J. Peng, A. Renzini, J. Rhodes, M. Salvato, D. B. Sanders, B. D. Sarvestani, C. Scarlata, E. Schinnerer, K. Sheth, P. L. Shopbell, V. Smolčić, Y. Taniguchi, J. E. Taylor, S. D. M. White, and L. Yan. Evolution of Galaxies and Their Environments at z = 0.1-3 in COSMOS. *ApJS*, 206:3, May 2013. doi: 10.1088/0067-0049/206/1/3.

J. M. Scudder, S. L. Ellison, P. Torrey, D. R. Patton, and J. T. Mendel. Galaxy pairs in the Sloan Digital Sky Survey - V. Tracing changes in star formation rate and metallicity out to separations of 80 kpc. *MNRAS*, 426:549–565, October 2012. doi: 10.1111/j.1365-2966.2012.21749.x.

J. L. Sérsic. Influence of the atmospheric and instrumental dispersion on the brightness distribution in a galaxy. *Boletin de la Asociacion Argentina de Astronomia La Plata Argentina*, 6:41, 1963.

L. Simard, C. N. A. Willmer, N. P. Vogt, V. L. Sarajedini, A. C. Phillips, B. J. Weiner, D. C. Koo, M. Im, G. D. Illingworth, and S. M. Faber. The DEEP Groth Strip Survey. II. Hubble Space Telescope Structural Parameters of Galaxies in the Groth Strip. *ApJS*, 142:1–33, September 2002. doi: 10.1086/341399.

L. Simard, J. T. Mendel, D. R. Patton, S. L. Ellison, and A. W. McConnachie. A Catalog of Bulge+disk Decompositions and Updated Photometry for 1.12 Million

Galaxies in the Sloan Digital Sky Survey. *ApJS*, 196:11, September 2011. doi: 10.1088/0067-0049/196/1/11.

S. A. Smee, J. E. Gunn, A. Uomoto, N. Roe, D. Schlegel, C. M. Rockosi, M. A. Carr, F. Leger, K. S. Dawson, M. D. Olmstead, J. Brinkmann, R. Owen, R. H. Barkhouser, K. Honscheid, P. Harding, D. Long, R. H. Lupton, C. Loomis, L. Anderson, J. Annis, M. Bernardi, V. Bhardwaj, D. Bizyaev, A. S. Bolton, H. Brewington, J. W. Briggs, S. Burles, J. G. Burns, F. J. Castander, A. Connolly, J. R. A. Davenport, G. Ebelke, H. Epps, P. D. Feldman, S. D. Friedman, J. Frieman, T. Heckman, C. L. Hull, G. R. Knapp, D. M. Lawrence, J. Loveday, E. J. Mannery, E. Malanushenko, V. Malanushenko, A. J. Merrelli, D. Muna, P. R. Newman, R. C. Nichol, D. Oravetz, K. Pan, A. C. Pope, P. G. Ricketts, A. Shelden, D. Sandford, W. Siegmund, A. Simmons, D. S. Smith, S. Snedden, D. P. Schneider, M. SubbaRao, C. Tremonti, P. Waddell, and D. G. York. The Multi-object, Fiber-fed Spectrographs for the Sloan Digital Sky Survey and the Baryon Oscillation Spectroscopic Survey. *AJ*, 146:32, August 2013. doi: 10.1088/0004-6256/146/2/32.

V. Springel, S. D. M. White, A. Jenkins, C. S. Frenk, N. Yoshida, L. Gao, J. Navarro, R. Thacker, D. Croton, J. Helly, J. A. Peacock, S. Cole, P. Thomas, H. Couchman, A. Evrard, J. Colberg, and F. Pearce. Simulations of the formation, evolution and clustering of galaxies and quasars. *Nature*, 435:629–636, June 2005. doi: 10.1038/nature03597.

I. Strateva, Ž. Ivezić, G. R. Knapp, V. K. Narayanan, M. A. Strauss, J. E. Gunn, R. H. Lupton, D. Schlegel, N. A. Bahcall, J. Brinkmann, R. J. Brunner, T. Budavári, I. Csabai, F. J. Castander, M. Doi, M. Fukugita, Z. Győry, M. Hamabe,

G. Hennessy, T. Ichikawa, P. Z. Kunszt, D. Q. Lamb, T. A. McKay, S. Okamura, J. Racusin, M. Sekiguchi, D. P. Schneider, K. Shimasaku, and D. York. Color Separation of Galaxy Types in the Sloan Digital Sky Survey Imaging Data. *AJ*, 122: 1861–1874, October 2001. doi: 10.1086/323301.

M. A. Strauss, D. H. Weinberg, R. H. Lupton, V. K. Narayanan, J. Annis, M. Bernardi, M. Blanton, S. Burles, A. J. Connolly, J. Dalcanton, M. Doi, D. Eisenstein, J. A. Frieman, M. Fukugita, and et al. Spectroscopic Target Selection in the Sloan Digital Sky Survey: The Main Galaxy Sample. *AJ*, 124:1810–1824, September 2002. doi: 10.1086/342343.

M. Tanaka, T. Goto, S. Okamura, K. Shimasaku, and J. Brinkmann. The Environmental Dependence of Galaxy Properties in the Local Universe: Dependences on Luminosity, Local Density, and System Richness. *AJ*, 128:2677–2695, December 2004. doi: 10.1086/425529.

M. Tanaka, A. Finoguenov, S. J. Lilly, M. Bolzonella, C. M. Carollo, T. Contini, A. Iovino, J.-P. Kneib, F. Lamareille, O. Le Fevre, V. Mainieri, V. Presotto, A. Renzini, M. Scodeggio, J. D. Silverman, G. Zamorani, S. Bardelli, A. Bongiorno, K. Caputi, O. Cucciati, S. de la Torre, L. de Ravel, P. Franzetti, B. Garilli, P. Kampczyk, C. Knobel, K. Kovač, J.-F. Le Borgne, V. Le Brun, C. López-Sanjuan, C. Maier, M. Mignoli, R. Pello, Y. Peng, E. Perez-Montero, L. Tasca, L. Tresse, D. Vergani, E. Zucca, L. Barnes, R. Bordoloi, A. Cappi, A. Cimatti, G. Coppa, A. M. Koekemoer, H. J. McCracken, M. Moresco, P. Nair, P. Oesch, L. Pozzetti, and N. Welikala. X-Ray Groups of Galaxies at $0.5 < z < 1$ in zCOSMOS: Increased AGN Activities in High Redshift Groups. *PASJ*, 64:22, April 2012.

doi: 10.1093/pasj/64.2.22.

A. Toomre and J. Toomre. Galactic bridges and tails. *ApJ*, 178:623–666, December 1972. doi: 10.1086/151823.

F. C. van den Bosch, D. Aquino, X. Yang, H. J. Mo, A. Pasquali, D. H. McIntosh, S. M. Weinmann, and X. Kang. The importance of satellite quenching for the build-up of the red sequence of present-day galaxies. *MNRAS*, 387:79–91, June 2008. doi: 10.1111/j.1365-2966.2008.13230.x.

A. van der Wel, E. F. Bell, B. P. Holden, R. A. Skibba, and H.-W. Rix. The Physical Origins of the Morphology-Density Relation: Evidence for Gas Stripping from the Sloan Digital Sky Survey. *ApJ*, 714:1779–1788, May 2010. doi: 10.1088/0004-637X/714/2/1779.

M. Vogelsberger, S. Genel, V. Springel, P. Torrey, D. Sijacki, D. Xu, G. Snyder, D. Nelson, and L. Hernquist. Introducing the Illustris Project: simulating the coevolution of dark and visible matter in the Universe. *MNRAS*, 444:1518–1547, October 2014. doi: 10.1093/mnras/stu1536.

B. A. Vorontsov-Vel'Iaminov. The Interaction of Galaxies and the Nature of Their Arms, Spanning Filaments and Tails. The Morphology of Galaxies. V. *Astronomicheskii Zhurnal*, 35:858, 1958.

K. E. Whitaker, P. G. van Dokkum, G. Brammer, and M. Franx. The Star Formation Mass Sequence Out to z = 2.5. *ApJL*, 754:L29, August 2012. doi: 10.1088/2041-8205/754/2/L29.

D. B. Wijesinghe, A. M. Hopkins, S. Brough, E. N. Taylor, P. Norberg, A. Bauer, M. J. I. Brown, E. Cameron, C. J. Conselice, S. Croom, S. Driver, M. W. Grootes, D. H. Jones, L. Kelvin, J. Loveday, K. A. Pimbblet, C. C. Popescu, M. Prescott, R. Sharp, I. Baldry, E. M. Sadler, J. Liske, A. S. G. Robotham, S. Bamford, J. Bland-Hawthorn, M. Gunawardhana, M. Meyer, H. Parkinson, M. J. Drinkwater, J. Peacock, and R. Tuffs. Galaxy And Mass Assembly (GAMA): galaxy environments and star formation rate variations. *MNRAS*, 423:3679–3691, July 2012. doi: 10.1111/j.1365-2966.2012.21164.x.

V. Wild, C. J. Walcher, P. H. Johansson, L. Tresse, S. Charlot, A. Pollo, O. Le Fèvre, and L. de Ravel. Post-starburst galaxies: more than just an interesting curiosity. *MNRAS*, 395:144–159, May 2009. doi: 10.1111/j.1365-2966.2009.14537.x.

K. W. Willett, C. J. Lintott, S. P. Bamford, K. L. Masters, B. D. Simmons, K. R. V. Casteels, E. M. Edmondson, L. F. Fortson, S. Kaviraj, W. C. Keel, T. Melvin, R. C. Nichol, M. J. Raddick, K. Schawinski, R. J. Simpson, R. A. Skibba, A. M. Smith, and D. Thomas. Galaxy Zoo 2: detailed morphological classifications for 304 122 galaxies from the Sloan Digital Sky Survey. *MNRAS*, 435:2835–2860, November 2013. doi: 10.1093/mnras/stt1458.

K. C. Wong, M. R. Blanton, S. M. Burles, A. L. Coil, R. J. Cool, D. J. Eisenstein, J. Moustakas, G. Zhu, and S. Arnouts. PRIMUS: Enhanced Specific Star Formation Rates in Close Galaxy Pairs. *ApJ*, 728:119, February 2011. doi: 10.1088/0004-637X/728/2/119.

X. Yang, H. J. Mo, and F. C. van den Bosch. Constraining galaxy formation and

cosmology with the conditional luminosity function of galaxies. *MNRAS*, 339:1057–1080, March 2003. doi: 10.1046/j.1365-8711.2003.06254.x.

X. Yang, H. J. Mo, F. C. van den Bosch, A. Pasquali, C. Li, and M. Barden. Galaxy Groups in the SDSS DR4. I. The Catalog and Basic Properties. *ApJ*, 671:153–170, December 2007. doi: 10.1086/522027.

D. G. York, J. Adelman, J. E. Anderson, Jr., S. F. Anderson, J. Annis, N. A. Bahcall, J. A. Bakken, and et al. The Sloan Digital Sky Survey: Technical Summary. *AJ*, 120:1579–1587, September 2000. doi: 10.1086/301513.

F. Zwicky. Multiple Galaxies. *Ergebnisse der exakten Naturwissenschaften*, 29:344–385, 1956.

F. Zwicky. Multiple Galaxies. *Handbuch der Physik*, 53:373, 1959.